Technische Universität München

Fakultät für Medizin

Institut für Neuroproteomik, TU München und

Deutsches Zentrum für neurodegenerative Erkrankungen (DZNE) München

Proteomic secretome analysis of primary brain cells

Johanna Tüshaus

Vollständiger Abdruck der von der Fakultät für Medizin der Technischen Universität München zur Erlangung des akademischen Grades eines

Doktors der Naturwissenschaften (Dr. rer. nat.)

genehmigten Dissertation.

Vorsitzender: Prof. Dr. Andreas Pichlmair

Prüfer der Dissertation:
1. Prof. Dr. Stefan Lichtenthaler
2. Prof. Dr. Franz Hagn
3. Prof. Chris Turck, Ph.D.

Die Dissertation wurde am 08.09.2020 bei der Technischen Universität München eingereicht und durch die Fakultät für Medizin am 16.02.2021 angenommen.

EIDESSTATTLICHE ERKLÄRUNG

Ich erkläre an Eides statt, dass ich die bei der Fakultät für Medizin der TUM zur Promotionsprüfung vorgelegte Arbeit mit dem Titel:

“Proteomic secretome analysis of primary brain cells”

im Institut für Neuroproteomik der TU München und dem Deutsches Zentrum für neurodegenerative Erkrankungen (DZNE) München unter der Anleitung und Betreuung durch:

Prof. Stefan F. Lichtenthaler

ohne sonstige Hilfe erstellt und bei der Abfassung nur die gemäß § 6 Abs. 6 und 7 Satz 2 angegebenen Hilfsmittel benutzt habe.

Ich habe keine Organisation eingeschaltet, die gegen Entgelt Betreuerinnen und Betreuer für die Anfertigung von Dissertationen sucht, oder die mir obliegenden Pflichten hinsichtlich der Prüfungsleistungen für mich ganz oder teilweise erledigt. Ich habe die Dissertation in dieser oder ähnlicher Form in keinem anderen Prüfungsverfahren als Prüfungsleistung vorgelegt. Ich habe den angestrebten Doktorgrad noch nicht erworben und bin nicht in einem früheren Promotionsverfahren für den angestrebten Doktorgrad endgültig gescheitert.

Die öffentlich zugängliche Promotionsordnung der TUM ist mir bekannt, insbesondere habe ich die Bedeutung von § 28 (Nichtigkeit der Promotion) und § 29 (Entzug des Doktorgrades) zur Kenntnis genommen. Ich bin mir der Konsequenzen einer falschen Eidesstattlichen Erklärung bewusst.

Mit der Aufnahme meiner personenbezogenen Daten in die Alumni-Datei bei der TUM bin ich einverstanden.

München, den

Johanna Tüshaus

PUBLICATIONS RELATED TO THIS THESIS

Tüshaus, J., Müller, S.A., Kataka, E.S., Zaucha, J., Monasor, L.S., Su, M., Güner, G., Jocher, G., Tahirovic, S., Frishman, D., Simons, M., and Lichtenthaler, S.F. (2020). Quantitative proteomics establishes the cell type-resolved mouse brain secretome. The EMBO journal,e105693.

Weskamp, G., **Tüshaus, J**., Li, D., Feederle, R., Maretzky, T., Swendemann, S., Falck-Pedersen, E., McIlwain, D.R., Mak, T.W., Salmon, J.E., Lichtenthaler, S.F., and Blobel, C.P. (2020). ADAM17 stabilizes its interacting partner inactive Rhomboid 2 (iRhom2) but not inactive Rhomboid 1 (iRhom1). The Journal of biological chemistry 295, 4350-4358.

Pigoni, M., Hsia, H.E., Hartmann, J., Rudan Njavro, J., Shmueli, M.D., Müller, S.A., Güner, G., **Tüshaus, J**., Kuhn, P.H., Kumar, R., Gao, P., Tran, M.L., Ramazanov, B., Blank, B., Hipgrave Ederveen, A.L., Von Blume, J., Mulle, C., Gunnersen, J.M., Wuhrer, M., Rammes, G., Busche, M.A., Koeglsperger, T., and Lichtenthaler, S.F. (2020). Seizure protein 6 controls glycosylation and trafficking of kainate receptor subunits GluK2 and GluK3. The EMBO journal, e103457.

Koo, C.Z., Harrison, N., Noy, P.J., Szyroka, J., Matthews, A.L., Hsia, H.E., Müller, S.A., **Tüshaus, J**., Goulding, J., Willis, K., Apicella, C., Cragoe, B., Davis, E., Keles, M., Malinova, A., McFarlane, T.A., Morrison, P.R., Nguyen, H.T.H., Sykes, M.C., Ahmed, H., Di Maio, A., Seipold, L., Saftig, P., Cull, E., Pliotas, C., Rubinstein, E., Poulter, N.S., Briddon, S.J., Holliday, N.D., Lichtenthaler, S.F., and Tomlinson, M.G. (2020). The tetraspanin Tspan15 is an essential subunit of an ADAM10 scissor complex [published online ahead of print, 2020 Feb 28]. J Biol Chem. 2020;jbc.RA120.012601. doi:10.1074/jbc.RA120.012601

Hsia, H.E., **Tüshaus, J**., Brummer, T., Zheng, Y., Scilabra, S.D., and Lichtenthaler, S.F. (2019). Functions of 'A disintegrin and metalloproteases (ADAMs)' in the mammalian nervous system. Cellular and molecular life sciences : CMLS 76, 3055-3081.

ABSTRACT

The secretome is one major driver of inter-cellular communication. It encompasses a multitude of signaling cues and consists of soluble secreted proteins as well as ectodomains of proteolytically shed membrane proteins. Thereby, the secretome plays a key role in diverse biological processes ranging from development to neurodegeneration. Mass spectrometry-based proteomics has the potential to decipher the cellular secretome and identify quantitative alterations in disease conditions. However, until today proteomic secretome analysis remains technically challenging. In order to perform secretome analysis more efficiently, I have developed the High-performance Secretome Protein Enrichment With Click Sugars (hiSPECS) method. hiSPECS allows miniaturization of secretome analysis of primary cells in the presence of serum supplements while increasing proteome coverage and quantification reproducibility.

Using hiSPECS, the secretome of the four major brain cell types neurons, astrocytes, microglia and oligodendrocytes was analyzed in order to establish the first cell type-resolved mouse brain secretome resource. Systematic analysis of the resource elucidated not only cell type-specific secretome differences including a pivotal role of ectodomain shedding in neurons, but also enabled to elaborate the cellular origin of CSF proteins. Moreover, the inflammatory response of *ex vivo* brain slices upon LPS stimulation was determined and pointed towards a joint response of all four brain cell types. Finally, hiSPECS was used to identify the substrate repertoire of ADAM17 in primary neurons and astrocytes which elucidated more than 50 new substrate candidates. These results together with proteomic CSF and brain vessel analysis of *iRhom1*$^{4\text{-}11/4\text{-}11}$ mice, a mouse model which we established to majorly lack ADAM17 activity in the brain, suggest a function of ADAM17 in brain vasculature.

In conclusion, in this thesis a new method, called hiSPECS, was developed to decipher the secretome of primary cells in a highly efficient manner. To elaborate the power of hiSPECS I established the first cell type-resolved mouse brain secretome resource, determined the inflammatory response of brain slices and elucidate the substrate repertoire of BACE1 and ADAM17 in the brain.

ZUSAMMENFASSUNG

Das Sekretom ist ein wichtiger Bestandteil der interzellulären Kommunikation und beeinflusst eine Vielzahl von Signalwegen. Es besteht sowohl aus löslich sezernierten Proteinen als auch aus Ektodomänen von Membranproteinen, die durch proteolytische Spaltung von der Zellmembran abgelöst werden. Daher spielt das Sekretom eine Schlüsselrolle in verschiedensten biologischen Prozessen, angefangen von der embryonalen Entwicklung bis hin zu neurodegenerativen Erkrankungen. Massenspektrometrie-basierte Proteomik ist in der Lage, das zelluläre Sekretom zu entschlüsseln und durch Erkrankungen bedingte, quantitative Veränderungen zu identifizieren. Die Analyse des proteomischen Sekretoms stellt sich jedoch bis heute technisch anspruchsvoll dar. Um die Sekretomanalyse effizienter durchführen zu können, habe ich die sogenannte High-performance Secretome Protein Enrichment With Click Sugars (hiSPECS)-Methode entwickelt. hiSPECS ermöglicht die Miniaturisierung der Sekretomanalyse von Primärzellen in Gegenwart von Serumzusätzen bei gleichzeitiger Erhöhung der Proteomabdeckung und der Reproduzierbarkeit der Quantifizierungen.

Um die erste Hirn-Sekretomressource der Maus zu etablieren, wurde mit der Hilfe von hiSPECS das Sekretom der vier häufigsten Hirnzelltypen Neuronen, Astrozyten, Mikroglia und Oligodendrozyten bestimmt. Die systematische Analyse der Ressource zeigt nicht nur zelltypspezifische Sekretomunterschiede einschließlich einer zentralen Rolle der Ektodomänenabgabe in Neuronen auf, sondern ermöglichte es auch, den zellulären Ursprung von Liquorproteinen herauszuarbeiten. Darüber hinaus wurde die Entzündungsreaktion von ex vivo Hirnschnitten nach LPS-Stimulation bestimmt, die auf eine gemeinsame Reaktion aller vier Hirnzelltypen hinweist. Schließlich wurde hiSPECS zur Identifizierung des Substratrepertoires von ADAM17 in primären Neuronen und Astrozyten verwendet, wodurch mehr als 50 neue Substratkandidaten detektiert werden konnten. Diese Ergebnisse deuten zusammen mit der proteomischen Analyse des Liquors und der Hirngefäße von *iRhom1*$^{4\text{-}11/4\text{-}11}$-Mäusen, einem Mausmodell, bei dem wir festgestellt haben, dass ADAM17-Aktivität im Gehirn weitgehend fehlt, auf eine Funktion von ADAM17 im Hirngefäßsystem hin.

Zusammenfassend lässt sich sagen, dass ich im Rahmen dieser Doktorarbeit eine neue Methode, genannt hiSPECS, entwickelt habe, um das Sekretom primärer Zellen auf hocheffiziente Weise zu entschlüsseln. Um die Leistungsfähigkeit von hiSPECS

herauszuarbeiten, habe ich die erste zelltypaufgelöste Hirn-Sekretomressource der Maus etabliert, die Entzündungsantwort von Hirnschnitten und das Substratrepertoire von BACE1 und ADAM17 im Gehirn bestimmt.

TABLE OF CONTENTS

ABBREVIATIONS

ACN	**Acetonitril**
AD	Alzheimer´s disease
ADAM	A disintegrin and metalloproteinases
AHA	Azidohomoalanine
AP	Alkaline Phosphatase
APP	Amyloid precursor protein
BACE	β-site APP cleaving enzyme
BP	Biological process
BSA	Bovine serum albumin
CC	Cellular compartment
CNS	central nervous system
CSF	Cerebrospinal fluid
CTSP	Cell type-specifically secreted proteins
DAPI	4′,6-diamidino-2-phenylindole
DBCO	Dibenzocyclooctyne
DDA	Data dependent acquisition
DIA	Data independent acquisition
DIV	Day in vitro
DNA	Deoxyribonucleic acid
DTT	Dithiothreitol
EDTA	Ethylenediaminetetraacetic acid
EGF	Epidermal growth factor
EGFR	Epidermal growth factor receptor
ELISA	Enzyme-Linked ImmunoSorbent Assay
ER	Endoplasmic reticulum
FBS	Fetal bovine serum
FDR	False discover rate
GFP	Green fluorescent protein
GFP	Green fluorescent protein
GPI	Glycosylphosphatidylinositol
hiSPECS	High-performance secretome protein enrichment with click sugars
HPLC	High-performance liquid chromatography
iRHOM	Inactive rhomboid
LFQ	Label-free quantification
LPS	Lipopolysaccharide
m/z	Mass to charge ratio
MACS	Magnetic Activated Cell Sorting
ManNAz	N-azidoacetylmannosamine-tetraacylated
MS	Mass spectrometry
PBS	Phosphate-buffered saline
PCA	Principal component analysis
PCR	Polymerase chain reaction
PFA	Paraformaldehyde
PMA	Phorbol 12-myristate 13-acetate
PPIN	Protein-protein interaction network
QARIP	Quantitative analysis of regulated intramembrane proteolysis

RNA	Ribonucleic acid
rpm	Revolution per minute
RT	Room temperature
SDS-PAGE	Sodium dodecyl sulfate polyacrylamide gel electrophoresis
SPECS	Secretome protein enrichment with click sugars
TGN	Trans-golgi network
TM	Single-pass transmembrane
UMAP	Uniform manifold approximation and projection

1 INTRODUCTION

1.1 The secretome

The central nervous system (CNS) is a complex cellular network in which cohesive communication between individual cells is key. One major driver of inter-cellular communication is the secretome, which encompasses all proteins actively released by a cell into the extracellular space (Lichtenthaler et al., 2018). Proteins harboring a signal peptide are secreted via the conventional secretory pathway by passing the trans-Golgi network (TGN) including soluble secreted proteins and ectodomains of transmembrane proteins released by proteolytic processing. In addition, proteins without signal peptide may be released by unconventional protein secretion (UPS) mechanisms (Figure 1) (Kim et al., 2018). Little is known about the mechanisms of secretion and systematic studies are lacking to elaborate their role in the CNS. The secretome contains a plethora of signaling proteins such as hormones, cytokines and growth factors. Thereby it plays an important role in basic mechanisms such cell growth or differentiation and also in disease conditions including neurodegenerative diseases such as Alzheimer disease (AD) (Lichtenthaler et al., 2018). For example, inflammation is triggering strong changes in the secretome of cells by increasing the release of proteins such as pro-inflammatory cytokines (e.g. TNFα) (Blobel, 2002).

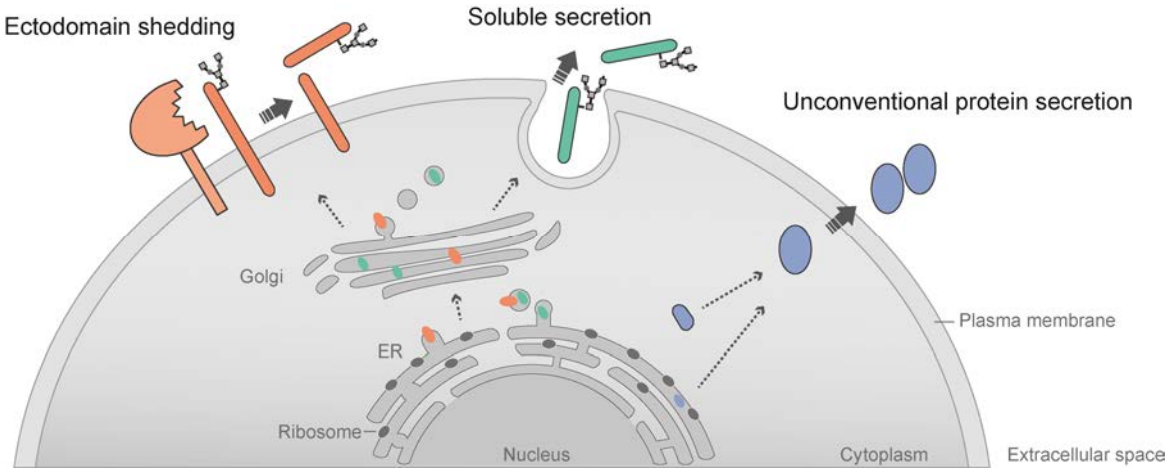

Figure 1: The secretome. The cellular secretome contains all actively released proteins including proteins which passed the conventional secretory pathway including soluble secreted (green) and soluble ectodomains of

transmembrane proteins released by ectodomain shedding (brown) as well as unconventionally secreted proteins (blue). Modified from (Kim et al., 2018).

1.2 Ectodomain shedding

Ectodomain shedding is defined as the proteolytic release of the extracellular domain from a membrane anchored protein by protease cleavage (Figure 2). Shedding is an evolutionary conserved process that strongly influences the fate of the shed protein because the cleavage step is irreversible. Many membrane proteins including single-pass transmembrane proteins with type 1 (TM1, cytosolic C-terminus) and type2 (TM2, cytosolic N-terminus) orientation, glycophosphatidylinositol (GPI)-anchored but also some multi-pass transmembrane proteins are subject to shedding (Lichtenthaler et al., 2018). The proteases, such as the ADAM (a-disintegrin-and-metalloproteinases) family members, are often themselves membrane bound and cleave their substrates in the juxtamembrane region. Ectodomain shedding plays a key role in diverse cellular processes in the CNS ranging from cell adhesion, axon and neurite outgrowth to transmembrane signaling and neuronal differentiation (Blobel, 2002; Hsia et al., 2019; Lichtenthaler et al., 2018; Saftig et al., 2015). Moreover, imbalances in this highly regulated process are linked to neurodegenerative diseases such as AD (Lichtenthaler et al., 2018). Therefore, it is important to study the regulation of ectodomain shedding and establish tools which allow detailed understanding of this process.

Ectodomain shedding can activate, terminate or alter the biological function of its target protein. The soluble ectodomain released by shedding into the secretome, may be the biologically active fragment of the protein. In contrast, other proteins, such as cell adhesion proteins or transmembrane receptors, act as full length proteins only and shedding terminates their biological function. This complex regulation can be nicely exemplified when taking a closer look to the tumor necrosis factor-α (TNFα). TNFα is synthesized as type 2 single-pass transmembrane protein in immune cells and reaches the plasma membrane via the TGN where it is shed by ADAM17(Black et al., 1997; Moss et al., 1997). The released ectodomain is soluble and acts as pro-inflammatory cytokine on distant cells by binding to TNFR1 and activating downstream signaling. In contrast, full-length TNFα acts anti-inflammatory by binding TNFR2 (Black et al., 1997; Grell, 1995). TNFR1 itself is shed by ADAM17 controlling its surface levels and terminating its signaling (Deng et al., 2015).

The initial shedding step is often followed by a second cleavage step within the transmembrane region by intramembrane proteases such as γ-secretase (TM1), rhomboid proteases (TM1), site-2 proteases (TM2) or signal-peptide peptidase (like) (TM2) proteases (Voss et al., 2013). The combination of both sequential cleavage steps is referred to as regulated intramembrane proteolysis (RIP) (Brown et al., 2000). One well studied example which undergoes RIP is NOTCH1. When cleaved initially by ADAM10 the ectodomain is released and the trimmed NOTCH1 protein undergoes cleavage by γ-secretase (De Strooper et al., 1999). The initial shedding step is a necessity for the second intramembrane cleavage step due to steric hindrance of the large ectodomain (Güner et al., 2020). Thereby, RIP regulates on the one hand the level of NOTCH1 on the cell surface and on the other hand releases the intracellular domain of NOTCH1 from the membrane. This domain is known to be allocated to the nucleus where it acts as transcription factor (Groot et al., 2014; Yatim et al., 2012). Together, ectodomain shedding controls the secretome as well as the surface of a cell and releases fragments of membrane proteins which trigger internal and external signaling pathways.

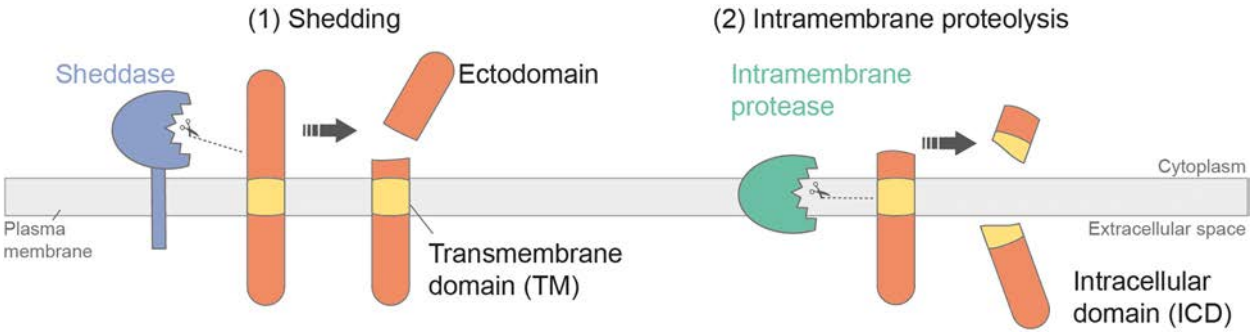

Figure 2 Illustration of regulated intramembrane proteolysis. First, the ectodomain of the single-pass transmembrane protein (orange) is cleaved by a sheddase such as BACE1 or ADAM17. In a second step, after shortening the large extracellular domain, intramembrane proteolysis can take place by cleavage within the transmembrane domain (yellow) releasing the intracellular domain (ICD) into the cytosol which may trigger intracellular signaling.

1.3 The Alzheimer´s disease protease BACE1

Extracellular amyloid-β (Aβ) plaques are, besides intracellular tau-tangles, the major hallmark of Alzheimer´s disease (AD) which was used for the first classification of the disease by Alois Alzheimer (Alzheimer, 1907) and is still used in diagnostics nowadays (Alzheimer et al., 1995; Vishal et al., 2011). The main building block of the plaques are oligomers of the Aβ peptide which is released by the cell via RIP of the amyloid precursor protein (APP). The initial APP cleavage step is performed by BACE1 (β-site APP cleaving enzyme 1) (Vassar et al., 1999; Yan et al., 1999). Followed by a second γ-secretase

cleavage step within the transmembrane region which releases the Aβ peptide. Hence, reducing the generation of the Aβ peptide by BACE1 inhibition was a major focus of AD therapy development during the past decade. However, several phase 3 clinical trials testing different BACE1 inhibitors failed due to a lack of efficacy and arising side effects, such as liver toxicity, suicidal ideation and sleeplessness (Egan et al., 2018; Hampel et al., 2020; Imbimbo et al., 2019). The side effects may partially be explained by the loss of cleavage of other BACE1 substrates besides APP or off-target inhibition of BACE2, the closest homolog of BACE1.

In general, BACE1 is an aspartyl protease which has higher activity in acidic compartments of the cell. It is highly expressed in the brain and primarily enriched in neurons. While only a small fraction of BACE1 is present on the cell surface due to rapid internalization, it is mainly present in endosomes and the trans-Golgi network (Vassar et al., 1999) (Huse et al., 2000). The substrate repertoire of BACE1 has been elaborated in several proteomic studies using cell lines (Hemming et al., 2009) (Stutzer et al., 2013), primary neurons (Herber et al., 2018; Kuhn et al., 2012; Zhou et al., 2012) or CSF analysis of BACE1 deficient mice (Dislich et al., 2015; Pigoni et al., 2016) elucidating more than 40 substrate candidates other than APP. Several of them were validated in follow-up studies as neuronal BACE1 substrates e.g. L1CAM and CHL1 (Zhou et al., 2012), SEZ6 and SZE6L (Pigoni et al., 2016), CACHD1 and MDGA1 (Rudan Njavro et al., 2020).

BACE1 knockout mice reveal pronounced phenotypes including seizures, reduced survival rates and body weight. Some of the molecular changes were attributed to the lack of cleavage of specific substrates, such as NRG1 (myelination), JAG1 (neurogenesis) or CHL1 (axon guidance) (Hampel et al., 2020). Noteworthy, a mouse model in which the BACE1 loss was introduced in adulthood revealed no major deficits, besides the axon guidance phenotype (Ou-Yang et al., 2018) or deficits in synaptic plasticity (Lombardo et al., 2019). These findings suggested, that many of the phenotypes seen in the BACE1 straight KO mice were originated from the developmental stage. Since Alzheimer´s disease affects mainly the elderly people, these non-developmental phenotypes are of even greater importance in terms of suggesting possible side effects when BACE1 is pharmacologically inhibited. Additional studies are needed to gain deeper knowledge of the biological functions and substrate repertoire of BACE1 to explain and thereby potentially circumvent the detected side effects in clinical trials of BACE1

inhibitors. Moreover, development of companion diagnostics and pharmacodynamics biomarkers to reflect the activity state of the protease are required to predict disease progression, determine treatment windows and enable safe drug development to minimize side effects.

1.4 The inflammatory protease ADAM17

ADAM17 (a-disintegrin-and-metalloprotease 17) also known as TACE (TNFα-converting-enzyme), is a highly conserved and ubiquitously expressed metalloprotease that plays key roles in inflammation, wound healing, development and many other cell functions (Hsia et al., 2019). Patients suffering from ADAM17 mutations which induces loss of function reveal severe symptoms such as skin and bowel lesions (Bandsma et al., 2015; Blaydon et al., 2011). The knockout of ADAM17 in mice leads to premature death around birth, which is potentially caused by hemorrhages and resembles in many regards the phenotype of epidermal growth factor receptor (EGFR) knockout mice, including e.g. an open-eye phenotype (Blobel, 2005; Jackson et al., 2003; Mine et al., 2005; Peschon et al., 1998). This is the case, because ADAM17 is cleaving and thereby systematically activating all EGFR ligands besides betacellulin (BTC) and EGF which in contrast are cleaved by ADAM10 (Blobel, 2005; Sahin et al., 2004). In addition, ADAM17 is cleaving TNFα (as discussed before) and more than 70 other substrates including several cell adhesion proteins and cytokines (Zunke et al., 2017). Interestingly, a hypomorphic ADAM17 knockout mouse (*ADAM17*$^{ex/ex}$) revealed that around 5% of its normal expression level is sufficient to ensure the survival of the mice (Chalaris et al., 2010). Due to its broad substrate repertoire, ADAM17 is involved in a plethora of biological functions and is linked to many diseases including many inflammation related diseases such as lupus (Qing et al., 2018), arthritis (Haxaire et al., 2018) and kidney fibrosis (Kefaloyianni et al., 2016).

The functions of ADAM17 in the CNS are less well established. However, due to its RNA expression profile (Black et al., 1997) as well as ADAM17-mediated cleavage of NCAM (Kalus et al., 2006), L1CAM (Maretzky et al., 2005) and EGFR ligands with a dominant role of HB-EGF (Blobel, 2005), ADAM17 has been linked to neuronal development including the development of dopaminergic neurons, which are the major cell type affected in Parkinson's disease (PD) (Yoon et al., 2013). The HB-EGF/EGFR signaling axis is also regulating myelination (Palazuelos et al., 2014) and ADAM17 deletion in

oligodendrocytes has been linked to reduced regeneration after demyelination (Palazuelos et al., 2015) and hypomyelination because of reduced cell survival (Fredrickx et al., 2020; Palazuelos et al., 2014) in the brain. In contrast, constitutive deletion of ADAM17 in motor neurons leads to hypermyelination due to reduced cleavage of NRG1 type III in the periphery (La Marca et al., 2011). Moreover, ADAM17 has been linked by cleavage of neuronal pentraxin (NPR) to an involvement in long term depression (LTD) and thereby synaptic plasticity and memory (Cho et al., 2008). In addition, ADAM17 and its natural regulator TIMP3 (tissue inhibitor of metalloproteinase 3) have been associated with the genetic variant of small vessel disease CADASIL (cerebral autosomal dominant arteriopathy with subcortical in facts and leukoencephalopathy) (Capone et al., 2016) and glioblastoma (Siney et al., 2017; Zhang et al., 2018).

In general, ADAM17 can be rapidly activated by stimuli such as LPS and PMA *in vitro* (Lorenzen et al., 2016; Mülberg et al., 1993). It has been suggested to play a role in the stimulated cleavage of APP while its closest homolog ADAM10 has been shown as the major α-secretase under constitutive conditions (Kuhn et al., 2010). Similar to APP, ADAM17 might be involved in the stimulated cleavage of TREM2 (triggering receptor expressed in myeloid cells 2), an AD genetic risk factor, which is known to be cleaved by ADAM10 under constitutive conditions (Feuerbach et al., 2017; Schlepckow et al., 2017). Furthermore, ADAM17 might be linked to AD due to its function in inflammation by releasing soluble TNFα and other pro-inflammatory cytokines. Interestingly, a recent study in drosophila showed a protective effect of TNFα/ADAM17 in age dependent degeneration of retinal cells. Defective TNFα/ADAM17 leads to accumulation of lipid droplets (LD) in glia cells which finally results in cell death of neurons and glia (Muliyil et al., 2020). Moreover, a GWAS study revealed ADAM17 loss of function mutations as an AD risk gene (Hartl et al., 2020). In summary, ADAM17 has a pivotal role during inflammation and is linked to several brain functions by cleaving a broad spectrum of substrates expressed in the brain. However, further studies are required to elucidate the detailed ADAM17 regulation mechanisms in health and disease to evaluate the role of ADAM17 in the CNS.

The proteolytic activity of ADAM17 is tightly regulated on several levels (Figure 3). At its N-terminus it contains a pro-domain that blocks the catalytic center and the release of this domain by furin cleavage at two sites is required for ADAM17 activation (Wong et al.,

2015). Interestingly, a synthetic peptide resembling this prodomain has been suggested as an ADAM17 specific inhibitor (Wong et al., 2016). Its catalytic domain is closely related to snake venom metalloproteases and requires zinc ion binding for proteolytic activity on its substrates. A connection between phosphatidylserine relocation and the conformation of ADAM17 has been actively discussed in the field and may potentially influence its activity state (Sommer et al., 2016). The short cytotail of ADAM17 can be phosphorylated and may be triggered by activators such as PMA. However, the regulatory function of this domain is not well understood and other studies suggested its dispensability (Reddy et al., 2000; Schwarz et al., 2013). Moreover, ADAM17 requires the binding of inactive rhomboid (iRHOM) proteins to pass the TGN and reach the cell surface where it mainly cleaves its substrates) (Adrain et al., 2012; McIlwain et al., 2012). This last step of ADAM17 activity regulation is described in more detail in the following section. Taken together, the current understanding of the brain functions of ADAM17 is limited and thus revealing its regulatory mechanisms as well as its substrate repertoire in primary brain cell types is of significant interest to evaluate ADAM17 as potential drug target in brain diseases such as AD.

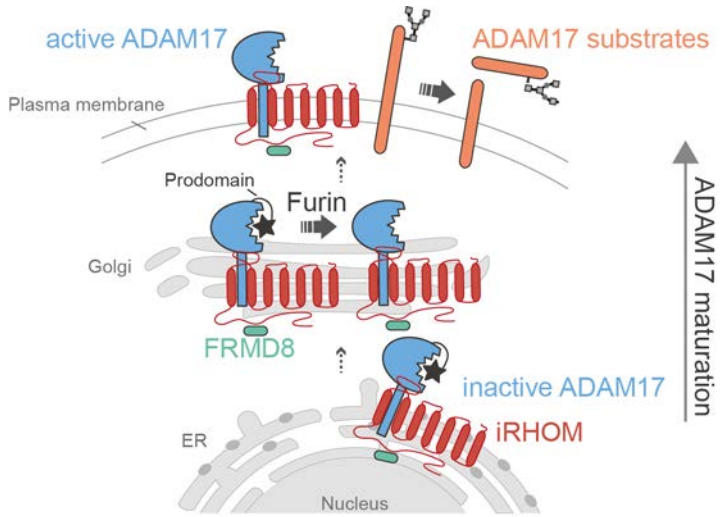

Figure 3 ADAM17 maturation. ADAM17 (blue) maturation is controlled by binding to its regulators iRHOM1 or iRHOM2 (red) and FRMD8 (green) which binds to the cytotail of the iRHOMs. The prodomain of ADAM17 is released by furin and mature ADAM17 reaches the cell surface where it can cleave its substrates (orange).

1.5 The ADAM17 regulator iRHOM1

In mammals, two iRHOM proteins, iRHOM1 and iRHOM2, are expressed. Regulation of ADAM17 activity and cell surface trafficking by iRHOMs are well characterized. iRHOMs bind ADAM17 in the ER and are required to guide it through the secretory pathway to the

plasma membrane (Figure 3) (Adrain et al., 2012; McIlwain et al., 2012). Both iRHOMs have a characteristic protein domain structure of seven transmembrane domains of which the first two are connected by an enlarged loop. It has a long intracellular domain (N-terminus) and a short C-terminus. The transmembrane domain of ADAM17 and the 1st transmembrane domain of iRHOM2 have been shown to be essential for their binding capability (Li et al., 2017; Tang et al., 2020). In addition, the cytotail of iRHOMs has been shown to be important for ADAM17 regulation. First, phosphorylation of the iRHOM2 cytotail is essential for the stimulated shedding activity of ADAM17, a process mediated by the recruitment of 14-3-3 protein family members to the phosphorylation sites (Cavadas et al., 2017; Grieve et al., 2017). Second, an additional protein named FRMD8 (or iTAP) binds to the cytotail of iRHOMs and is a third binding partner required for the maturation complex shuttling ADAM17 to the cell surface (Kunzel et al., 2018; Oikonomidi et al., 2018). Third, a spontaneous mutation in *Rhbdf2*, the gene encoding the iRHOM2 protein that causes a deletion of the first 268 amino acids of the cytotail, results in a loss of hair phenotype (Siggs et al., 2014). Last, two mutations in the cytotail of iRHOM2 have been shown to cause tylosis in patients (Blaydon et al., 2012).

The lack of both iRHOMs prevents ADAM17 activation and thereby the shedding of its substrates, which is important for cell growth and survival. Hence, iRHOM1 and 2 double knockout mice reveal severe phenotypes, mimicking ADAM17 knockout mice, including premature death, hemorrhages and an open-eye phenotype (Christova et al., 2013; Li et al., 2015). Interestingly, depending on the targeting strategy used for editing the *Rhbdf1* gene, encoding the iRHOM1 protein, knockout mice reveal differently pronounced phenotypes (Christova et al., 2013; Hosur et al., 2020; Li et al., 2015) (detailed comparison shown in Figure 4). iRHOM1 knockout mice reported by Christova et al. lack the whole coding region of *Rhbdf1* (exon 2-18) and they suffer from severe phenotypes including intracerebral hemorrhages and premature death within week 1 to 6 after birth, depending on the genetic background of the mice. Crossing these mice with iRHOM2 KO mice caused embryonic lethality before E9.5 (Christova et al., 2013). In contrast, targeting strategy used by Li et al. deleted exon 4 to 11 from the *Rhbdf1* locus, which encodes e.g. the first transmembrane domain (TMD) of iRHOM1. These mice (from now on referred to as *iRhom1*$^{4\text{-}11/4\text{-}11}$) are viable, fertile and indistinguishable from wild type littermates. Crossing the *iRhom1*$^{4\text{-}11/4\text{-}11}$ mice with iRHOM2 knockout mice causes perinatal lethality

and an open eye phenotype which mimics the phenotype of ADAM17 and EGFR knockout mice (Li et al., 2015). In the brain, *iRhom1*$^{4\text{-}11/4\text{-}11}$ mice have been reported to lack mature ADAM17 while in other tissues mature ADAM17 was detectable probably due to the compensatory effect of iRHOM2. This indicates a predominate role of iRHOM1 in ADAM17 regulation in the brain (Li et al., 2015). In contrast, in macrophages, iRHOM2 was shown to be the solely expressed iRHOM and knockout of iRHOM2 was sufficient to prevent ADAM17 maturation and ADAM17-dependent shedding of e.g. TNFα (Adrain et al., 2012; McIlwain et al., 2012). While both iRHOM1 and iRHOM2 are trafficking ADAM17, they have been suggested to differentially influence the substrate selectivity of ADAM17 (Maretzky et al., 2013). In general, little is known about the detailed mechanism including cellular differences and further studies are needed to pinpoint the diverse biological functions of iRHOM1 and iRHOM2. While most studies to date focus on iRHOM2 mainly in the context of ADAM17–dependent TNFα release, it is of significant interest to understand the biological function of iRHOM1, especially in the context of the brain and brain diseases.

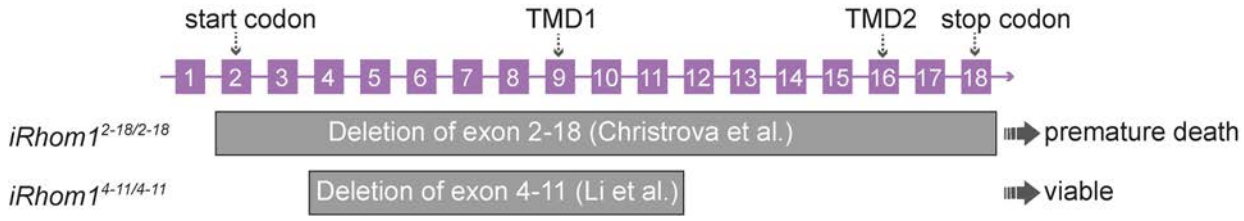

Figure 4 iRHOM1 targeting strategies in different mouse models. (Christova et al., 2013) published a mouse model which lacks the whole coding region of Rhbdf1, the gene encoding iRHOM1. *iRhom1*$^{2\text{-}18/2\text{-}18}$ mice reveal a severe phenotype including premature death. In contrast, the mouse model *iRhom1*$^{4\text{-}11/4\text{-}11}$ introduced by (Li et al., 2015) is viable and reveals no major phenotypes. In this mouse model exon 4 to 11 were deleted including the region encoding the first transmembrane domain (TMD) of iRHOM1.

1.6 Proteome analysis by mass spectrometry

The proteome, the union of all proteins, of a cell is not fixed. It is rather a flexible system adaptable to internal or external stimuli, meaning that it carries the information of systematic changes happening e.g. during disease progression or aging. In recent years, Mass spectrometry (MS) has proven its potential to enlighten the proteome and technical advances of the past decades enable deep proteome coverage with high precision and speed (Aebersold et al., 2016). Therefore, MS is often used for explorative studies by comparing protein abundance changes relative to each other e.g. between body fluids of patients and healthy controls aiming to pinpoint biomarkers or elucidating new drug targets. Moreover, measuring proteome-wide changes happening upon drug treatment

or knockout of a target gene in model systems is an unbiased way to determine disease mechanisms, pharmacodynamics changes and potentially foresee/prevent side effects during drug development. In addition, MS may become a tool for diagnostics in the clinic if technology, sample preparation and data analysis can be standardized and simplified in a cost-efficient and robust manner (Aebersold et al., 2016).

For discovery studies, such as those being performed in the scope of this thesis, bottom up proteomics in combination with LC-MS/MS (liquid chromatography - tandem mass spectrometry) analysis is commonly used. The workflow applied in this thesis is summarized (Figure 5), starting with denaturation of the proteins to be analyzed, followed by chemical derivatization of the cysteines to ensure no disulfide-bonds are being formed. Next, proteins are digested with trypsin, a sequence sensitive protease that cleaves C-terminal to arginine and lysine. This digestion results in peptides with an average length of nine amino acids which is a good balance between keeping specificity of the peptide and being in the ideal range for MS analysis. Additionally, in acidic environment peptides generated by trypsin digestions carry two positive charges at the N-terminus and the terminating amino acid (C-terminus), which brings the advantage of better ionization-ability of the peptide (Swaney et al., 2010). Using nano high-performance liquid chromatography (HPLC) peptides are separated, e.g. due to their hydrophobic properties by eluting with increasing percentage of organic solvent in the mobile phase from the hydrophobic C18 stationary phase. This technique is used in our set up.

In this thesis, the HPLC was online coupled to a Q-exactive™ HF hybrid quadrupole-orbitrap™ mass spectrometer which was used for all MS measurements throughout this research project. An electrospray ionization (ESI) interface, a technique honored with the Noble prize in 2002 (Fenn et al., 1990), is used to ionize the peptides which are guided through electric fields to the mass analyzer while uncharged particles are filtered out. Positively charged ions are accumulated, stabilized and focused in a narrow ion cloud in the C-trap before ions are injected into the orbitrap where their mass to charge ratio (*m/z*) is detected and analyzed. An orbitrap combines mass analyzer and detector functions and is built up of a negatively charged inner electrode and an outer electrode. The peptide ions, which are positively charged, rotate in an orbit-like movement around the inner electrode while at the same time oscillating along the z-axis. The frequencies of oscillation around the inner electrode is depend on the individual *m/z* of each peptide and induce a

characteristic current which is recorded by the detector (outer electrode). Signal amplification and fast Fourier transformation (FFT) are used to compute the *m/z* of the peptide ions according to the frequency and their intensities based on the amplitude of the induction current (Makarov, 2000; Perry et al., 2008).

The first so called MS1 scan, which determines the mass to charge ratios of the intact peptides (precursor ions), is not sufficient to predict the amino acid sequence as peptides build up by the same amino acids in different order may carry the same mass. Therefore, subsequent MS2 scans to gain information about the amino acid sequence of the peptides are required. The mass information of the MS1 scan is used to sequentially isolate the peptides of interest in a quadrupole mass filter. Those peptides enter the higher-energy collisional dissociation (HCD) cell where the inert gas nitrogen is used induce fragmentation along the peptide backbone (Olsen et al., 2007). These so-called fragment ions are transferred back through the C-trap into the orbitrap to acquire the fragment ion or also called MS2 spectra. The combined *m/z* information of the MS1 and MS2 scans are sufficient to accurately determine the sequence of the peptide For this purpose, a database search is applied which compares the detected peptide masses and its fragment ion masses to *in silico* digested protein databases of the analyzed species. The peptide identification is based on a scoring algorithm which determines the best hit in the protein database. Finally, the identified peptides can be mapped onto the protein sequences for further data analysis. Importantly, the quality of the individual matches are scored and a false discovery rate (FDR) filter is used to regulate for false positive identifications for peptides and proteins (Aebersold et al., 2016).

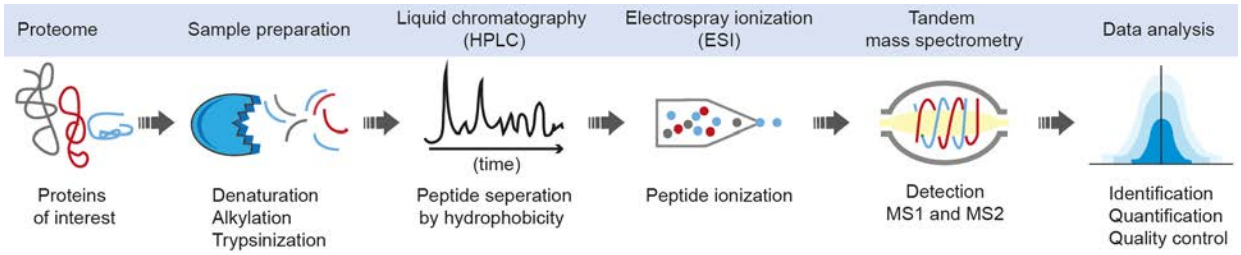

Figure 5 Illustration of a typical bottom-up proteomic workflow. Sample preparation of the proteins of interest is performed including denaturation, alkylation and digestion with a sequence sensitive enzyme such as trypsin. The tryptic peptides are separated according to their hydrophobicity using high-performance liquid chromatography (HPLC) and ionized using an electrospray ionization (ESI) source. In the mass spectrometer the MS1 scan, which is used for

detection of the precursor ion, is followed by MS2 scans of the fragmented precursor ions, allowing their identification using computational data analysis.

1.7 Quantitative proteomics

In order to compare proteomes, e.g. of different cell types or to investigate the effect of pharmacological treatments, not only the identity of the proteins (qualitative information) is important, but also their abundance levels (quantitative information). Quantification with MS is possible in an absolute or relative manner. However, absolute protein quantification requires the usage of synthetic peptide standards of known concentration for absolute quantification, which is very expensive, involves laborious method optimization, and only allows the quantification of a few selected proteins in one analysis. Therefore, relative quantification is the method of choice for whole proteome comparisons, which facilitates the relative quantification of abundances from hundreds to thousands proteins between two or more experimental groups. Relative quantification can be performed by introducing isotope labels e.g. by using synthetic amino acids in the stable isotope labeling by amino acids in cell culture (SILAC) method (Ong et al., 2002). Alternatively, isotope labeling can also be introduced chemically with amino-reactive isobaric tags such as tandem mass tags (TMT). This method facilitates to mix and analyze up to 16 samples in one analysis. However, since the relative quantification is based on reporter ions which are released during fragmentation in the low *m/z* area, this method has the disadvantage that co-isolation and fragmentation of multiple peptides can lead to an effect called ratio compression. This can lead to inaccurate relative protein quantification if sample preparation, e.g. peptide fractionation, and MS analysis is not performed properly (Aggarwal et al., 2019). In general, label-based quantification has the advantage of multiplexing different samples and being more precise than label-free quantification (LFQ), but the sample complexity and sample preparation time/costs are increased.

As LFQ is applicable to all sample types, including clinical samples and primary cells which may be influenced by the potential toxic effect of e.g. SILAC labels, LFQ is used in most discovery studies nowadays (Hauck et al., 2010). Technical improvements of the MS instruments and the algorithms used for data analysis greatly increased the power of LFQ over the last years (Cox et al., 2011), but reproducibility from sample preparation to chromatography are the key determinant for reliable and robust LFQ between different samples (Aebersold et al., 2016).

In order to quantify a given peptide by LFQ, it is required to collect distinct intensity values of a precursor ion within a defined *m/z* tolerance range in several subsequent scans. In general, around eight data points per precursor are needed to reliably extrapolate a chromatographic peak over these discrete intensity values as function over time (extracted ion chromatogram: XIC) which is used to integrate the area under the curve as quantity measurement. The integrated areas of the XIC of individual peptides of one protein are compared between different samples after a normalization step that controls for experimental variation to finally gain the protein LFQ value. In traditional data dependent acquisition (DDA), also named shotgun proteomics, a full MS1 scan is followed by 10 to 15 MS2 sequencing scans of the most abundant peptide ions (MS2 top N) (Figure 6). Typically, precursors, that were successfully isolated and fragmented, are excluded for a certain amount of time from following MS2 cycles to ensure the sequence information of a large variety of peptides is acquired. Since peptide quantification requires a series of intensity values of the same precursor, in DDA peptide quantification is achieved exclusively on MS1 level.

In the recently developed data independent acquisition (DIA) not the top N precursors are analyzed, instead all precursors belonging to a defined *m/z* window are fragmented and analyzed together in an unbiased manner (Figure 6). Multiple *m/z* windows are set to cover the desired *m/z* area in a way to balance the amount of precursors to be analyzed within each window. Thereby, DIA is not limited to the top N precursors, but the resulting fragment spectra become highly complex and an additional dimension is required to enable the computation of assigning the spectra to specific peptide precursors and their protein origin. This additional dimension are peptide spectral libraries generated by previously acquired DDA runs of the same sample type which contain not only the fragment ion information but also their retention time which is normalized to reference peptides (Bruderer et al., 2015; Bruderer et al., 2016; Ludwig et al., 2018). Throughout this thesis a DIA variant based on peptide-centric scoring named sequential window acquisition of all theoretical mass spectra (SWATH-MS) was used (Gillet et al., 2012). Here, distinct intensity values of the precursor and the fragment ions in subsequent MS1 and MS2 scans are collected meaning quantification is possible on both levels. For this purpose, either peptide peaks from MS1 spectra or multiple fragment ion peaks from MS2 spectra are integrated for peptide quantification. The biggest drawback of DIA compared

to DDA is the additional effort of producing the spectral libraries upfront and the completeness of the library directly defines the final DIA analysis results. In the future, library-free DIA may have the potential to overcome this drawback using newly released software such as directDIA™ in Spectronaut-14 by Biognosys. Interestingly, samples analyzed in DIA mode can be reanalyzed to a later time point if e.g. an improved spectral library is available. In general, DIA has been shown to acquire more complete data sets containing less missing values especially of low-concentrated proteins compared to DDA (Bruderer et al., 2015; Bruderer et al., 2017). Naturally, CSF and secretome samples contain mainly low abundant proteins, but also some very abundant proteins such as albumin in CSF, which require a highly sensitive analysis covering a broad concentration range. Therefore, one aim of this thesis was the establishment of DIA analysis for secretome analysis including the generation of required spectral libraries for these low-concentrated sample types.

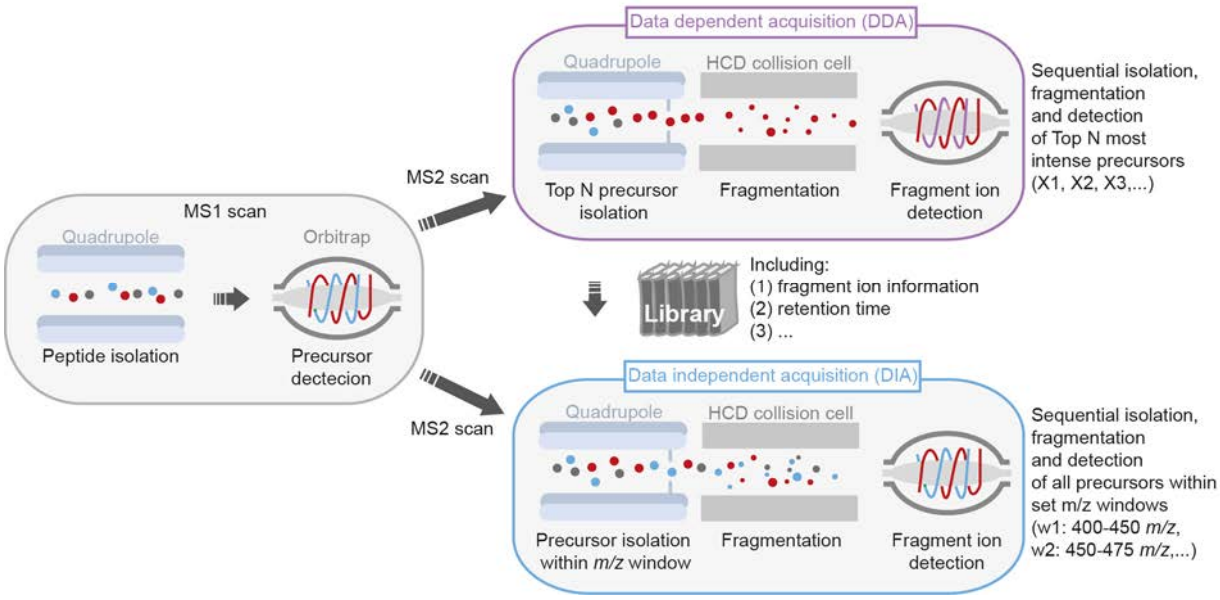

Figure 6 Comparison of DDA and DIA MS2 scans. In data dependent acquisition (DDA) mode a MS1 full scan is followed by N MS2 scans allowing the sequential analysis of the top N most intense precursor peptides. In contrast, in data independent acquisition (DIA) mode all precursor peptides of a defined mass range are analyzed in one MS2 scan. Typically, around twenty *m/z* windows are defined, meaning one MS1 scans is followed by twenty MS2 scans and each MS2 scan includes all precursors within the set mass range. Due to the higher complexity of the resulting data, a previously established library of DDA runs is required, which includes, among other things, information about the retention time of the precursor peptides to be analyzed.

1.8 Secretome analysis

Quantitative MS is commonly used to perform secretome analysis of cell lines or primary cultured cells by analyzing their conditioned media which contains the proteins secreted

by cells. The majority of cells require the presence of high abundant media supplements including albumin for vital growths and proliferation. This is a huge challenge for quantitative secretome analysis by MS because the high concentrated supplement proteins disturb the detection of low concentrated cell-derived secretome proteins. Commonly, LC-MS/MS based proteomics covers three to four orders of magnitude related to the protein with the highest concentration. This means that the limit of detection is roughly 1/10,000 1/1,000 of the protein concentration with the highest abundance in the sample. Therefore, most secretome studies are performed under serum/protein supplement starvation conditions (Deshmukh et al., 2015; Meissner et al., 2013), which however can rapidly trigger a stress response and alter the secretome composition of cells (Eichelbaum et al., 2012). In order to perform secretome analysis under more physiological-like conditions two methods were established in the past that combine metabolic labeling with click chemistry to select cell-derived proteins (Eichelbaum et al., 2012; Kuhn et al., 2012). The first method developed by Eichelbaum and colleagues is based on the integration of azidohomoalanine (AHA), a methionine analog carrying an azide-group, into newly formed proteins which is used for click chemistry-mediated enrichment (Eichelbaum et al., 2012). However, AHA labeling has been linked to cellular toxicity before (Müller et al., 2016) and therefore requires precise optimization and control of cell culture conditions. The second method called SPECS (secretome protein enrichment with click sugars) developed in the Lichtenthaler laboratory performs the metabolic labeling step using tetra-acetylated N-azidomannosamine (ManNAz), an azide-containing mannose derivate, which is metabolized and incorporated as sialic acid derivate into the glycotrees of proteins. The large majority of secreted proteins are glycosylated and thereby targetable with SPECS (Herber et al., 2018; Kuhn et al., 2012). Several secretome studies have been successfully conducted using this method with a focus on protease substrate identification (Kuhn et al., 2016; Kuhn et al., 2012; Kuhn et al., 2015). However, limitations of this method, which are discussed in more detail in the results part, are the requirement of large amounts of cells and involve highly laborious sample preparation including a high degree of fractionation rendering this method very time-consuming. To this end, one major aim of this thesis was the optimization and miniaturization of SPECS to the improved high-performance SPECS (hiSPECS) method.

1.9 The brain and its secretome

In the brain highly specialized cells are organized in brain regions which are responsible for diverse tasks. Within recent years, large-scale studies such as the Allen brain atlas and several transcriptome studies elaborated their expression patterns. In addition, mass spectrometry-based quantitative proteome analysis of the mouse brain revealed their overall lysate proteome in a region and cell type specific manner (Carlyle et al., 2017) (Sharma et al., 2015). The diverse protein expression profiles of the major brain cells neurons, oligodendrocytes, astrocytes and microglia are mirrored in their distinct functions in the CNS. Neurons transmit and process information and this action is supported by oligodendrocytes which built a fatty myelin sheath around neuronal axons. Astrocytes protect the CNS by shaping the blood-brain barrier and housekeeping nutrients. Microglia mainly maintain the brain in a homeostatic state by eliminating imbalances or the phagocytosis of cell debris, proteins, but also pathogens. As complex as their functions is the communication between the brain cells, which constantly communicate with each other through cell-cell contact, but also through protein secretion. In this thesis, one of the tasks was to establish a method to investigate protein secretion of the four major cell types in the brain to investigate this complex communication network.

In humans the secreted proteins of the brain cells are released into the cerebrospinal fluid (CSF) which is therefore also known as the *in vivo* secretome. CSF is the only non-organ invasive accessible biological sample of patients via lumbar puncture, which is in direct contact with the brain. This makes it the major target for biomarker studies, which aim to diagnose or reflect the pathological stage of brain diseases. Numerous proteomic data sets of murine and human CSF samples are available and recent advances in the MS technology allow in-depth coverage of the CSF proteome (Bader et al., 2020; Bai et al., 2020; Johnson et al., 2020; Sathe et al., 2019; Whelan et al., 2019). For example, two recent large-scale studies elucidated new biomarkers for AD pathology including elevated levels of soluble CD44 – a protein released into the secretome via shedding by ADAM17 – in the CSF of AD patients (Bai et al., 2020; Johnson et al., 2020). Given that the brain is embedded in CSF, we ask whether the CSF proteins reflect the secretome of the highly specialized brain cells and if we can trace back the cellular origin of the CSF proteins to a specific cell type using a cell type-resolved murine brain secretome resource.

2 OBJECTIVE

The overall aim of this doctoral thesis is the development of a tool to enable efficient secretome analysis of primary cells using quantitative proteomics and its application in order to broaden the fundamental knowledge about the brain secretome. CSF, the *in vivo* brain secretome, is a rich source of proteins secreted by brain cells which carry the potential to serve as biomarkers by reflecting the health state of the brain. However, their cellular origin often remains elusive which hampers follow-up studies aiming to understand underlying molecular mechanisms. By releasing ectodomains of transmembrane proteins from the cell into the secretome, proteases such as ADAM17 significantly shape the composition of the secretome. While ADAM17 fulfills well-established functions in the periphery its substrate repertoire and cellular tasks in the highly specialized brain cells remains to be determined.

Therefore, this study targets the following three major aims:

1) Development of the novel hiSPECS method in order to decipher the secretome of small amounts of primary cells in a highly reproducible and robust manner.

2) Establishing the first murine brain secretome resource in order to trace back the cellular origin of CSF proteins.

3) Elucidating the brain substrate repertoire of ADAM17 in order to identify pathways regulated by its proteolytic activity.

In summary, the successful conduction of this thesis project should not only advance our fundamental knowledge of ADAM17 activity in the brain, but also establish a new method to perform efficient secretome analysis, which can be used to build the first brain secretome resource to study systematic differences between secretion mechanisms of brain cell types.

3 MATERIAL AND METHODS

3.1 Material

Table 1 Antibodies

Antibodies	Source	Identifier
Mouse monoclonal anti-**ADAM22**	UC Davis/NIH NeuroMab Facility	Cat#75-093; RRID:AB_2223817
Rabbit polyclonal anti-**ADAM17**	Blobel laboratory	C-terminal
Rabbit polyclonal anti-**Calnexin**	Enzo Life Sciences	Cat#ADI-SPA-860, RRID:AB_10616095
Goat polyclonal anti-**CD200**	R and D systems	Cat# AF2724, RRID:AB_416669
Rat monoclonal anti-**SEZ6**	Lichtenthaler laboratory	Clone: 14E5, (Pigoni et al., 2016)
Rabbit polyclonal anti-**GFAP**	Abcam	Cat#ab7260, RRID:AB_305808
Rat monoclonal anti-**iRHOM1**	Lichtenthaler laboratory	Clone: 20A8, (Weskamp et al., 2020)
Chicken polyclonal anti-**β-galactosidase**	Abcam	Cat#ab9361, RRID:AB_307210

Table 2 Equipment

Equipment	Source
1-10 phenanthroline	Sigma-Aldrich
Automated cell counter	BioRad
C18 extraction disks (47 mm) Empore	SUPELCO
Cell strainer, nylon (40 µm)	BD Falcon
Confocal laser scanning microscope LSM 800	Carl Zeiss
Corning® Costar® Spin-X® centrifuge tube filters	Sigma-Aldrich
Falcon tubes	Sarstedt
Gel electrophoresis System Mini-Protean	Bio-Rad Laboratories
Glass coverslips	Marienfeld
ImageQuant LAS-4000	Applied Biosystems
Ion source NanoFlex with column oven	Sonation
Liquid chromatograph EASY-nLC 1200	Thermo Fisher Scientific
Liquid-repellent slide marker pen	Science Services
Mass spectrometer Q-Exactive HF	Thermo Fisher Scientific
Microplate reader	Tecan
Nanodrop	Tecan
Nitrocellulose membrane	BioRad
Precellys homogenization tubes	Bertin Instruments
Protein LoBind tubes	Eppendorf
ReproSil-Pur 120 C18-AQ, 1.9 µm	Dr. Maisch

Equipment	Source
SDS-PAGE system (including electrophoresis and transfer system)	BioRad
Sterile pipettes	Sarstedt
STAGE-tip centrifuge	Sonation
Uncoated SilicaTip Emitters (30xm)	New Objective
Vacuum centrifuge MaxiVac	ScanVac

Table 3 Mouse models

Mouse models	Source
ADAM17 flox mice	The Jackson Laboratory, Stock#009597
C57BL/6J wildtype mice	The Jackson Laboratory/ Charles River
iRhom1$^{4\text{-}11/4\text{-}11}$ mice	Li et al. (2015)

Table 4 Reagents

Reagent	Source
Acetonitrile (ULC/MS – CC/SCF)	Biosolve
Acrylamid/Bis (37.5:1)	Serva Electrophoresis GmbH
Ammonium bicarbonate	Sigma-Aldrich
Ammoniumpersulfate (APS)	Roche
Bovine serum albumin (BSA)	Sigma-Aldrich
Bromphenol blue	BioRad
B-27	Thermo Fisher Scientific
Concanavalin A (ConA) agarose beads	Sigma-Aldrich
DAPI	Life technologies
DBCO beads (34agnetic)	Jena Bioscience
Dimethyl sulfoxide	Roth
Dithiothreitol (DTT)	Sigma-Aldrich
Dithiothreitol (for SDT buffer)	GE Healthcare
DMEM high glucose, GlutaMAX supplemented	Thermo Fisher Scientific
ECL solution	GE Healthcare
Ethanol	Merck
Ethylenediaminetetraacetic acid (EDTA)	Sigma-Aldrich
Fetal bovine serum (FBS)	Life Technologies
Ficoll PM400	Sigma-Aldrich
Formic acid	Sigma-Aldrich
Iodoacetamide	Sigma-Aldrich
Lipofectamin 2000	Thermo Fisher Scientific

Reagent	Source
LysC (mass spec grade)	Promega
MEM	Thermo Fisher Scientific
Neurobasal	Thermo Fisher Scientific
Opti-MEM	Thermo Fisher Scientific
Papain	Sigma-Aldrich
Paraformaldehyde (PFA)	Merck
Penicillin-streptomycin	Life technologies
Phosphate buffered saline	Thermo Fisher Scientific
Poly-D-lysine	Sigma-Aldrich
Potassium hexacyanoferrate(III)	Sigma-Aldrich
Potassium hexacyanoferrate(II) trihydrate	Sigma-Aldrich
Protease inhibitor	Sigma-Aldrich
Restriction enzyme	New England Biolabs
Dry milk powder	Sigma-Aldrich
Sodium butyrate	Sigma-Aldrich
Sodium dodecyl sulfate	Sigma-Aldrich
Sodium Deoxycholate	Sigma-Aldrich
tetra-acetylated N-azidomannosamine (ManNAz)	Thermo Fisher Scientific
TEMED (99%)	Roth
Tris base (Trizma)	Sigma-Aldrich
Tris ultrapure	AppliChem
Trypsin (mass spec grade)	Promega
Trypsin- EDTA	Thermo Fisher Scientific
Triton X-100	Merck
Tween-20	Merck
Urea	Merck
Western HRP substrate Immobilon	Merck
X-Gal, 5-Bromo-4-chloro-3-indolyl β-D-galactoside	Sigma Aldrich
β-Secretase Inhibitor IV – C3, Calbiochem	Sigma Aldrich

Table 5 Software

Software	Source
ImageJ-win64	NIH
MaxQuant (1.5.5.1 or 1.6.1.0)	Jürgen Cox and Max-Planck-Institute of Biochemistry
Perseus (1.6.6.0)	Jürgen Cox andMax-Planck-Institute of Biochemistry.
R	The R Foundation for Statistical Computing
Spectronaut™ Pulsar X (12.0.20491.14)	Biognosys

3.2 Methods

All methods conducted in the scope of this thesis are listed below in alphabetical order to accelerate search. Moreover, point-by-point protocols are listed in the appendix: hiSPECS and vessel isolation (see 125).

3.2.1 Animal work

All mouse work was performed in accordance with the European Communities Council Directive and animal experiments were approved by the Regierung von Oberbayern under the license code #02-19-067. Primary cells analyzed to establish the secretome resource were isolated from C57BL/6J mice. *ADAM17*$^{flox/flox}$ mice were purchased from the Jackson laboratory and *iRhom1*$^{4\text{-}11/4\text{-}11}$ mice were obtained from the laboratory of Carl Blobel, the group who established and characterized the mouse line (Christova et al., 2013). Breeding and housing of the mice took place at the pathogen-free animal facility in the German Center for Neurodegenerative diseases (DZNE) Munich.

3.2.2 AP-shedding-assay

AP-assay (alkaline phosphatase-assay) was performed in order to validate ADAM17 substrate candidates according to (Tang et al., 2020). On the first day wildtype and *ADAM17*$^{-/-}$ mouse embryonic fibroblasts (MEFs) were seeded onto PDL coated 12-well plates (200.000 cells per well). Live count of the cells was acquired using an automated cell counter in combination with trypan blue according to the manufacturer's manual (BioRad). On the next morning, cells were cultured for 30 min in Opti-MEM media and afterwards transfected with Lipofectamine 2000 according to the supplier's manual (per well: 1 µg DNA in 100 µL Opti-MEM, 2 µL Lipofectamine in 100 µL Opti-MEM). 5 h post transfection, the transfection mixture was removed and cells were cultured in cultivation media for 24 h. On day three of the experiment, the full media was exchanged to 1 mL Opti-MEM and cells were incubated for 1 h. Next, cells were stimulated with PMA (25 ng/mL final concentration) or not stimulated for 45 min. Afterwards, the media of the cells was harvested, spin down at maximum speed for 10 min in a precooled centrifuge and stored on ice until further use. The cells were lysed in 500 µL triton-buffer (2.5% Triton, 1 mM EDTA in ddH_2O). To ensure sufficient lysis the plates were incubated on a plate shaker for 10 min at 4°C before harvesting the lysate. Lysates were cleared as described for the cultivation media above. Next, either 100 µL cultivation media or 20 µL lysate with 80 µL AP-buffer (100 mM NaCl, 20 mM MgCl2 in 100 mM Tris pH 9.5) were added to 96-

well. Each sample was measured in triplicates. After, 100 µL AP-substrate (0.5 mg/mL pNPP in AP-buffer) were added to each well. Plates were incubated at 37°C for 2h prior to the measurement of the colometric changed at 405 nm. GFP transfected cells were used as background control, TGFα as positive and BTC as negative control for ADAM17 cleavage activity. Background subtraction and normalization to the expression level in the lysate and finally the unstimulated condition (no PMA) were performed to evaluate ADAM17 shedding activity. Truncated substrate candidates (70-100 amino acids N-terminal of transmembrane domain) were cloned into the AP-5 backbone (Maretzky et al., 2013; Tang et al., 2020) using the following primers:

Table 6: Cloning strategy for ADAM17 substrate candidates into the AP-5 backbone.

Primer 5´→3´	Sequence	Restriction enzyme
SEMA5B_F	TAAGCAGTCGACTCTGAGTGGGGTGTCTGC	SalI
SEMA5B _R	TGCTTATCTAGAGAGCTGTTGGGGAAACAGCG	XbaI
MEGF10_F	TAAGCA CTCGAGTGCCCTGCGGGAACATAC	XhoI
MEGF10_R	TGCTTAGCTAGCGA TTCACTGCTGCTGCTGCT	NheI
EPHB6_F	TAAGCA GTCGACACCATGACCAGTGAGACC	SalI
EPHB6_R	TGCTTAGCTAGCGACACTTCCACTGAGCCTGG	XbaI
MRC2_F	TAAGCACTCGAGGTCTGGCAAGACAACACA	XhoI
MRC2_R	TGCTTATCTAGAGATTCTTGCTGT TCGTTCAT	XbaI
PTK7_F	TAAGCAGTCGACCCTACCAAGCTGGGACCC	SalI
PTK7_R	TGCTTATCTAGAGACTGCTTGCTG TCTGCAGG	XbaI
TREM2_F	TAAGCACTCGAG CAGAGTCTCCGAGGCCGA	XhoI
TREM2_R	TGCTTAGCTAGCGACGTACCTCCGGGTCCAGT	NheI
SORL1_F	TAAGCACTCGAGAGGGGCTATGAGATACACATGTTT	XhoI
SORL1_R	TGCTTATCTAG AGA GGCTATCACCATGGGGAC	XbaI

3.2.3 Bioinformatic analysis

Bioinformatic analysis of the secretome resource was limited to the 995 proteins, which were quantified in at least one of the cell types with a minimum of 5 biological replicates. Using Perseus the data were processed including log2 transformation, determination of Pearson correlation coefficients between each sample and imputation. All imputations conducted in the scope of this thesis are based on replacement of missing values by a randomly chosen value of a normal distribution which is left-shifted by 1.8 standard deviation and the width was set to 0.3.

3.2.3.1 Cell type specific secretion

In order to decipher the secretion profiles of the individual brain cell types we defined a protein to be specifically secreted if it was either 5-fold enriched in a pair-wise comparison to the other 3 cell types, or if it was quantified in one cell type with more than 4 biological replicates and in the other cell types with a maximum of 2 biological replicates.

3.2.3.2 Disease association of CSF proteins

In order to see if proteins detected in murine CSF and specifically secreted from one cell type in the secretome resource are linked to human brain disease, we scanned DisGeNet (Pinero et al., 2017) for gene-disease associations (GDA). 31 known diseases of the CNS were included in the search and the evidence index (EI) was set to 0.95.

3.2.3.3 Interaction map

To visualize the complexity of inter-cellular communication between the brain cell types, we mapped known interactions between proteins enriched in a cell types secretome or lysate. Binary interactions listed on UniProt (UniProt Consortium, 2018) or the protein-protein interaction network (PPIN) of BioGRID (Chatr-Aryamontri et al., 2015) were considered. Proteins specifically enriched in the secretome of one brain cell type were included on the secretome site and mapped to transmembrane proteins enriched in the lysate of one brain cell type according to (Sharma et al., 2015).

3.2.3.4 Meta-analysis: Correlating secretome and lysate data

A meta-analysis was performed comparing the cell type-specifically secreted proteins of our resource to a previously published data set by (Sharma et al., 2015). This data set contains proteomic characterization of the cellular lysates of the same four brain cell types. The LFQ data published by Sharma et al in Supplementary Table 1 (Sharma et al., 2015) of cultivated primary cells were used for the cross-comparison. All proteins quantified with at least two biological replicates in one cell type were considered and data of the same cell type were grouped intendent of the duration of cultivation or age of the isolated mice. Using Perseus missing values were placed according to the imputation method (left-shifted 1.8 standard deviation, width = 0.3) described before. In order to facilitate comparison of the data sets, we defined cell type specifically enriched lysate proteins to require a 2.5-fold enrichment in a pairwise comparison to the other three cell types. The comparison allowed us to estimate if cell type-specific secretion is based on high expression in the particular cell type or if potential other mechanism are in place.

3.2.3.5 Pathway analysis

Functional annotation clustering was conducted using DAVID 6.8 (Huang da et al., 2009a, b). Enrichment scores based on medium classification stringency were used for visualization. The backgrounds used are indicated in the individual figure captions. In general, KEGG pathway or gene ontology terms for cellular compartment (GOTERM_CC_FAT), molecular function (GOTERM_MF_FAT) or biological process (GOTERM_BP_FAT) were individually analyzed.

3.2.3.6 QARIP analysis

Peptide matting to protein domains was performed using the online software QARIP (Ivankov et al., 2013).

3.2.3.7 UMPA and PCA

In order to depict the relationship between the secretome of different cell types and/or their biological replicates included in the mouse secretome resource uniform manifold approximation and projection (UMAP) (Diaz-Papkovich et al., 2019) as well as principal component (PCA) analysis were conducted.

3.2.4 Cell culture

All cells used in the scope of this thesis were cultured using standard conditions at 37°C, 5% CO_2 and DMEM media with 10% FBS and 1% Pen/Strep, if not highlighted otherwise. In general, experiments containing primary isolated cells were harvested from at least two different preparations procedures. Of note, the sex of the primary cells was either mixed or was not demined due to the lack of tools for easily determination due to the youth of the mice.

Primary murine neurons were isolated and cultured as described by (Kuhn et al., 2012) using E16.5 embryos. In brief, the skull was opened, the brain extracted, the meninges removed, the hippocampus and cerebral cortex cleared and either used jointly or collected separately in HBSS according to the experiment. The tissue was digested with pre-activated Papain (Sigma Aldrich, 30 min), dissociated by repetitive pipetting and seeded on dishes coated with poly-D-lysine for at least 2 h. To ensure proper attachment of the cells the media was exchanged carefully 4h after seeding to Neurobasal media supplemented with 2% B27, 0.5 mM glutamine and 1% Pen/Step.

Primary murine astrocytes were isolated according to the neuronal isolation described above. However, cells were seeded onto uncoated dishes, grown until reaching confluence, trypsinized and split 1:3 into new dishes. After the third splitting procedure the cells were used for the final experiment.

Primary microglia and oligodendrocytes were isolated using magnetic-activated cell sorting (MACS). Microglia were isolated from P5 pups using CD11b MicroBeads as published by Daria et al. (Daria et al., 2017). After the isolation cells were cultured in DMEM/F12 media supplemented with 10% FBS and 1% Pen/Strep for 4 days prior to the 48 h ManNAz labeling. In contrast, for the oligodendrocyte cultures, 6 days old pups and anti-AN2 MicroBeads were used. Cells were cultured in OPC MACS cultivation medium for one day prior to the 48 h ManNAz labeling step for the hiSPECS protocol.

Four organotypic brain slice per biological replicate were prepared according to Daria et al. (Daria et al., 2017) and cultured in horse serum (25%), HBSS (25%), HEPES-buffered MEM (50%) and 1 mM L-glutamine. The ManNAz labeling was performed after 2 weeks in culture while changing media on the first as well as every third day.

3.2.5 CSF isolation

CSF was isolated from 3-month old *iRhom1*$^{4\text{-}11/4\text{-}11}$ and control littermates (n=6) according to (Liu et al., 2008) with small optimizations. Animals were anesthetized with isoflurane and afterwards injected with medetomidine, midazolam, fentanyl 0.05/5/0.5 mg/kg i.p. for deep anesthesia. Anesthetized mice were placed into a stereotaxic frame in order to adjust the head in an angle of around 130° to the spinal cord. A 1 cm long cut was vertically placed at the back of the head. The cisterna magna was laid bare by separating the muscles and tissue above and fixing it with two hooks to each side. The head position was adjusted to gain ideal pressure and sight of the cisterna magna. Next, a sharp capillary which was attached to sterile tubing (PEG-free) was placed into the arm of the stereotactic aperture. At an angle of 45°C the dura was punctuated with the capillary without touching other tissue. The CSF was slowly socked into the capillary by applying negative pressure through a syringe attached to the other end of the tubing. Of note, blood contamination must be avoided through the CSF collection procedure. Finally the CSF was transferred into low binding tubes, centrifuged (3000 x g, 4°C, 20 min) and frozen on dry ice in 5 µL aliquots. Samples were stored at -80°C until used for in-solution digest and analysis by mass spectrometry.

3.2.6 ELISA of soluble CD200

The murine CD200 ELISA kit was used according to the manual provided by the supplier to detect the ectodomain of CD200 in the cultivation media of primary neurons. 1.5 Million neurons were cultured for 48 h in 1 mL neuronal cultivation media (N=6). 25% of the supernatant was used per technical replicate. Uncultured neuronal media was used as negative control and the standard curve of the kit was applied.

3.2.7 Mass spectrometry

All mass spectrometry analysis performed in the scope of this thesis were conducted using an LC-MS/MS set up containing an EASY-nLC 1200 UHPLC system, a NanoFlex ion source with a column oven and a Q-Exactive™ HF Hybrid Quadrupol-Orbitrap™ mass spectrometer. Injected samples were separated on hand-made C-18 columns (ID: 75 µm, length: 30 cm) which were equipped with C18-AQ resin (ReproSil-Pur 120). For the secretome and CSF samples a gradient of MS-H_2O and 80% acetonitrile (ACN-80) was run as following for a total of 120 min (flow rate: 250 nL/min, column temperature 50 °C): 3% ACN-80 at 0 min, 6% ACN-80 at 2 min, 30% ACN-80 at 92 min, 44% ACN-80 at 112min and 75% ACN-80 at 121 min.

3.2.7.1 Data dependent acquisition (DDA)

DDA runs were performed within a scan range of 300-1400 *m/z*, a resolution of 120,000 at MS1 level, 50 ms max. injection-time and automatic gain control of 3 Million ions. A top 15 precursor's method was applied with 1.6 *m/z* isolation windows, a resolution of 15,000, 100 ms max injection-time and automatic gain control of 100,000 ions. The dynamic exclusion time for redundant precursors was set to 120 s.

3.2.7.2 Data independent acquisition (DIA)

DIA runs were acquired within a scan range of 300-1400 *m/z* by alteration of a single MS1 scan and twenty MS2 scans using the window width summarized in table x. Each window overlapped with adjacent windows by one *m/z*. Window widths were custom designed for hiSPECS secretome samples to compensate for high peptide density with smaller window sizes aiming for detection of 8 measurement points per peak (based on representative neuronal secretome DDA run shown in Figure 8). MS1 scans were performed as following: resolution 120,000, 120 ms max. injection-time and automatic gain control of 0.5 Million ions. The twenty MS2 scans were performed as following: resolution 30,000, auto max. injection-time and automatic gain control of 3 Million ions.

Table 7 MS2 customized window widths used for DIA. Unit is *m/z*.

Window	**1**	**2**	**3**	**4**	**5**	**6**	**7**	**8**	**9**	**10**
Width	85	40	30	28	26	25	24	24	24	24
Mid-point	341.5	403	437	465	491	515.5	539	562	585	608
Start	299	383	422	451	478	503	527	550	573	596
End	384	423	452	479	504	528	551	574	597	620

Window	**11**	**12**	**13**	**14**	**15**	**16**	**17**	**18**	**19**	**20**
Width	25	27	28	29	34	38	46	61	151	352
Mid-point	631.5	656.5	683	710.5	741	776	817	869.5	974.5	1225
Start	619	643	669	696	724	757	794	839	899	1049
End	644	670	697	725	758	795	840	900	1050	1401

3.2.7.3 Analysis of proteomic raw data

Using MaxQuant (version 1.5.5.1 or 1.6.1.0), DDA data were analyzed. Matching was performed against the reference database for *mus musculus* provided by UniProt on the 17th of January 2018 (16,954 entries, canonical) and the iRT reference peptides, which were used for retention time calibration, provided by Biognosys. MaxQuant default settings were applied for the analysis with the small variation that the minimal peptide length was defined as 6 amino acids. Methionine oxidation and acetylation of the N-terminus were defined as variable modification, while carbamidomethylation was assigned as fixed modification. The FDR cut-off was set to 1% on protein and peptide level. Customized-libraries for the DIA analysis were built based on the MaxQuant results using Spectronaut Pulsar X (Biognosys). In the scope of this thesis, four different customized-libraries were generated: 1) neuronal secretome, 2) brain cell secretome, 3) murine CSF samples and 4) brain slice secretome. Details are summarized in Table 8. DIA raw data were analyzed using the Spectronaut Pulsar X software with standard settings provided by Biognosys (1% FDR, MS2 quantification, quantification based on top 1 to 3 precursors). In addition for neuronal samples the custom-library #1 was used, for the samples of the brain secretome resource and astrocyte samples custom-library #2, for CSF samples custom-library #3 and for brain slices custom-library #4 was used.

Table 8: Customized-Libraries for DIA analysis. The following table summarizes the four custom-made libraries used in this thesis including information about the sample type used to generate the library, the number of entries and the number of figures they are used in.

Library	Used for	Entries	Figure
#1	Secretome of neurons	UP modified: 4,585 UP precursors: 5,957 Protein groups: 646	Figure 9 Figure 30 Figure 20
#2	Secretome resource, Secretome of astrocytes	UP modified: 12,695 UP precursors: 15,886 Protein groups: 1,540	Figure 12 Figure 31
#3	Murine CSF	UP modified: 20,100 UP precursors: 24,985 Protein groups: 2,550	Figure 25
#4	Brain slices	UP modified: 2,675 UP precursors: 3,375 Protein groups: 431	Figure 26

3.2.8 Pharmacological treatments

3.2.8.1 BACE1 inhibition using C3

The well-established BACE inhibitor C3 dissolved in DMSO (β-secretase inhibitor IV) was added to primary neurons at a final concentration of 2 µM for 48h in accordance with (Kuhn et al., 2012). Of note, C3 is inhibiting BACE1 and BACE2 but neurons express only BACE1 at a detectable level (Voytyuk et al., 2018).

3.2.8.2 LPS treatment

The cortico-hippocampal brain slices were cultured for 2 weeks post isolation to ensure recovery of the cells from the isolation procedure and labeled for 48 h with ManNAz in full media (horse serum (25%), HBSS (25%), HEPES-buffered MEM (50%) and 1 mM L-glutamine). In a subsequent step, the media was exchanged to horse serum-free conditions supplemented with 500 ng/mL LPS and ManNAz. After a 6 h LPS treatment step, media was exchanged once more and replaced by horse serum-free media containing ManNAz. The cultivated media was harvested 24 h after and processed using the hiSPECS protocol.

3.2.8.3 PMA treatment

PMA was used at a final concentration of 25 ng/mL and applied to the cells for 2h or 6h in the hiSPECS secretome analysis and for 45 min in the AP-shedding assay.

3.2.9 Sample preparation for mass spectrometry analysis

3.2.9.1 hiSPECS secretome analysis

The first major aim of this thesis was the development of the hiSPECS method. In order to facilitate broad applicability of the newly established method a detailed point-by-point protocol is attached in the appendix. For the secretome resource the supernatant equivalent to 1 Million cells per cell type was used for the analysis (N=6). The iRHOM and ADAM17 related secretome analysis was performed using 1.5 Million cells per biological replicate. Samples were obtained from at least two different isolations.

3.2.9.2 In-solution digest of CSF samples

CSF samples were prepared for analysis on the mass spectrometer by in-solution digestion as described by (Pigoni et al., 2016). However, in the end peptides were not only dissolved in 0.1% FA but also 2µL of iRT peptides were added (diluted 1:10). Of each biological replicate/mouse 5 µL were used for the proteomic analysis.

3.2.9.3 SP3 protocol

Isolated brain vessels lysed in SDT buffer were prepared for mass spectrometry analysis using the SP3 protocol according to (Hughes et al., 2019).

3.2.10 Sholl analysis

Seed primary hippocampal neurons were onto PDL coated glass cover slips placed into 12-well plates (100,000 neurons per well). Cover slips were incubated with nitric acid on, washed 3x with dH_20 and dried for 2 h in the oven at 100°C followed by 8 h at 200°C. On DIV1 perform Calcium Phosphate (CaP) transfection, as following: Cultivation media of neurons was removed and immediately replaced by adding 600 µl of pre-warmed Opti-MEM into each well. Transfection mixture was prepared by adding 4 µg plasmid of interest and 7.5 µL 2 M $CaCl_2$. Using H_2O the mixture was filled up to 60 µL. 60 µl of 2× HBS was added to the transfection mixture in a drop-wise manner. Next, the transfection mixture was incubated for 30 min at RT in the dark. After resuspension by pipetting, 60 µL transfection mixture was added to each well. The cells were placed back into the incubator for 20 min. Afterwards, the transfection mixture was replaced with 1 mL HBSS.

The cells were placed back into the incubator for 5 min and the HBSS was removed and replaced by fresh HBSS. The HBSS washing step was repeated three more times. Finally 1 mL neuronal cultivation media was added per well. On DIV6, cells were fixed using 4% PFA for 1 0min at RT and washed twice with 1 mL 1xPBS. Nuclei were stained by adding DAPI (1:10,000) for 2 min. After performing two additional PBS-washing-steps the cover slips were mounted. Images were acquired at the confocal microscope (25x objective) of neurons from three independent preparations. Basic Sholl analysis was performed using ImageJ according to the standard procedure of (Hsia et al., 2014; Langhammer et al., 2010).

3.2.11 Staining

3.2.11.1 Immunofluorescence staining

Brains were isolated from adult *iRhom1*$^{4\text{-}11/4\text{-}11}$ or wildtype mice which were perfused with 1x PBS and 4% PFA. Dehydration was performed using a sucrose gradient and afterwards snap frozen. Next, brains were cut at a cryostat into 40 µm coronal sections and mounted onto glass slides. Sections were stored at -80°C until further use. In order to perform the immunofluorescence (IF) staining, slides were thawed in 1x PBS at RT for 20 min. Next, tissue was permeabilized by incubating the sections in 0.1% Trition in 1xPBS for 5 min. The sections were washed 3x with 1x PBS and blocked with 1% BSA in PBS for 1 h at RT. Next, the primary antibodies (1:500) in blocking buffer was added for 1 h at RT. After three washing steps with 1xPBS for 10 min each, the secondary antibodies (1:1000) were added. Next the sections were washed twice with 1xPBS, stained for 2 min with DAPI (1:10,000), washed again twice with 1xPBS and mounted for final image acquisition at the confocal microscope.

3.2.11.2 X-Gal staining

Mice were sacrificed and perfused with 5-10 mL 1xPBS. Next, brains were isolated, placed in precooled 1xPBS on ice until further use, fixed with 2 % PFA for 15 min on ice, washed with 5 mL 1xPBS, placed in brain slicer and cut into 2 mm sagittal brain slices using racer plates. For staining each brain slices was transferred into a well of a 12-well plate, permeabylized by washing three times with 2 mL wash buffer for 20 min at RT and stained over night at 37°C with X-Gal staining solution. Wash buffer (200 mL total): 0.4 mL 1 M MgCl2, 2.0 mL 2% NP-40, 197.6 mL PBS pH7.3. X-Gal Stock: 250 mg X-Gal (5-Bromo-4-chloro-3-indolyl β-D-galactoside) in 10 mL DMSO. X-Gal staining solution (50

mL total): 2.0 mL 25 mg/mL X-gal stock, 0.106 g potassium ferrocyanide, 0.082 g potassium ferricyanide in 48 mL wash buffer.

3.2.12 Vessel isolation

Whole brain vessels were isolated from adult *iRhom1*$^{4\text{-}11/4\text{-}11}$ mice according to the protocol by (Zellner et al., 2018) (N=6). In brief, mice were sacrificed at 3-months of age, perfused with 1x PBS and brains were snap frozen on dry ice. Brains were stored at -80°C until use. At the day of vessel isolation, frozen brains were cut into small pieces and homogenized in MEM. Next, ficoll (final concentration 15%) was added to the homogenates and a centrifugation step (6000xg; 20 min; 4°C) allowed isolation of the vessel-enriched pellet. The vessels were placed on a 40µm- nylon mesh and washed with cold 1xPBS to reduce cellular contamination. Vessels were collected and lysed in vessel-lysis-buffer (100 mM Tris, 100 mM DTT, 4% SDS) using a dounce tissue grinder for homogenization. Next, samples were sonicated, protein concentration was determined using 660 nm-assay and used for SP3 sample preparation.

3.2.13 Viral infection

Lentiviral transfection was on the one hand conducted to knockdown the newly identified BACE1 substrates ADAM22 and CD200 using shRNAs in order to validate the specificity of the commercially purchased antibodies. On the other hand, to induce Cre recombinase based gene knockout in primary cells isolated from ADAM17 flox mice. Of note, all experiments performed with lentiviral particles were conducted under biosafety level 2.

Lentiviral particles were generated in HEK293-t cells by co-transfection of the envelope, packaging and transfer vector. First, two times 16 Million cells were seeded on two PDL coated 15 cm dishes. 16 h after seeding, cells were transfected with 60 µg transfer vector, 30 µg psPAX2 and 20 µg pcDNA3.1-VSVG using Lipofectamine 2000 standard protocol (80 µL Lipofectamine in 2 mL Opti-MEM). However, the final incubation step of Lipofectamine and DNA was prolonged from 20 to 60 min. During this incubation step, the cellular cultivation medium was exchanged to 20 mL Opi-MEM supplemented with 10% FBS. The transfection mixture was added gently in a dropwise manner to cover the two plates equally. The media of the cells was exchanged carefully 20 h post transfection to DMEM (high glucose) supplemented with 2%FBS, 1% Pen/Strep, 1% GlutaMax and 10 mM sodium butyrate. 19 mL media was added to each 15 cm dish. 48 h after the transfection, the supernatant containing the lentiviral particles of both dishes was

combined and was filtered using a 0.45 µm nylon filter. For long-term storage the filtered supernatant was concentrated using ultracentrifugation (SW28 swing rotor) at 22,000 rpm for 2 h at 4°C. The viral pellet was suspended in 2 mL TBS-5 buffer (130 mM NaCl, 10 mM KCl, 5 mM MgCl2, 10% BSA, 50 mM Tris-HCl pH 7.5) after incubation over night at 4°C and viral aliquots were stored at -80°C.

Primary neurons were infected on the first day *in vitro* (DIV) with lentiviral particles using codon-optimized Cre recombinase or a GFP control virus (1:200) as described by (Kuhn et al., 2016). The same virus was used for primary astrocytes which were cultured 5 days before performing the final experiments.

The shRNA knockdown of CD200 and ADAM22 was performed using the shRNAs cloned into the pLKO2 plasmid (Kuhn et al., 2010) using the primers summarized in Table 9. Neurons were infection on DIV1 (1:100) and lysed on DIV7.

Table 9. Primers used for cloning the shRNA constructs targeting Cd200 or Adam22 into the pLKO2 plasmid.

Target	Forward Reverse
Cd200.1	CGCGTCCGGCCCATAGTACACCTTCACTACTCGAGTAGTGAAGGTGTACTATGGGCTTTTTGGAAA
	CCGGTTTCCAAAAACCCATAGTACACCTTCACTACTCGAGTAGTGAAGGTGTACTATGGGCCCGGA
AD22.1	CGCGTCCGGCATGGCAGATGTGATCTATAACTCGAGTTATAGATCACATCTGCCATGTTTTTGGAAA
	CCGGTTTCCAAAAACATGGCAGATGTGATCTATAACTCGAGTTATAGATCACATCTGCCATGCCGGA
AD22.2	CGCGTCCGGTCAGGTTATGTAGAGAGACAGCTCGAGCTGTCTCTCTACATAACCTGATTTTTGGAAA
	CCGGTTTCCAAAAATCAGGTTATGTAGAGAGACAGCTCGAGCTGTCTCTCTACATAACCTGACCGGA
AD22.3	CGCGTCCGGAACCAGAGATAGACAATGCAACTCGAGTTGCATTGTCTATCTCTGGTTTTTTTGGAAA
	CCGGTTTCCAAAAAAACCAGAGATAGACAATGCAACTCGAGTTGCATTGTCTATCTCTGGTTCCGGA

3.2.14 Western blotting

Western blot analysis was performed using standard procedures. In brief, cultured cells are washed twice with 1x PBS and lysed in STET buffer (50 mM Tris, 2 mM EDTA, 150 mM NaCl, 1% Triton X-100 at pH 7.5). 250 µL STET buffer supplemented with protease inhibitor (1:500) for one well of a 6-well plate was used and scaled accordingly if needed for larger or smaller sample sizes. Noteworthy, if ADAM17 blots were conducted 10 nM 1,10-phenanthroline was added to the lysis buffer to block self-digestion (Brummer et al., 2018). To ensure sufficient lysis of the cells, samples were incubated for 20 min on ice. Lysates were transferred to 1.5 mL tubes and cleared from cellular derby by centrifugation

at maximum speed for 10 min at 4°C. Next, the whole protein concentration was measured using a BCA kit according to the instructions supplied by the manufacturer Interchim. Next, in most cases samples were heated at 95°C for 10 min in 4x Laemmli buffer, which contained β-mercaptoethanol for denaturation of the proteins. Of note, if iRHOM1 blots were conducted the samples were not boiled to prevent aggregation of the protein and ensure efficient separation on the gel. Instead samples were incubated for 15 min in Leammli buffer at RT. After, samples were separated on self-made SDS-polyacrylamide gels (8 up to 12%). In general, nitrocellulose membranes were used for the transfer in a wet-tank-blotting system of BioRad. Blocking was performed in blocking buffer (5% dried milk powder dissolved in 1xPBS with 1% Tween) for 20 min at RT. Incubation with the primary antibody was conducted over night at 4°C, followed by a 1 h incubation step with the secondary HRP-coupled antibody at RT and visualization of the signal using ECL solution. After the blocking and the antibody incubation steps the membrane was washed with 1xPBS with 1% Tween. Starting with the blocking step the membrane was gently agitated at all time until final development.

3.3 Data availability

Proteomic data published in (Tüshaus et al., 2020) are publically available via PRIDE using the following project accession codes: PXD018171, PXD020503.

4 RESULTS

4.1 Development and benchmarking of the hiSPECS method

The secretome is an essential part of inter-cellular communication which allows the orchestration of cellular networks. It contains soluble secreted, unconventionally secreted as well as ectodomains of proteolytically-shed transmembrane proteins. Until today, quantitative proteomic analysis of the cellular secretome remains challenging, not only because of the requirement of large cell numbers, which are unlikely to be gained if working with primary cells, but also due to high abundant serum supplements which may disturb the detection of the lower abundant secretome proteins by mass spectrometry. The first major aim of this PhD thesis was optimizing and miniaturizing the secretome protein enrichment with click sugars (SPECS) method in order to decipher the secretome of minute amounts of primary cells in a highly reproducible and robust manner while aiming for deep proteome coverage. To that end, the high-performance SPECS (hiSPECS) method (Figure 7) was established by introducing four key changes into the previously published SPECS protocol (Kuhn et al., 2016; Kuhn et al., 2012; Serdaroglu et al., 2017):

1) Concanavalin A (ConA) glycoprotein enrichment
2) Covalent immobilization of metabolically labeled glycoproteins on magnetic beads
3) Stringent washing and on-bead digestion
4) Data-independent acquisition (DIA) for label-free protein quantification

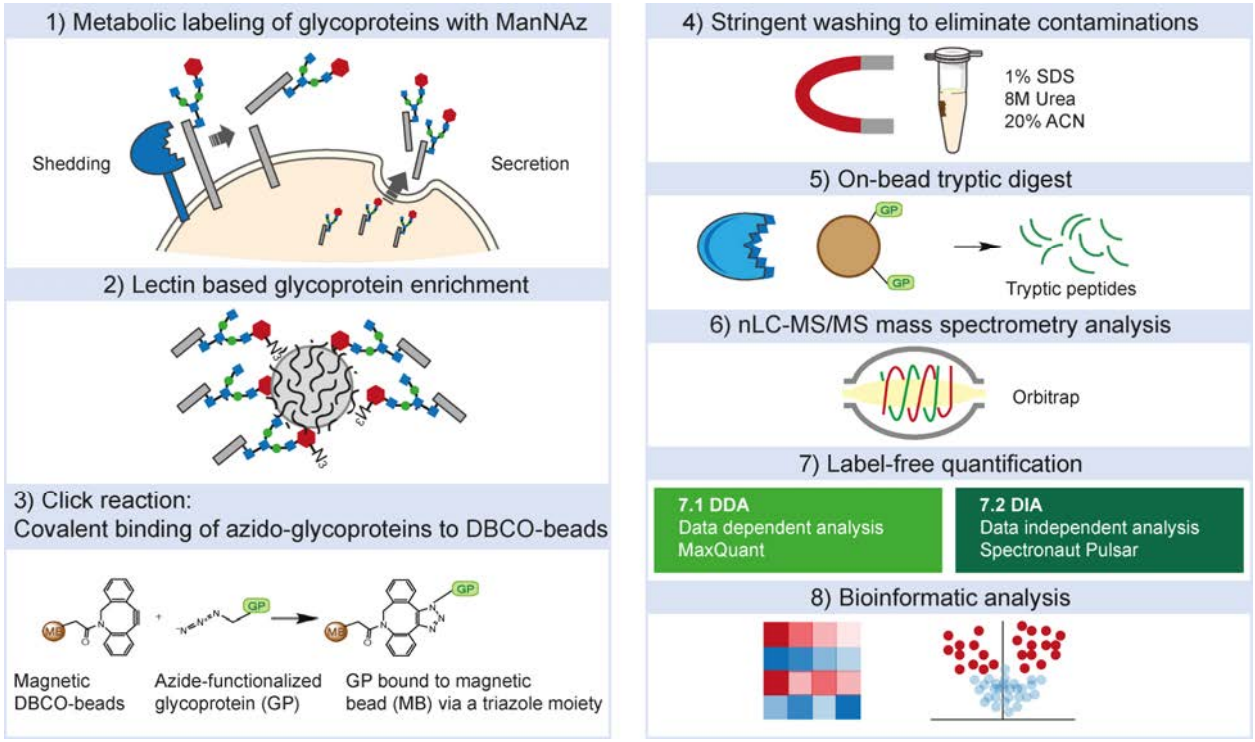

Figure 7: hiSPECS workflow. Cells are cultured in the presence of ManNAz enabling metabolic labeling of newly formed glycoproteins (GP) and their functionalization with an azide-group used for click-mediated binding to DBCO-beads after a ConA precipitation step. After stringent washing GP are released by tryptic digest and analyzed by mass spectrometry using DDA and DIA followed by bioinformatics evaluation of the results. ManNAz: N-azido-mannosamine; GP: glycoproteins DBCO: Dibenzocyclooctyne; ConA: Concanavalin A; DDA: data dependent acquisition; DIA: data independent acquisition. Figure retrieved from (Tüshaus et al., 2020).

In detail, cells are metabolically labeled with tetra-acetylated N-azido-mannosamine (ManNAz) for 48 h. The membrane permeable sugar derivate is metabolized by cells to N-azido-sialic acid and incorporated into the glycotrees of newly formed proteins (Kuhn et al., 2012). In the first optimization step, glycoproteins of the secretome were precipitated with Concanavalin A (ConA), a lectin which preferably binds N-glycans (Guan et al., 2015). This step strongly reduced albumin contamination, a high abundant media supplement (Figure 8a). Next, copper-free click chemistry was used to covalently immobilize the metabolically labeled azido-glycoproteins. In hiSPECS, the azido-glycoproteins were covalently bound on magnetic dibenzocyclooctyne (DBCO)-beads. This enabled further reduction of contaminating proteins by stringent washing with 1% sodium dodecyl sulfate (SDS), 8 M urea and 20% acetonitrile. Subsequently, the proteins were denatured, alkylated and finally released from the beads by digestion with Lys-C and trypsin. In contrast, the previous SPECS protocol relied on biotinylation of the azido-glycoproteins by click reaction, followed by streptavidin precipitation, fractionation by SDS-polyacrylamide gel electrophoresis (PAGE) and in-gel digestion. The fraction in close approximation to albumin (around 65 kDa) needed to be discarded to prevent strong

interference by this contaminant which means secretome proteins of this particular size range were lost (Figure 8a). Of note, using the hiSPECS method those proteins could be retained and no fractionation on peptide or protein level was required.

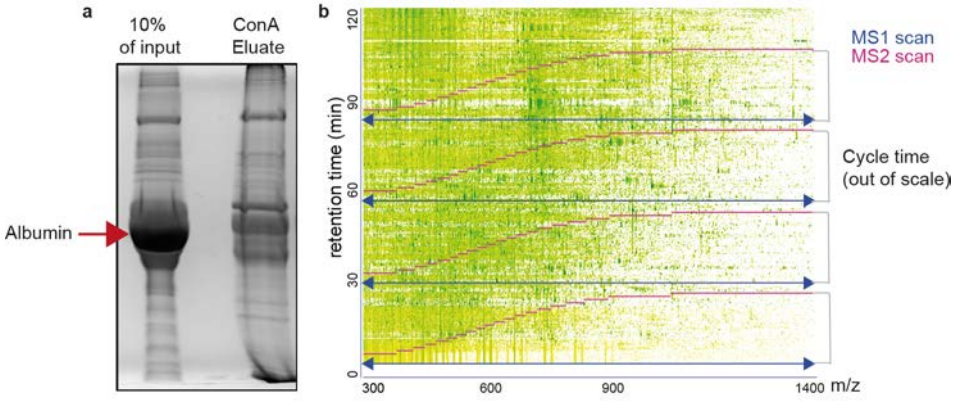

Figure 8: Glycoprotein precipitation and DIA windows. a) Albumin reduction due to lectin based glycoprotein enrichment with ConA shown on a gel stained with Coomassie. The left lane shows conditioned media of primary neurons (10% of the input) and the right lane shows the eluted proteins after ConA precipitation. **b)** Twenty MS2 window widths (pink) were chosen according to a peptide density plot representing the secretome of neurons measured with hiSPECS DDA aiming for a balanced number of peptides per window. Adjacent windows overlap by 1 *m/z* and cover in total the range between 300 and 1400 *m/z*. Figures retrieved from (Tüshaus et al., 2020).

After a final desalting step, peptides were subject to label-free quantification (LFQ) by mass spectrometry. Liquid chromatography-tandem mass spectrometry (LC/MS-MS) analysis with 120 min gradients were used to analyze the secretome samples on a Q-Exactive™ HF hybrid quadrupole-orbitrap™ mass spectrometer. The SPECS protocol used data-dependent acquisition (DDA) analysis. For the hiSPECS protocol DDA and data-independent acquisition (DIA) analyses was established for secretome analysis and benchmarking against each other. The MaxQuant software was used to perform the combined analysis of the DDA samples applying a false discover rate (FDR) of 1%. Based on the DDA search results from MaxQuant, a spectral library was generated for the DIA analysis using Spectronaut Pulsar and the peptide density map was consulted to set the width of the 20 variable *m/z* windows for optimal peptide recovery for DIA. Smaller width windows were chosen for *m/z* areas with higher peptide densities whereas larger ones were defined for lower peptide densities (Figure 8b). Taken together, the optimization of the hiSPECS method was built on a combination of improved glycoprotein enrichment and advanced proteomic analysis (for a detailed comparison of the hiSPECS and SPECS workflow see (Figure 9)).

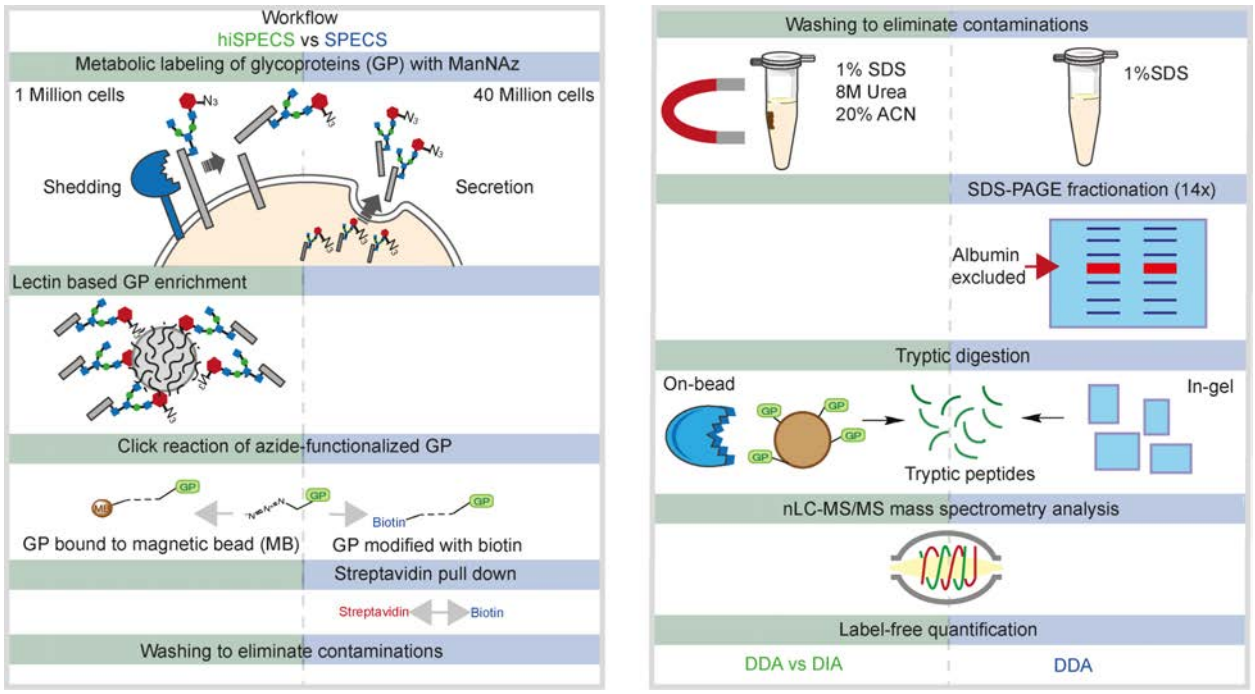

Figure 9: Comparison of the hiSPECS and SPECS workflow. Illustration of the differences of the optimized hiSPECS and the SPECS workflow by Kuhn et al.(Kuhn et al., 2012). Both protocols start with a 48 h metabolic labeling step of glycoproteins with ManNAz. hiSPECS is based on 1 Million cells, lectin enrichment to reduce contaminations, covalent binding to DBCO-beads and on-bead digestion. Finally DDA and DIA mode is used for LFQ. The previous SPECS protocol required 40 Million cells and utilized biotinylation of the glycoproteins, streptavidin enrichment, SDS-PAGE fractionation, in-gel digestion and DDA analysis. LFQ: label free quantification; SDS PAGE: sodium dodecyl sulfate polyacrylamide gel electrophoresis. Figures retrieved from (Tüshaus et al., 2020).

In order to benchmark the newly established hiSPECS against the SPECS protocol, we analyzed the secretome of primary neurons as previously published (Kuhn et al., 2012)). However, instead of the originally used 40 million neurons per biological replicate only one million neurons were used for hiSPECS. In accordance, the volume of cultivated media was reduced from 40 mL (4x 10 cm dishes) to 1 mL (6-well). The efficient reduction of contaminants in the hiSPECS method allowed us to skip the protein fractionation step by SDS-PAGE of SPECS. Running single-shot experiments reduced the sample preparation and measurement time on the mass spectrometer substantially by 5-fold (Figure 10a). Despite this miniaturization, the protein LFQ was more reproducible between biological replicates with hiSPECS. On average, hiSPECS showed an improved Pearson correlation coefficient of 0.97 compared to 0.84 using SPECS (Figure 10b).

Previously, SPECS required a direct ratio comparison of samples that were run on the same SDS-PAGE, because protein LFQ intensities varied strongly for biological replicates separated on different gels due to differences in separation, gel fractionation and in-gel digestion (Figure 10b). In contrast, hiSPECS strongly improved the

reproducibility between biological replicates facilitating direct protein LFQ comparisons between all samples (Figure 10b). In summary, hiSPECS increases reproducibility while miniaturizing the required amount of cells and time.

a

	SPECS	hiSPECS	fold reduction
Cell number per sample	$40x10^6$	$1x10^6$	40
Volume cell media per sample	40 mL	1 mL	40
Sample preparation time for 12 samples	15 d	3 d	5
Measurement time for 12 samples	7.5 d	1.5 d	5

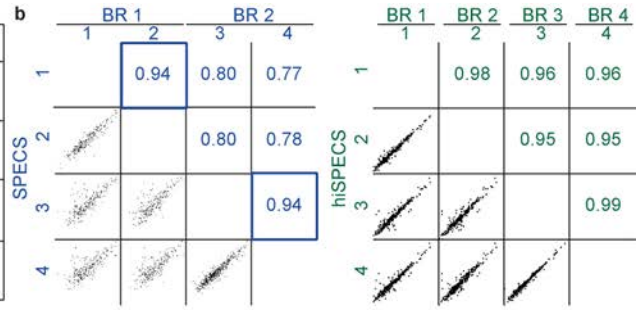

Figure 10 Miniaturization and reproducibility of hiSPECS. a) Comparison between SPECS (blue) and hiSPECS (green) with regard to the requirement of cells, conditioned media, and time. **b)** Pearson correlation coefficients and multiple scatter plots of log2 transformed LFQ intensity values of neuronal secretomes analyzed with SPECS or hiSPECS. Blue squares indicate samples fractionated together on one SDS PAGE. SPECS data shown in blue were extracted from (Kuhn et al., 2012). Figures retrieved from (Tüshaus et al., 2020).

The secretome contains soluble secreted proteins and the ectodomains of proteolytically-processed transmembrane proteins. Therefore, we closely inspected the proteins quantified in the neuronal secretome datasets. Overall, more proteins were quantified in the dataset using hiSPECS DDA (light green) and DIA (dark green) compared to the dataset obtained with SPECS (blue) (Figure 11a). Proteins were included if quantified in 4 of 5 or in 9 of 11 biological replicates in the SPECS and hiSPECS dataset, respectively. In addition, more potential target proteins (secreted, membrane, transmembrane + glycosylphosphatidylinositol-anchored (TM+GPI)) were quantified with hiSPECS according to UniProt (Figure 11a). The potential contaminating proteins, which are not expected to be found in the secretome, such as cytoplasmic, nuclear or mitochondrial proteins were also increased with hiSPECS (Figure 11a). However, many transmembrane proteins, such as APP, have several annotations on UniProt due to different processing by proteases and subsequent shuttling of protein fragments to other compartments of the cell. Conclusively, these results clearly demonstrate that hiSPECS DIA/DDA mainly quantifies secretome-specific proteins, whereas the increase of contaminating proteins might be a result of increased sensitivity.

Due to the ManNAz labeling step, (hi)SPECS targets exclusively glycoproteins which represent the majority of secreted proteins (Kuhn et al., 2016). According to four large-scale proteomic studies that mapped glycosylation sites (Fang et al., 2016; Joshi et al., 2018; Liu et al., 2017; Zielinska et al., 2010), we have extended the UniProt glycoprotein

list to achieve a more complete data comparison (Figure 11b,c). Accordingly, hiSPECS increased the quantification of glycoproteins by 186% (DDA) or 236% (DIA) compared to SPECS (Figure 11d). Noteworthy, DIA outperformed DDA by quantifying more glycoproteins (18%), TM+GPI proteins (11%) (Figure 11d) and increasing the dynamic range of protein quantification by one order of magnitude (Figure 11e). Eventually, we have chosen hiSPECS DIA as the method of choice thought my thesis due to its clear superiority.

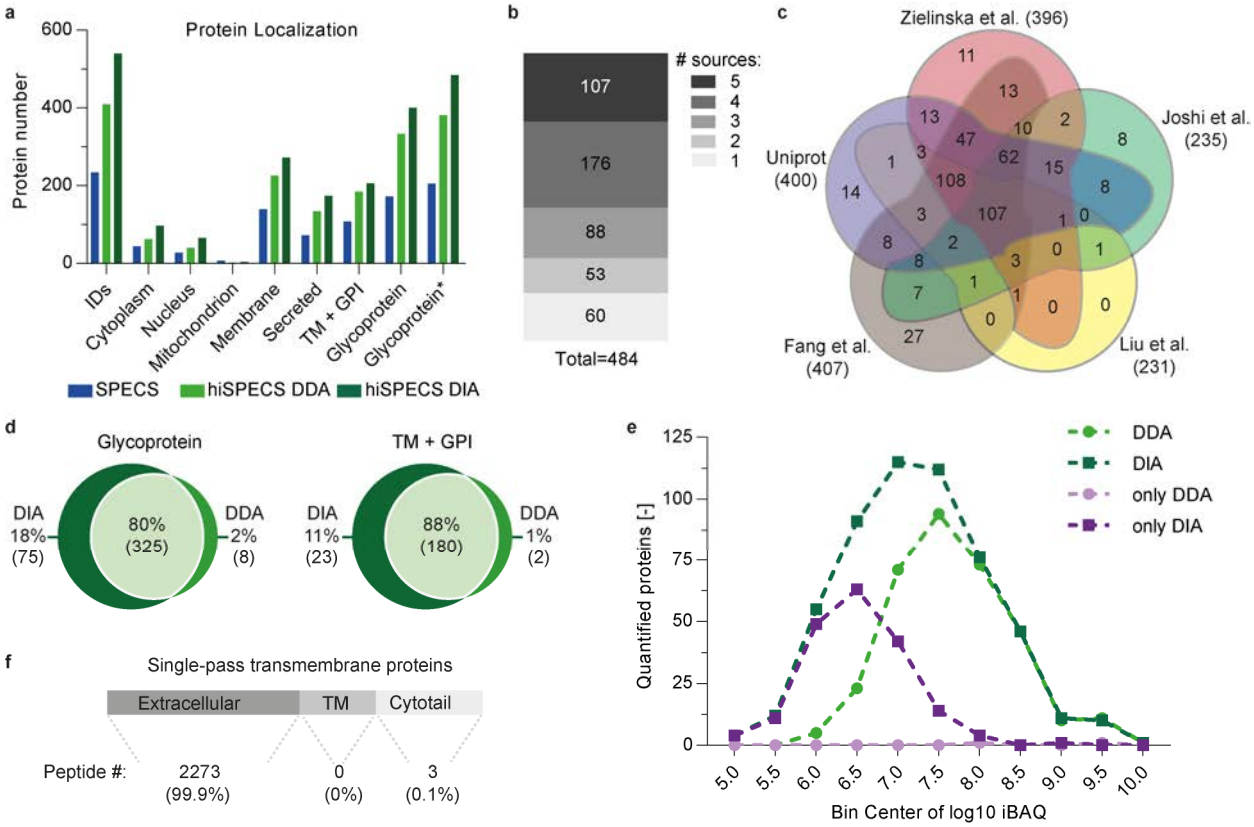

Figure 11 Benchmarking hiSPECS against SPECS. a) Comparison between SPECS (blue), hiSPECS DDA (light green) and DIA (dark green) used for secretome analysis of primary neurons. The bar chart shows the number of quantified proteins number and their localizations according to UniProt considering proteins quantified in at least 4 of 5 (SPECS dataset) or 9 of 11 biological replicates (hiSPECS dataset). SPECS data shown in blue were extracted from (Kuhn et al., 2012). Glycoprotein* combines proteins determined to contain a glycosylation site according to UniProt or previous glycoproteomic studies (Fang et al., 2016; Joshi et al., 2018; Liu et al., 2017; Zielinska et al., 2010) **b-c)** Distribution of the glycoprotein* fraction of hiSPECS DIA indicating in which source a protein was found to contain a glycosylation. **d)** Comparison of the quantified proteins of the category glycoprotein and TM+GPI between hiSPECS DIA and DDA in a Venn diagram. **e)** The protein number identified within a bin size of 0.5 of log10 LFQ values indicated for total hiSPECS DDA (light green), total hiSPECS DIA (dark green), only in hiSPECS DDA (light purple) and only in hiSPECS DIA (light purple) (min. 3/6 biological replicates). **f)** Tryptic peptides of TM proteins grouped according to protein domains. Figures retrieved from (Tüshaus et al., 2020). TM: single-pass transmembrane protein; GPI: Glycosylphosphatidylinositol-anchored membrane protein

In order to test if we detect full-length transmembrane proteins or only the secretome-specific ectodomains released by shedding, we mapped all identified peptides of single-

pass transmembrane proteins to their amino acid sequence and domains. Of 2276 peptides derived from transmembrane proteins only 3 mapped to the cytotail and none to the transmembrane region. This quality control underlines the utility of hiSPECS for secretome analysis. In summary, hiSPECS outperforms SPECS in terms of time requirement and necessary cell number, but also gains deeper secretome coverage while increasing protein quantification reproducibility.

4.2 Establishing the murine brain secretome resource

Secretome proteins, namely soluble secreted and shed ectodomains, function as soluble signaling cues and thereby play an essential role in inter-cellular signal transduction in the brain. However, their cellular origin remains often elusive. Hence, the second major aim of my PhD thesis was the generation of a murine brain secretome resource. To this end, we used the newly established hiSPECS DIA method to analyze the secretome of neurons and glia cells (microglia, oligodendrocytes and astrocytes) - the four dominant cell types of the brain. Next, we illustrated the utility of the brain secretome resource by tracing back the cellular origin of cerebrospinal fluid (CSF) proteins and pinpoint the cellular response to inflammatory stimulation by LPS in cortico-hippocampal brain slices (Figure 12a).

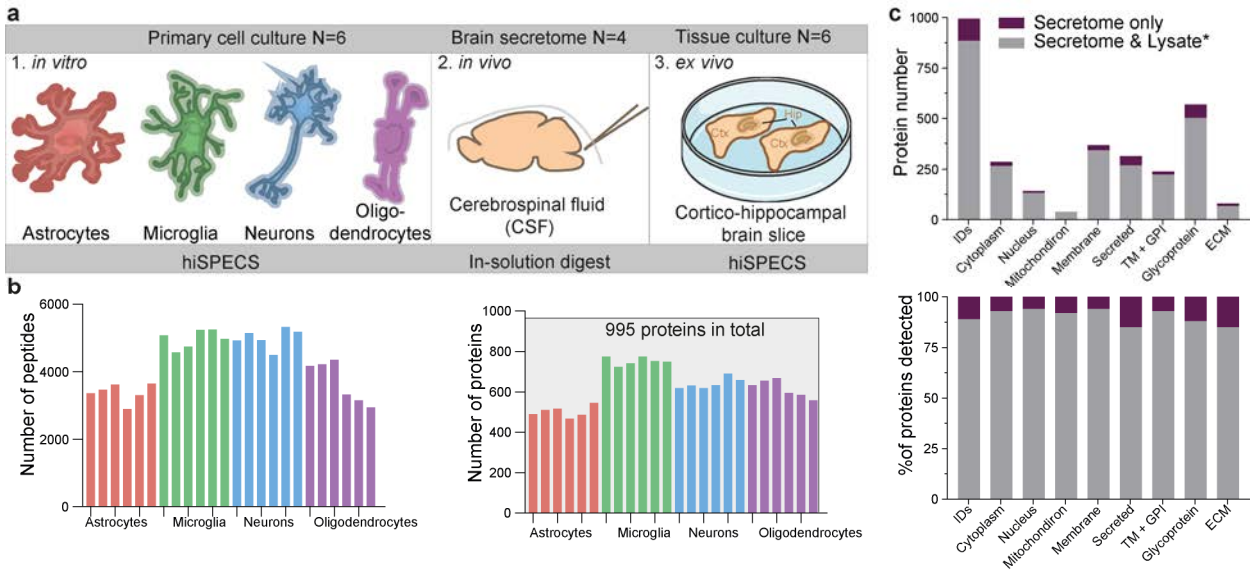

Figure 12 Experimental set up of the mouse brain secretome resource. a) Overview of the cell type-resolved mouse brain secretome resource and its applications to study secretome *in vitro, in vivo* and *ex vivo*. **b)** Peptides and protein groups of the individual brain cell types included in the brain secretome resource considering proteins quantified with at least 5/6 biological replicates in one cell type. **c)** Coverage of the secretome resource proteins in a previous

proteomic study which established the lysate proteome of brain cells is depicted in grey (Sharma et al., 2015). Figures retrieved from (Tüshaus et al., 2020).

To establish the brain secretome resource, one million astrocytes, microglia, neurons and oligodendrocytes were used for hiSPECS DIA analysis (N=6) and yielded 995 robustly quantified protein groups (min. 5/6 biological replicates in one cell type). On average astrocytes revealed the least (503 with 3367 unique peptides) whereas microglia showed the most (753 with 4955 unique peptides) protein groups (Figure 12b). The majority (89%) of the secretome proteins (884/995) were also found in a proteomic dataset by Sharma et al (Sharma et al., 2015) which investigated the lysates of the same cultured brain cell types. Noteworthy, 111 proteins were only detected in our secretome study of which 42% were annotated as secreted according to UniProt, e.g. SEMA3F, MMP2 and TIMP1. Proteins annotated as secreted or related to the extra cellular matrix (ECM) contained with 15% most proteins which were only detected in the secretome (Figure 12c).

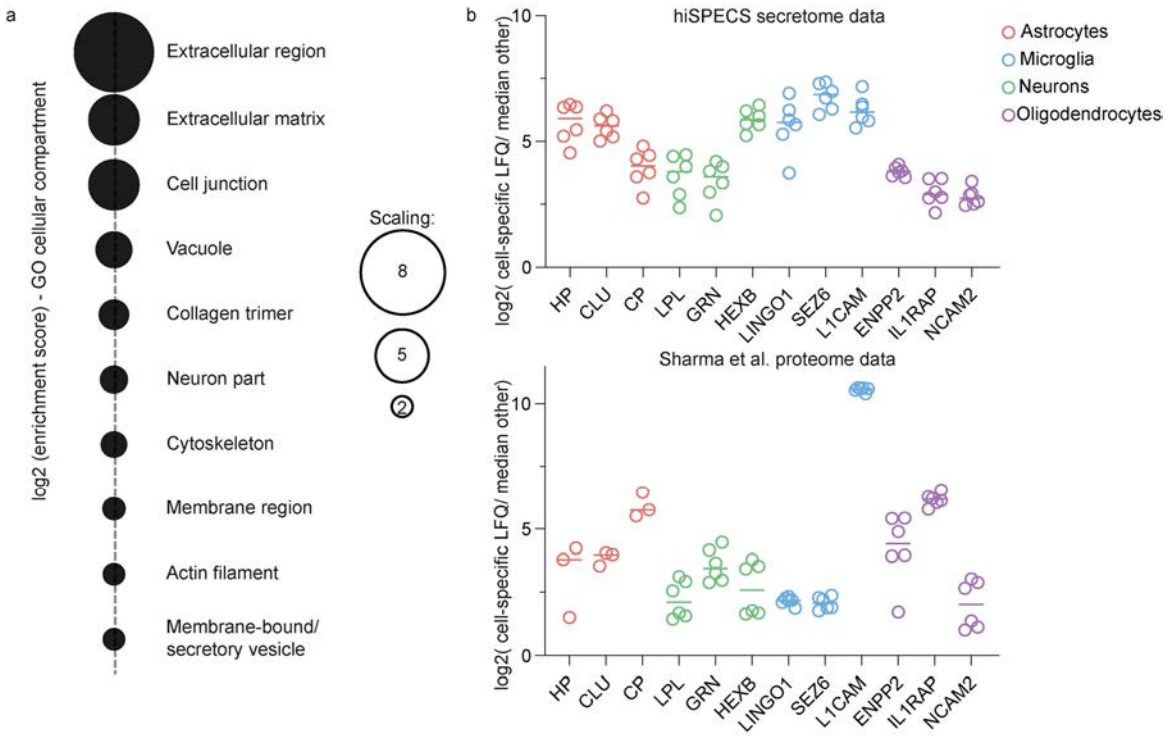

Figure 13 Quality control of the mouse brain secretome resource. a) GO analysis by functional annotation clustering of the proteins quantified in the secretome resource compared to the whole mouse proteome (background) for the term cellular component (FAT) using DAVID 6.8 (Huang da et al., 2009a, b). Log2 enrichment scores are represented in the dot size. **b)** Enrichment of characteristic proteins in the individual brain cell types. Of each biological replicate the log2 ratio of the cell type specific LFQ to the median of the other three cell types is depicted for secretome and lysate data (Sharma et al., 2015). Figures retrieved from (Tüshaus et al., 2020). GO: gene ontology

In order to verify the quality of the secretome resource, a pathway analysis based on gene ontology (GO) cellular compartment was performed and extracellular region/ matrix were the most enriched terms (Figure 13a). Moreover, the primary cultures were validated

by determining the enrichment of known cell type-specific proteins in the secretome of astrocytes (HP, CLU, CP), microglia (LPL, GRN, HEXB), neurons (LINGO1, SEZ6, L1CAM) and oligodendrocytes (ENPP2, IL1RAP, NCAM2) compared to the other cell types. All of those cell marker proteins were also found to be enriched in a cell type-specific manner in lysates of the same cell type (Sharma et al., 2015) (Figure 13b). In addition, the Pearson correlation coefficients (based on LFQ values) indicate high reproducibility between all 6 biological replicates of each brain cell type. On the other side, the Pearson correlation coefficients between the different brain cell types vary dramatically between 0.29 and 0.68 indicating strong differences in the secretome composition, whereby glia cell secretomes (astrocytes, microglia and oligodendrocytes) revealed higher correlations between each other compared to neuronal secretome due to their closer relationship (Figure 14a). In summary, these findings underline the quality of our brain secretome resource.

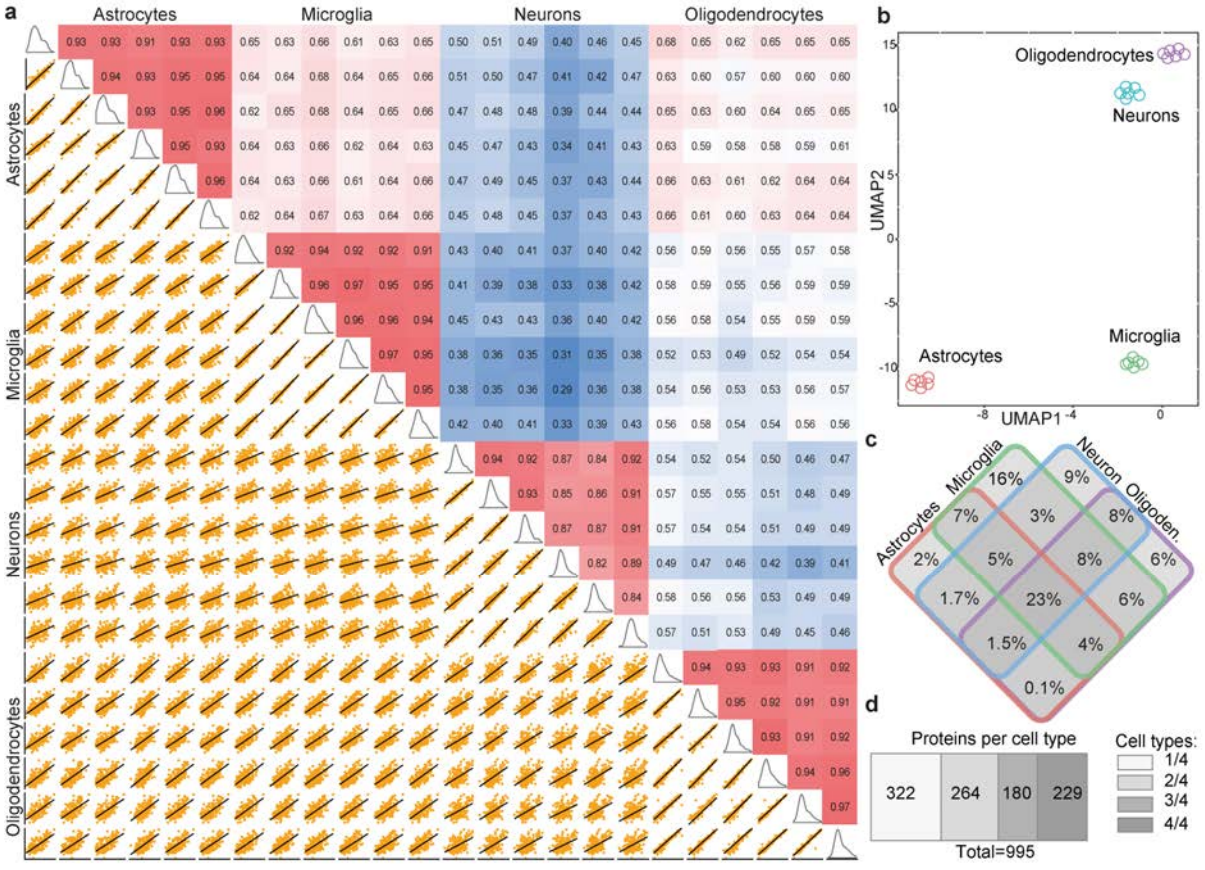

Figure 14 Protein segregation in the mouse brain secretome resource. a) Pearson correlation coefficients and the corresponding log2 LFQ scatter plots of all biological samples included in the secretome resource. Red indicates higher correlation and blue lower correlation. **b)** UMAP blot revealing distinct secretome separation of the individual brain cell

types. **c-d)** Distribution of the proteins quantified in the secretome of the individual brain cell types. UMAP: Uniform Manifold Approximation and Projection. Figures retrieved from (Tüshaus et al., 2020).

In the next step, we aimed to pinpoint the most prominent differences in the secretome of the four brain cell types. Their high degree of variation is not only reflected in the low Pearson correlation coefficients between the different cell types (Figure 14a), but also the uniform manifold approximation and projection (UMAP) plot illustrates their clear separation (Figure 14b). Only 23% of the proteins were robustly detected in all 4 cell types, whereas 32% of the proteins were only robustly detected in one cell type (5/6 biological replicates) (Figure 14e,d). Considering all proteins with at least 5-fold enrichment in a pairwise comparison to the other 3 cell types and proteins detected exclusively in one cell type (with min. 5/6 biological replicates and in the other cell types with max. 3/6 biological replicates), we obtained a list of 420 cell type-specific secretome proteins (CTSP) in our resource (42%). These dramatic protein level changes in the secretome were also illustrated in a pairwise comparison, which revealed differences of more than 350-fold, such as CHL1 in neuronal vs microglia secretome (Figure 15), demonstrating a specific secretome fingerprint of individual brain cell types.

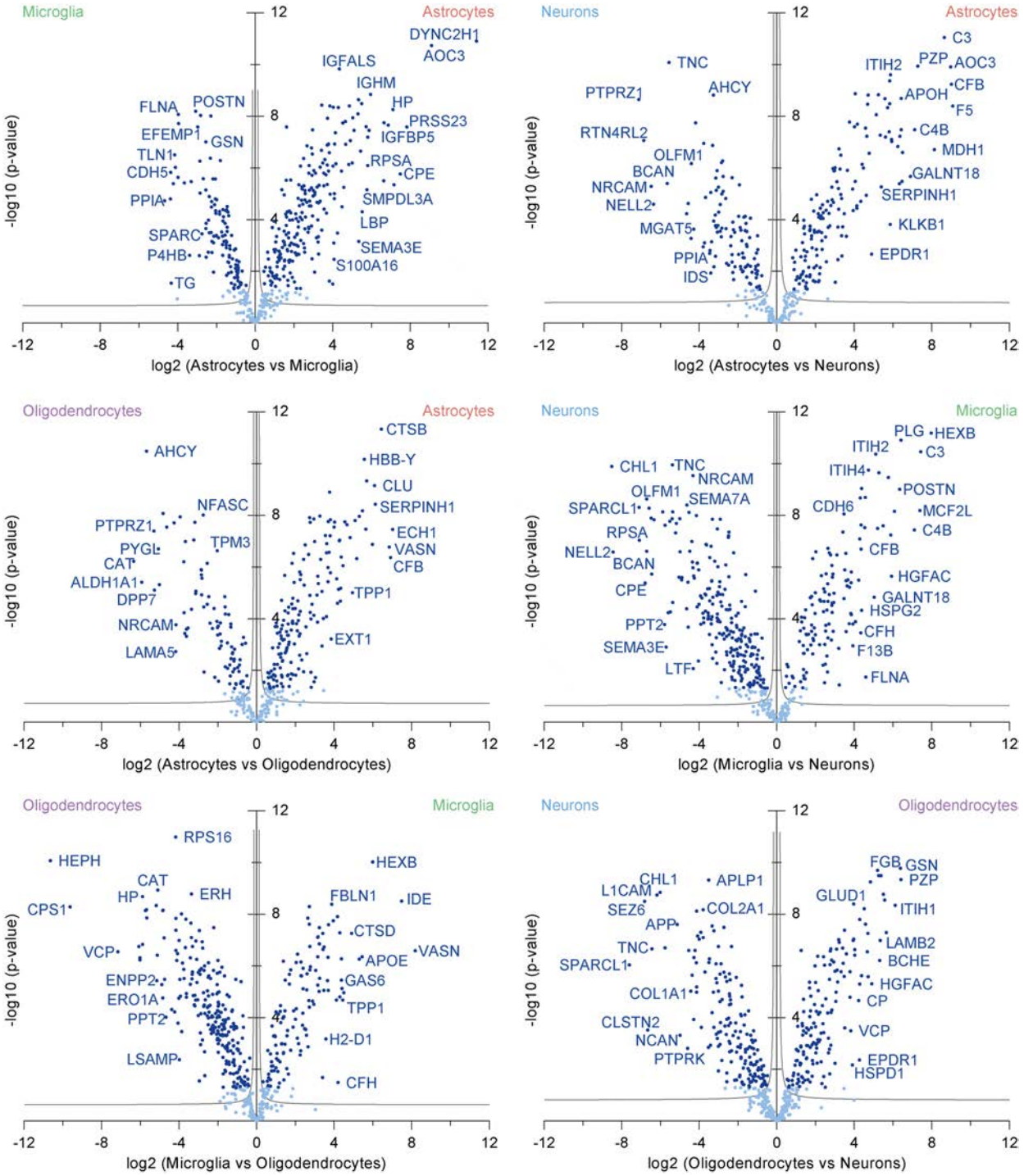

Figure 15 Volcano plots for pairwise secretome comparison of the four brain cell types. Six volcano plots depicting the differences in the secretome of primary astrocytes, microglia, neurons and oligodendrocytes in a pairwise format using hiSPECS DIA. The fold change (log2) is plotted against the p-value (negative log10) with dark blue dots indicating significant regulation meaning a p-value below 0.05. Hyperbolic selection curves colored in grey illustrate a permutation-based false discovery rate (FDR) estimation of 5% (N=6). Figure retrieved from (Tüshaus et al., 2020).

Heat map visualization of all 995 secretome proteins (z-scored LFQ intensities) revealed protein clusters enriched in the individual brain cell types (Figure 16a). GO term enrichment analysis for the category biological process for these protein clusters indicate

general terms typical for cell surface proteins such as cell adhesion. On top, terms characteristic for the key functions of each brain cell type were identified. For example, in the microglia cluster the terms phagocytosis and autophagy (e.g. TREM2 and GFB1), in the astrocyte cluster the immune response and gliogenesis (e.g. LBP and CD14), in the neuronal clusters synaptic signaling and axon guidance (e.g. SEZ6 and CHL1) and in the oligodendrocyte cluster myelination and lipid metabolic process (e.g. TNFRSR21 and OMG) were identified. Performing the same GO analysis but only focusing on the cell type-specific proteins revealed concomitant terms (Figure 16b). Together, the GO analysis highlight that not only the lysate proteome but also the proteins found the secretome of brain cells are linked to their biological key functions.

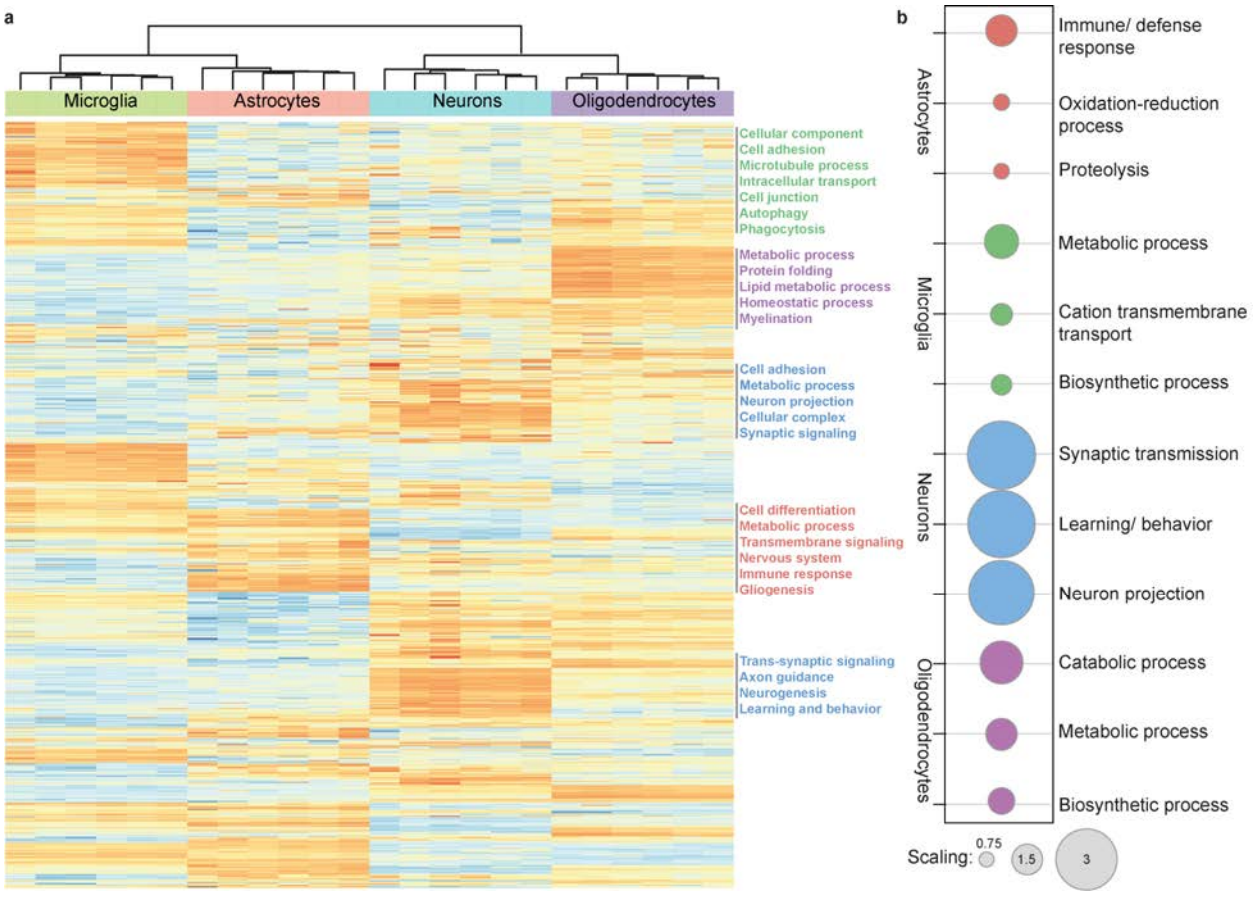

Figure 16 Heat map of the brain secretome resource. a) Heat map of proteins quantified in the brain secretome resource indicating z-scored LFQ values with red indicating high and blue low abundance levels. Top terms revealed by GO analysis by functional annotation clustering of protein clusters of the individual brain cell types compared to all proteins quantified in the secretome resource (background) for the term biological process (FAT) using DAVID 6.8 (Huang da et al., 2009a, b) are listed. **b)** Top three terms identified by GO analysis as described in a) of the cell type-specifically secreted proteins of the individual brain cell types. Enrichment scores are mirrored in the dot size. Figures retrieved from (Tüshaus et al., 2020).

Next, a systematic analysis of the secretome composition was conducted. Therefore proteins were grouped either into shed proteins, if annotated as single-pass

transmembrane or GPI-anchored proteins (TM+GPI), of which peptides were almost exclusively mapped to their ectodomains (99.9%; Figure 11f); or soluble secreted (annotated as secreted but not TM+GPI). Both groups, soluble secreted (244/568) and shed proteins (242/568), made up 43% of the glycoproteins in the secretome resource. Interestingly, the distribution strongly varies between the different brain cell types. While glia cells (astrocytes, microglia and oligodendrocytes) released more soluble secreted proteins, the neuronal secretome contained more shed proteins (Figure 17a). This trend became even more pronounced when focusing on the cell type-specifically secreted proteins (CTSP) only (Figure 17b). 71% of the neuron-specific proteins were shed proteins of which many play a role in neuron projection and synaptic signaling, such as SEZ6, CHL1 and NRXN1. This may point towards a modulatory role of ectodomain shedding in synapse function and neuronal maturation. In contrast, in glia cell secretomes shed proteins made up a smaller fraction, e.g. in astrocytes 21% (9/43) of the CTSP. In the glia secretome, especially in the microglia and astrocyte secretome the majority of proteins were soluble secreted with 62% (38/61) and 70% (30/43), respectively. Several of these proteins play a role in inflammatory response, such as TGFB1, MMP9 and GRN in microglia and TIMP1 as well as complement proteins, e.g. C1QA and C1QB, in astrocytes (according to DAVID (Huang da et al., 2009b)). Overall, these results point towards a central role of soluble secreted proteins in glia cells and ectodomain shedding in neurons.

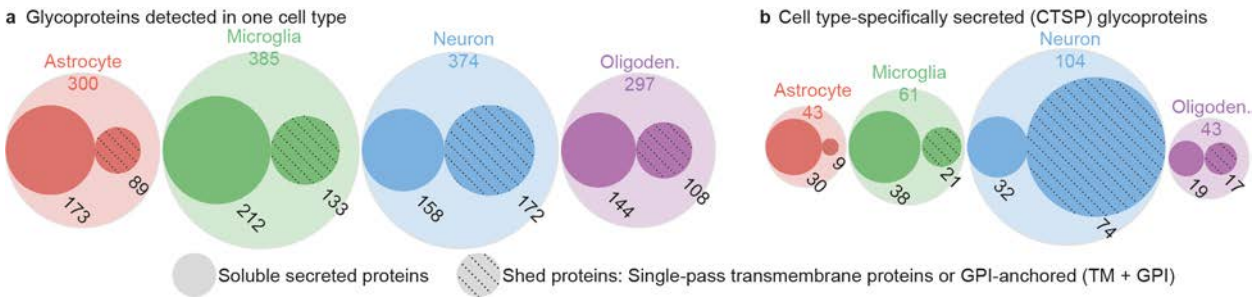

Figure 17 Shedding vs soluble secretion in brain cell types. a) Glycoproteins detected in the individual brain cell types (min. 5 of 6 biological replicates) indicating the amount of proteins annotated as TM+GPI or secreted but not TM+GPI according to UniProt. The diameter of the circles follow the protein count. **b)** Corresponding analysis to a) but of the CTSP only. CTSP: cell type-specifically secreted proteins; TM: single-pass transmembrane protein; GPI: Glycosylphosphatidylinositol-anchored membrane protein. Figures retrieved from (Tüshaus et al., 2020).

Secreted proteins released into the extracellular space function as soluble signaling cues that may bind to their interaction partners/receptors on the surface of distant cells and trigger a cellular response. In order to gain the first cell type-resolved interaction map of the brain, we fused the information of cell type-specific secretion of the cues (secretome

resource), cell type-specific protein levels of transmembrane proteins of the receptors (Sharma et al., 2015) and known protein-protein interaction partners (UniProt and BioGRID) (Chatr-Aryamontri et al., 2015; UniProt Consortium, 2018) (Figure 18a). On the one hand, we mapped known interactions between cells of one cell type, such as between soluble CHL1, which was specifically secreted form neurons, and CNTN6 specifically expressed in neurons. On the other hand, we detected known cell type specific interactions between two cell types, such as soluble CD200 (neurons) and its receptor CD200R1 (microglia) (Yi et al., 2016). Additionally, we elucidated potential cell type-specific interactions based on known binding partners. One example is the interaction between the soluble secreted ADIPOQ and CDH13. ADIPOQ was assumed to be secreted exclusively by adipocytes reaching the brain though the blood-brain-barrier (BBB) where it plays a role in neurodegeneration, neurogenesis and metabolism (Lee et al., 2019). Here, ADIPOQ was identified to be specifically secreted from oligodendrocytes (Figure 18c) and therefore may bind to neurons where its receptor CDH13 is highly expressed (Sharma et al., 2015). Hence, this cell type-resolved interaction map, elucidated a new communication path between neurons and oligodendrocytes and may help to understand the incomplete understood brain functions of ADIPOQ and other soluble signaling cues. In summary, the cell type resolved mouse brain secretome resource unravels an unique secretome fingerprint for astrocytes, microglia, neurons and oligodendrocytes and is a rich resource to systematically study protein interaction and shedding in a cell type-resolved manner.

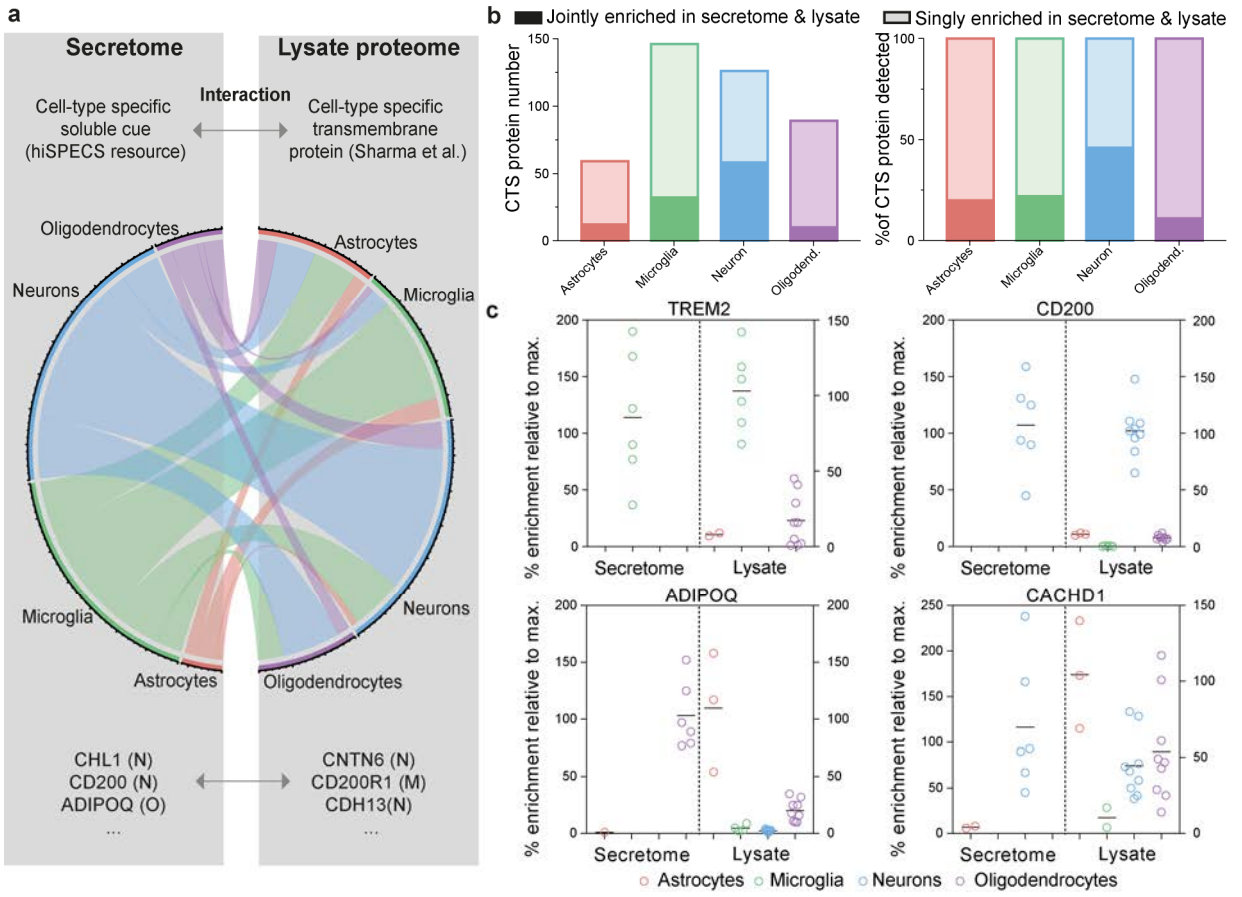

Figure 18 Secretome interaction map. a) The inter-cellular communication network showing on the left CTSP from the secretome resource connected to their transmembrane interaction partners, which may act as cell surface receptors, enriched in the lysate of one brain cell type according to (Sharma et al., 2015). Protein interaction data are extracted from BioGRID and UniProt (Chatr-Aryamontri et al., 2015; UniProt Consortium, 2018). **b)** Bar graph indicating the CTSP of the secretome resource according to the individual cell types. Joint enrichment in the same cell type in lysate (Sharma et al., 2015) and secretome is indicated with solid color. **c)** Examples of proteins secreted in a cell type-specific manner and their corresponding levels in lysates of astrocytes, microglia, neurons and oligodendrocytes (lysate data extracted from (Sharma et al., 2015)). Illustrated is the enrichment in % normalized to the individual cell type with the maximal average LFQ value. Figures retrieved from (Tüshaus et al., 2020).

4.3 Mechanisms controlling cell type-specific secretome composition

The unique fingerprint detected in the secretome of the individual brain cell types includes several CTSP (42% of the secretome resource) and we aimed to unravel underlying mechanisms controlling cell type-specific secretion. Microglia revealed the most CTSP (146), followed by neurons (126), oligodendrocytes (89) and lastly astrocytes (59) in our brain secretome resource (Figure 18b). An obvious mechanism that may control cell-type specific secretion is the higher degree of protein level present in the particular cell type. Actually, the vast majority (around 85%) of proteins was shown to reveal similar protein levels between the individual brain cell types (Sharma et al., 2015). Hence, we used that previous dataset by Sharma et al. (Sharma et al., 2015) to define proteins specifically enriched in the lysate of one brain cell type (2.5-fold in pairwise comparison) and

compared it to our CTSP secretion list. Unexpectedly, only 27% of the proteins revealed an enrichment in both, the lysate and secretome of the same cell type (112/420), ranking from only 11% in oligodendrocytes up to 46% in neurons. Two examples for joined enrichment in secretome and lysate were TREM2 in microglia and CD200 in neurons. In contrast, ADIPOQ and CACHD1 are specifically secreted from one cell type but reveal high protein abundance levels in another or several other cell types (Figure 18c, for more examples see Figure 19). Together, protein abundance levels is one mechanism that can explain cell type-specific secretion, however additional other mechanism must be in place to control secretion.

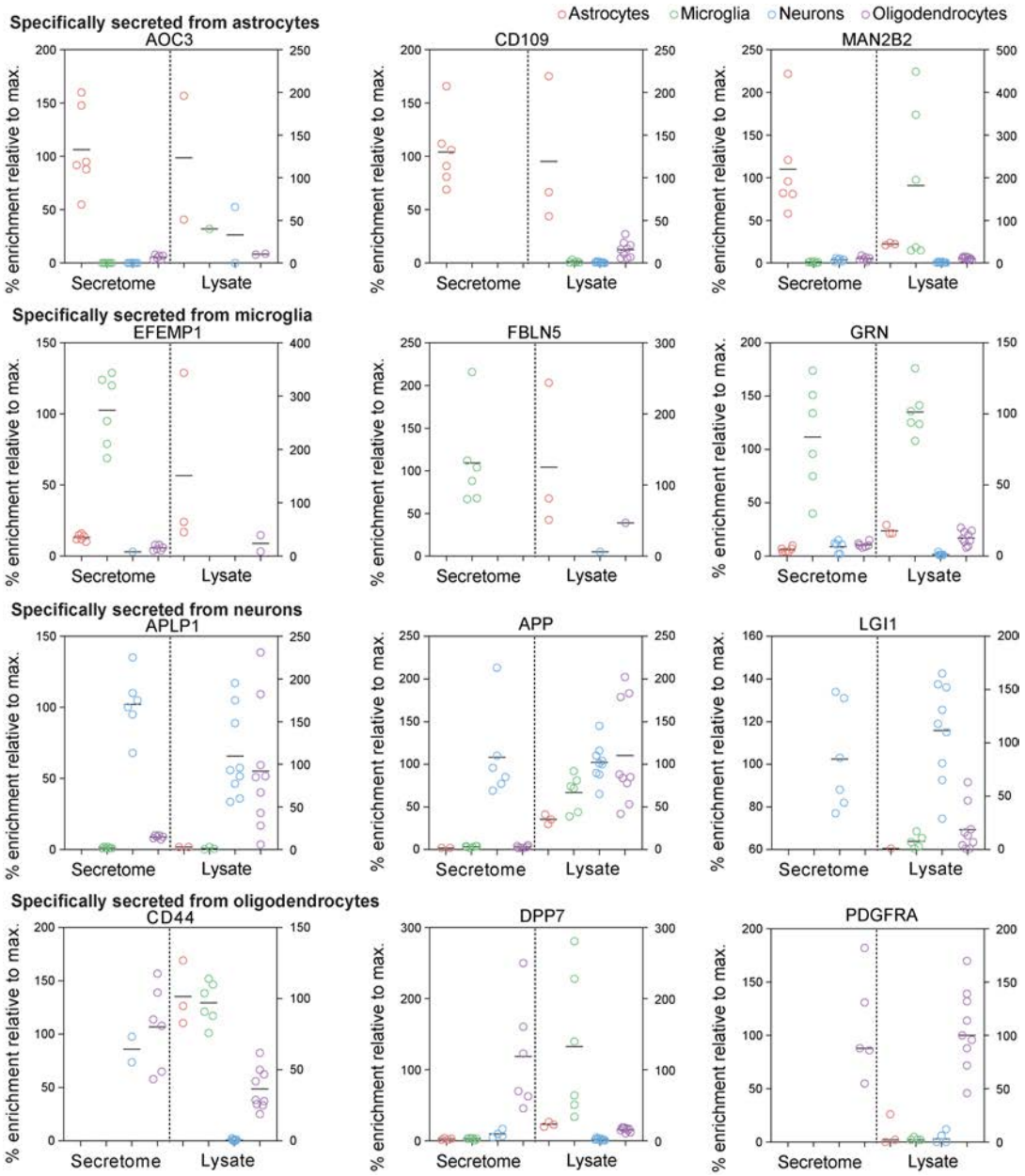

Figure 19 Secretome vs. lysate protein abundances. See Figure 12 c) Examples of proteins secreted in a cell type-specific manner and their corresponding levels in lysates of astrocytes, microglia, neurons and oligodendrocytes (lysate data extracted from (Sharma et al., 2015)). Illustrated is the enrichment in % normalized to the individual cell type with the maximal average LFQ value. Figure retrieved from (Tüshaus et al., 2020).

As shown before, ectodomain shedding strongly contributes to the composition of the cellular secretome, especially the neuronal secretome. Therefore, specific expression of the responsible protease might be one of the mechanisms controlling cell type-specific secretion. The Alzheimer´s disease protease BACE1 (β-site APP cleaving enzyme) (Hu et al., 2006; Vassar et al., 1999) is known to be highly enriched in neurons and no other brain cell type (Voytyuk et al., 2018). Several previous proteomic studies established the BACE1 substrate repertoire in the brain (Dislich et al., 2015; Kuhn et al., 2012) also using

the previously published SPECS protocol (Kuhn et al., 2012). Interestingly, a number of these transmembrane proteins cleaved by BACE1, such as SEZ6L, CACHD1 and APLP1, reveal high expression in more than one cell type but we found them to be specifically secreted by neurons (examples in Figure 18, Figure 19). Noteworthy, APP, which is mainly cleaved by BACE1 and ADAM10 but also to a minor extend by other proteases in the central nervous system, showed a clear enrichment in the secretome of neurons whereas it is equally abundant in oligodendrocytes. In summary, the comparison of shed transmembrane proteins in the secretome and their cellular abundances clearly show that other secretory mechanisms such as protease activities play a major role in protein secretion.

4.4 Investigating the substrate repertoire of BACE1 in primary neurons

In addition to the investigation of the cell type resolved brain secretome, the hiSPECS method is also suitable to decipher the substrate repertoire membrane bound proteases. In order to find additional BACE1 substrates, which may explain their specific secretion from neurons, we used the hiSPECS DIA method to analyze the secretome of primary cortical neurons cultured in the presence or absence of a protease inhibitor C3 (Stachel et al., 2004). The inhibition of BACE1 reduces its shedding activity which is reflected by reduced abundances of its substrates in the neuronal secretome. Overall, we found 29 membrane proteins to be reduced in the secretome upon BACE1 inhibition including several known BACE1 substrates, such as SEZ6, SEZ6L, CACHD1 and CHL1. On top, we identified several additional BACE1 substrate candidates: MMP24, IL6ST, CXADR, CD200 and ADAM22 (Figure 20a-c). Noteworthy, the well-established BACE1 substrate APP, was not significantly reduced in the neuronal secretome upon C3 treatment. This is likely the case because APP is additionally also cleaved by other proteases besides BACE1 (Lichtenthaler et al., 2018) and hiSPECS only measures total protein abundance changes and cannot distinguish between different cleavage products of APP. Moreover, we repeated the analysis using specifically neurons of the hippocampus which revealed a highly correlating BACE1 substrate repertoire independent of the brain region (Figure 20d). This analysis allowed us not only to highlight again the superiority of hiSPECS over the SPECS method, but also to identify new BACE1 substrate candidates. Furthermore, cell type-specific secretion depends on several mechanism such as the expression of proteases and only to a small extent on cell type-specific protein abundance.

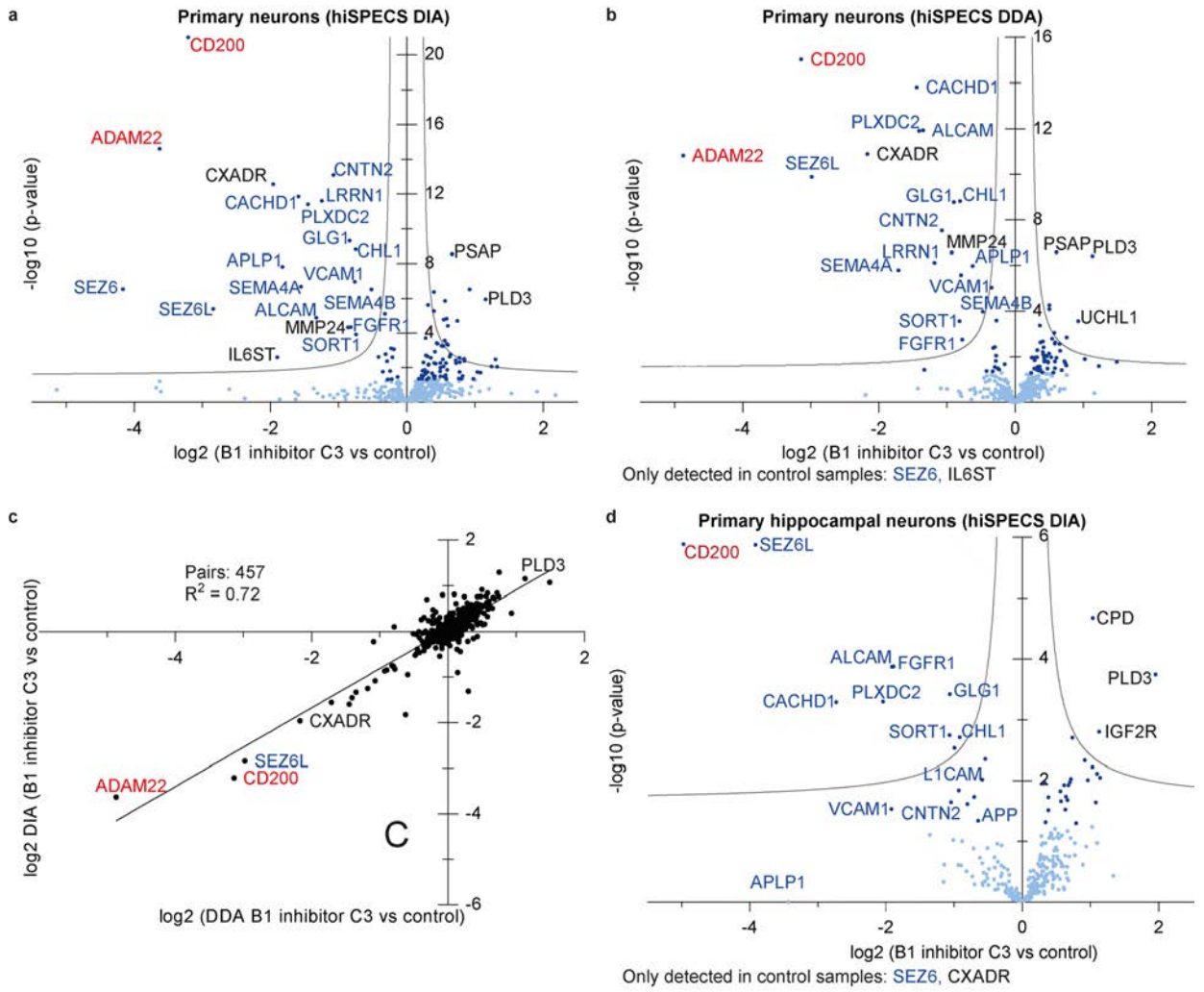

Figure 20 The substrate repertoire of BACE1. a-b) Volcano plot indicating protein abundance changes in the secretome of cortical primary neurons treated with the BACE1 inhibitor C3 vs untreated control using hiSPECS DIA in a) or DDA in b). The fold change (log2) is plotted against the p-value (negative log10) with dark blue dots indicating significant regulation meaning a p-value below 0.05. Hyperbolic selection curves colored in grey illustrate a permutation-based false discovery rate (FDR) estimation of 5%. (N=11) **c)** Correlation plot of the log2 fold changes detected in a) and b). **d)** hiSPECS DIA analysis as described in a) but using hippocampal primary neurons. Figures retrieved from (Tüshaus et al., 2020).

4.4.1 Validation of CD200 and ADAM22 as BACE1 substrates

In the next step, we aimed to validate the two substrate candidates ADAM22 and CD200 using Western Blot analysis. Of note, CD200 was previously reported to be cleaved by BACE1 in a peripheral cell line (Stutzer et al., 2013) and both ADAM22 and CD200 have been shown to accumulate on the cell surface of primary neurons upon BACE1 inhibition (Herber et al., 2018). In a first step, shRNA against the two target proteins ADAM22 and CD200 were established in order to knock-down the proteins and validate the antibodies used in the following experiments (Figure 21a). Afterwards, we validated the accumulation of full-length (fl) CD200 and ADAM22 in the lysate and the reduction of

soluble ADAM22 in the conditioned media upon BACE1 inhibition (Figure 20b,c). Due to the lack of sensitivity of the CD200 antibody in the conditioned media, the reduction of soluble CD200 was validated by ELISA (Figure 20d).

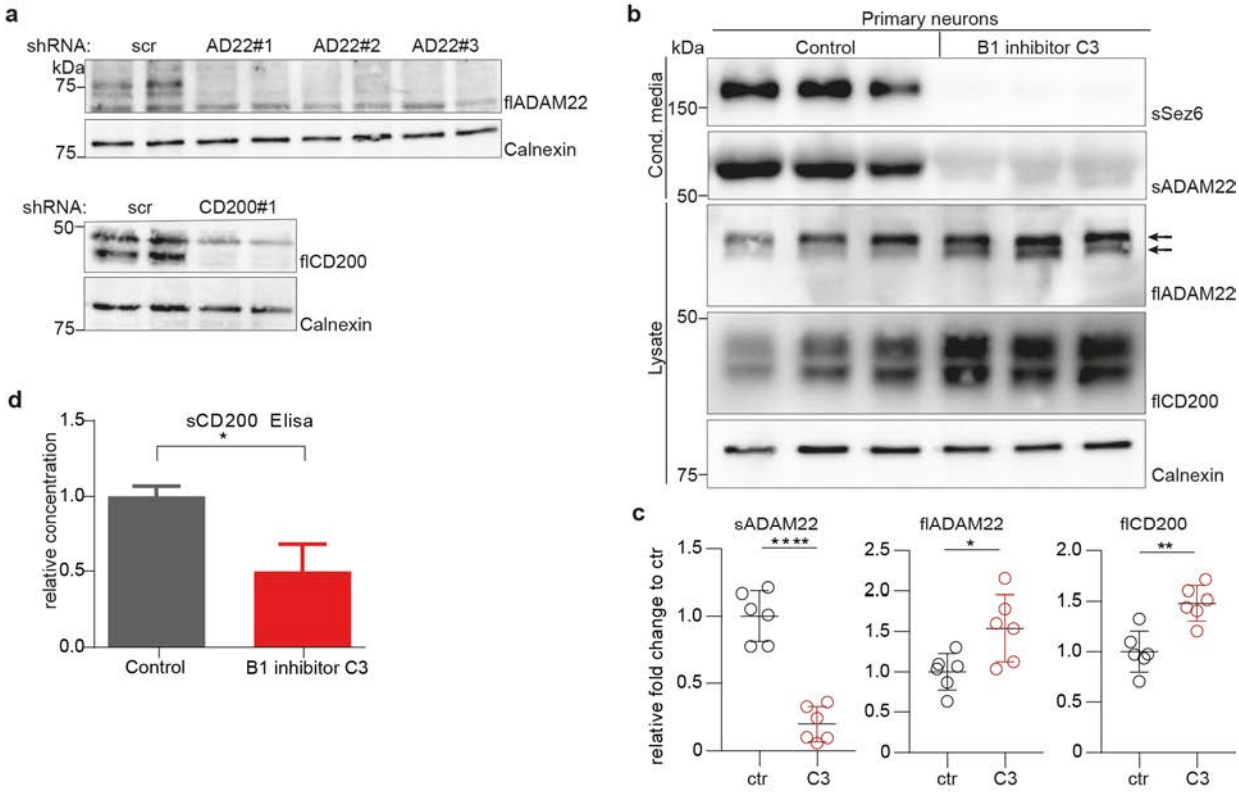

Figure 21 Validation of Cd200 and ADAM22 as BACE1 substrates in neurons. a) Western blotting of neuronal lysate treated with scrambled control (scr) or ADAM22/CD200 targeting shRNAs for 5 days to verify the specificity of the antibodies. **b + d)** Neurons were cultured for 48 h with or without the BACE1 inhibitor C3. Western blot of full length (fl) and shed (s) ADAM22, CD200 and calnexin (loading control) in the neuronal lysates upon BACE1 inhibition or control lysates. In the supernatant of these neurons soluble SEZ6, ADAM22 were detected by Western blotting and soluble CD200 by ELISA (N=6) (d) (p-value = 0.0116, one sample t-test) **c)** Western blot quantification of b) using calexin levels for normalization and quantifying relative to the non treated control condition (black). A one sample t-test was used with N=6 (flADAM22: p-value= 0.0251, flCD200: p-value = 0.011, sADAM22: p-value <0.0001). Figures adapted from (Tüshaus et al., 2020).

BACE1 cleavage of a substrate generates a new protein C-terminus for the shed substrates. Therefore, we investigated different mass spectrometric datasets based on DDA and searched for semi-tryptic peptides, which are characterized by one tryptic cleavage at one peptide terminus and a non-tryptic cleavage at the other terminus. Conclusively, after tryptic digestion during the sample preparation, one dedicated peptide at the very C-terminus of the shed protein substrate will be generated, which can be used to identify the BACE1 cleavage site. However, since peptide identification by mass spectrometry strongly depends on the peptide length, hydrophobicity and ionization behavior, those peptides are often hard to detect. Especially peptides with a non-

specifically cleaved C-term lack the terminal lysine or arginine, which carry a positive charge. Hence, those peptides are harder to ionize for mass spectrometry.

Fortunately, we identified a semi-tryptic peptide for CD200 in a BACE1 activity dependent manner. First, it was detected in the supernatant of control primary neurons in the hiSPECS DDA analysis but not upon BACE1 inhibitor C3 treatment (Figure 22a). Second, it was detected when overexpressing BACE1 together with flCD200 in HEK cells but not upon BACE1 inhibition or in the control missing BACE1 (Figure 22b). Third, the same semi-tryptic peptide of CD200 was detected in the CSF of wild type mice but not in BACE1 and 2 double knockout mice (Pigoni et al., 2016). Moreover, the peptide is located in the ectodomain of CD200 in close proximity to the transmembrane region and therefore it very likely represents the BACE1 cleavage site in CD200 (Figure 22c).

Together, we validated the two BACE1 substrates CD200 and ADAM22 in primary neurons and showed the power of the hiSPECS method to elucidate the substrate repertoire of membrane bound proteases thorough quantification of their shed substrates.

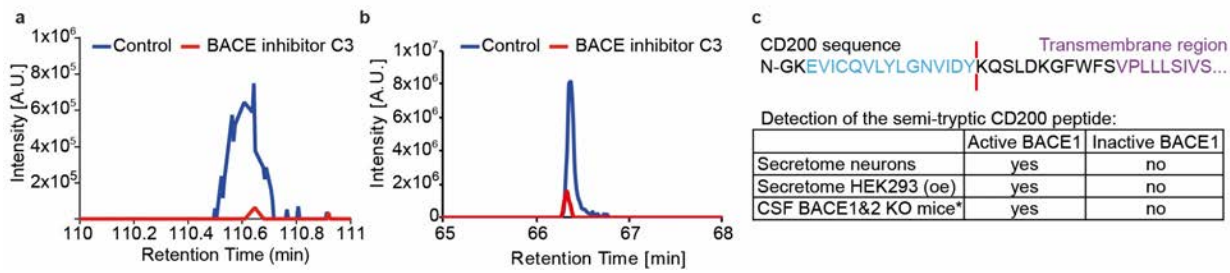

	Active BACE1	Inactive BACE1
Secretome neurons	yes	no
Secretome HEK293 (oe)	yes	no
CSF BACE1&2 KO mice*	yes	no

Figure 22 The BACE1 cleavage site in CD200. a) Extracted ion chromatogram of the peptide EVICQVLYLGNVIDY, which is semi-tryptic and belongs to CD200, detected in neuronal secretome upon BACE1 inhibition (red) or the control sample (blue) using hiSPECS DDA. **b)** Extracted ion chromatogram of the same semi-tryptic peptide in the secretome of HEK 293 cells overexpressing BACE1 and CD200 with BACE1 inhibition (red) or without (blue). **c)** Overview of the detection of the semi-tryptic CD200 peptide in BACE1 activity dependent manner in the secretome of neurons, overexpressing HEK 293 cells and CSF of BACE1 and 2 knockout mice (data obtained from a re-analysis of the raw files by (Pigoni et al., 2016)). The transmembrane region is indicated in purple, the semi-tryptic peptide in blue and the potential BACE1 cleavage site with a red line. Figures adapted from (Tüshaus et al., 2020).

4.5 Elaborating the cellular origin of CSF proteins

Cerebrospinal fluid (CSF) embeds the brain and its protein composition changes upon aging, neurodegeneration or other pathological conditions. This means that the proteins secreted by the brain cells into the CSF can mirror the brains health state. Therefore, CSF is also called *in vivo* secretome and is frequently used for biomarker studies in clinical and basic research. While protein level changes may be detected, the cellular origin of these proteins remains often elusive, because most proteins are produced in

more than one cell type. To this end, we used the established cell type-resolved mouse brain secretome resource to systematically trace back the cellular origin of CSF proteins.

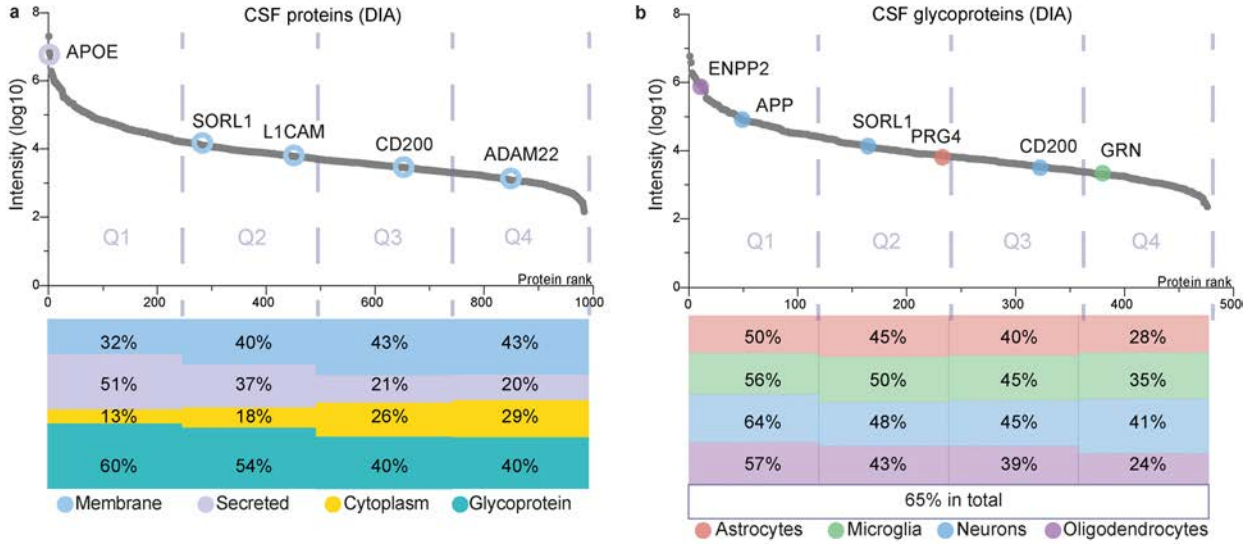

Figure 23 The composition of murine CSF. a) Proteins detected in murine CSF (min. 3/4 biological replicates) visualized in a dynamic range plot according to their log10 LFQ intensities. The percentage of proteins in each quartile annotated as membrane, secrete, cytoplasm, or glycoprotein according to UniProt is indicated. **b)** Glycoproteins detected in murine CSF (min 3/4 biological replicates) visualized in a dynamic range plot according to the log10 LFQ intensity. The percentage of proteins in each quartile covered in the secretome resource in the individual cell types (min. 5/6 biological replicates) is indicated. Dedicated CTSP are indicated with color. Figures retrieved from (Tüshaus et al., 2020).

In total, 984 protein groups were quantified in the CSF (min. 3/4 biological replicates) using DIA and a custom made murine CSF library (Figure 25d). The higher coverage compared to other proteomic murine CSF datasets (Dislich et al., 2015; Pigoni et al., 2016) suggests a general superiority of DIA in secretome studies *in vitro* and *in vivo* (CSF). Protein groups were sorted according to their LFQ intensities and split into quartiles with the 1st quartile representing the 25% most abundant CSF proteins. APOE, a soluble secreted protein, was detected as one of the most abundant proteins in CSF. In general, soluble secreted proteins were more abundant in the 1st quartile and decreased continually to the 4th quartile. In contrast, membrane proteins were least abundant in the 1st quartile indicating in general a lower abundance of shed proteins such as the two BACE1 substrates CD200 and ADAM22 in CSF (Figure 23a).

Next, we focused on the 476 glycoproteins in the CSF (according to UniProt) and illustrated their coverage by the established cell type-resolved mouse brain secretome resource. Overall 65% of the CSF glycoproteins were also identified in our resource with the highest coverage in the 1st quartile of each cell type. With an average of 50% per quartile, neurons revealed the best coverage (Figure 23b) which hold also true when

focusing on the top 25 most abundant CSF proteins per cell type, where a coverage of 76% was achieved (Figure 24) e.g. the cell adhesion protein NRCAM. The predominant role of neuronally derived glycoproteins in the CSF was also visible when focusing on the CTSP of which 123 were detected in the CSF (Figure 25a). Given that neurons are outnumbered by glia cells in the brain this dominant role was not to be expected. Again we found examples of proteins being expressed in several brain cell types, although secreted specifically by one. For example, SEZ6L and CACHD1 are broadly expressed (Sharma et al., 2015) and specifically secreted by neurons due to ectodomain shedding by BACE1 (Pigoni et al., 2016; Rudan Njavro et al., 2020). Thus, mechanisms controlling cell type specificity observed in the secretome resource were also detected in CSF, the *in vivo* secretome.

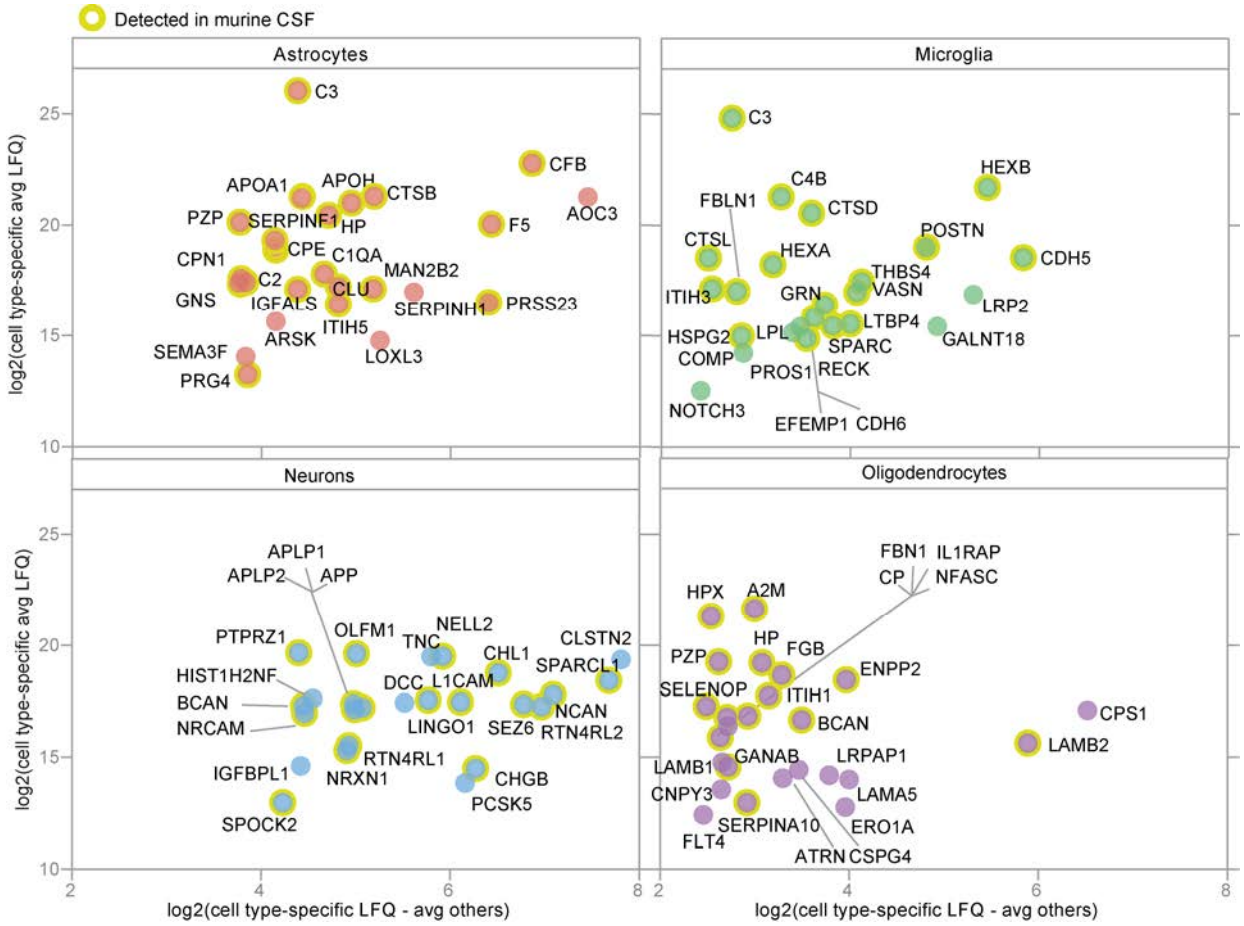

Figure 24 CSF coverage of the top 25 abundant secretome glycoproteins of the individual brain cell types. The 25 most abundant glycoproteins are illustrated by plotting their average log2 LFQ values of the enriched cell type against the log2 transformed ratio of the average cell type-specific LFQ intensities and the average of the other cell

types. Proteins which are also quantified in murine CSF are highlighted with a yellow circle. Figure retrieved from (Tüshaus et al., 2020).

Numerous proteins both detected in the secretome resource and the CSF, are homologs of human proteins linked to diseases of the nervous system according to DisGeNET (Pinero et al., 2017). In order to trace back their cellular origin, we mapped them to our secretome resource (Figure 25c). One example, the amyloid precursor protein (APP) is linked to Alzheimer´s disease (AD) and was found to be mainly secreted by neurons (O'Brien et al., 2011). Another AD-linked example is SORL1 (Yin et al., 2015), which was also specifically released by neurons while being expressed in similar levels in astrocytes, microglia, neurons and oligodendrocytes. This means that changes of CSF protein levels of APP and SORL1 during AD pathogenesis are likely to be triggered by neurons. In general, the assignment of the disease linked proteins to an individual brain cell type might help to target studies on this cell type during the pathogenesis of the specific disease.

AD biomarkers reflecting the pathogenesis of the disease are urgently needed and many large-scale studies focused on proteomic analysis of postmortem AD tissue and CSF (Bai et al., 2020; Johnson et al., 2020) to detect systematic protein level changes. For example, a recent study by Johnson et al (Johnson et al., 2020) reported elevated CSF levels of the protein CD44 in AD patients. Interestingly, CD44 was found to be specifically released by oligodendrocytes in out secretome resource while showing highest protein levels in the lysates of astrocytes and microglia (Sharma et al., 2015)(Figure 19). This suggests, that follow up studies trying to understand the mechanism behind the increase of soluble CD44 in AD CSF samples may be focused on oligodendrocytes. In summary, the cell-type resolved secretome resource can be used to trace back the cellular origin of soluble CSF proteins and study brain diseases.

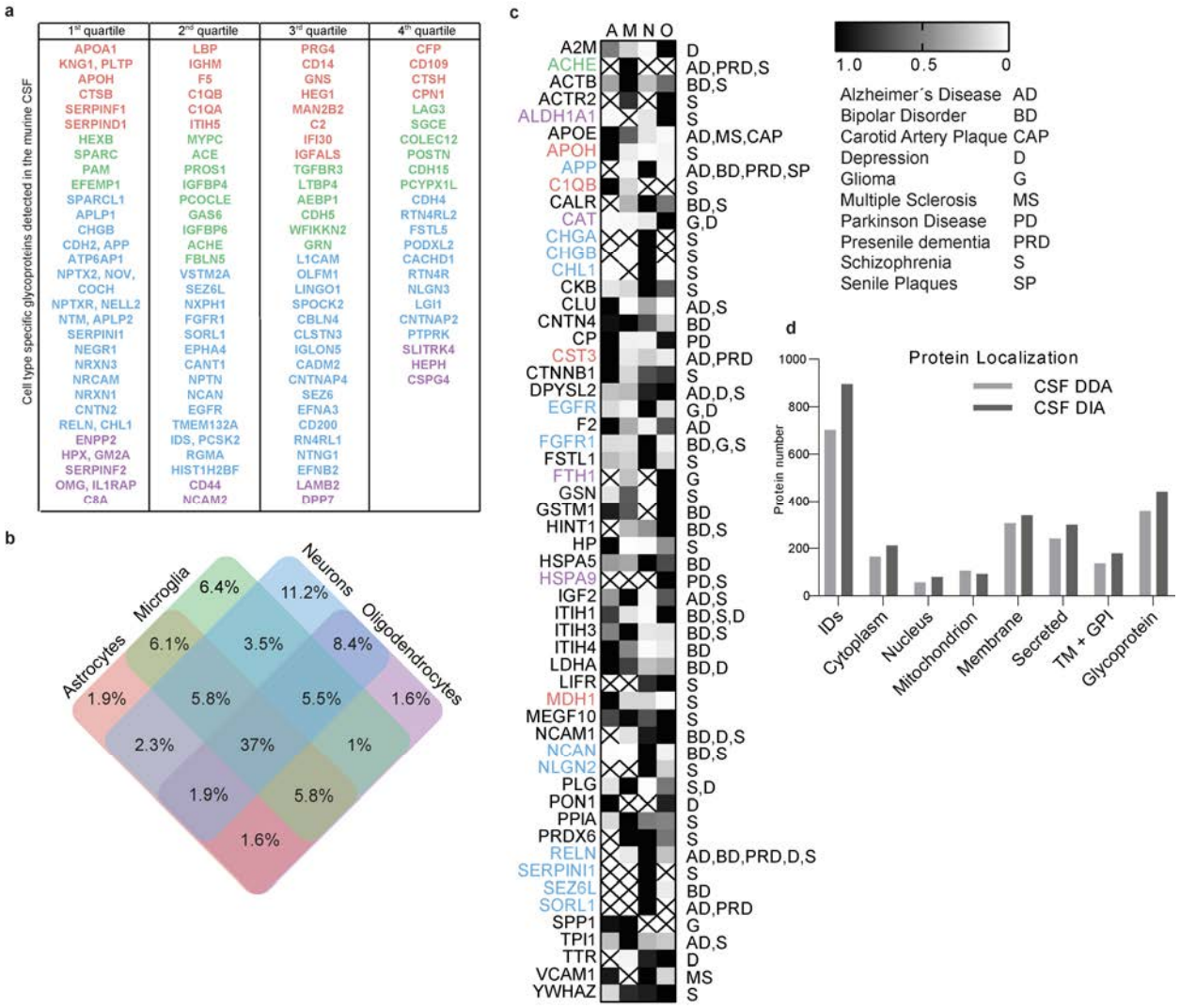

Figure 25 Tracing the cellular origin of CSF proteins. a) CTSP of the secretome resource detected in murine CSF listed according to their quartiles. **b)** Venn diagramm showing the the overlap between glycoproteins detected in the CSF and the secretome resource in the individual brain cell types (min 5/6 biological replicates). **c)** Proteins detected in both the secretome resource and CSF with a disease association of the nervous system according to DisGeNet (experimental index >= 0.9) (Pinero et al., 2017). Colored protein names indicate secretion in a cell type specific manner and the relative protein abundance level in the secretome of the individual brain cell types is indicated in the heat map with black indicating high, white indicating low and crosses indicating no detection. **d)** Bar chart indicating the quantified proteins (min. 3/4 biological replicates) and their location according to UniProt in the in the CSF samples comparing DDA (light grey) to DIA (dark grey) analysis. Figures adapted from (Tüshaus et al., 2020).

4.6 Deciphering the secretome of brain slices

Finally, hiSPECS was used to identify the secretome of brain slices which in combination with the secretome resource allowed us to map the secreted proteins to their cellular origin. The advantage of studying cortico-hippocampal brain slices as an *ex vivo* model system is the maintenance of the divers cellular connections between the individual cell types. Although the brain slices were cultured in the presence of 25% serum supplements, we reproducibly quantified 249 protein groups using hiSPECS DIA and a custom-made brain slice library (min. 5/6 biological replicates) (Figure 26a). Ranking and

grouping of the proteins according to their LFQ intensities revealed a comparable picture to the CSF analysis. In the 1st quartile only 18% of the proteins were annotated as membrane proteins according to UniProt while this percentage increased up to 35% in the 3rd and 4th quartile. Secreted proteins revealed opposing distribution with the highest percentage of 56% in the 1st quartile. Comparable to CSF, soluble secreted proteins were higher abundant and shed ectodomains were lower abundant in the secretome of brain slices. In total 89% of the quantified proteins were also included in the secretome resource. In contrast to CSF, where neurons were the predominant contributing cell type, in the secretome of brain slices neurons contributed on average the least (66.5%) and the most proteins were traced back to microglia (74%) (Figure 26b). Of note, among the highest abundant proteins (1st quartile) the highest percentage of coverage and number of CTSP originated from oligodendrocytes (Figure 26c).

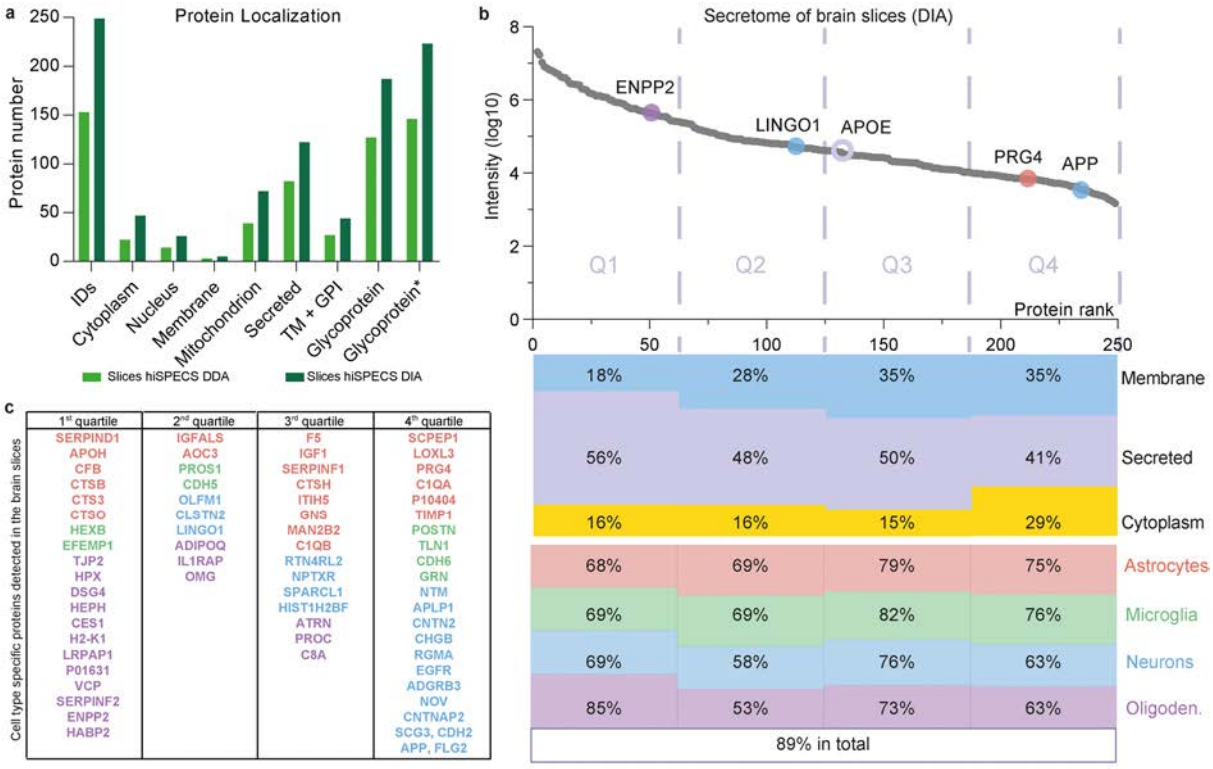

Figure 26 Secretome analysis of brain tissue using hiSPECS. a) Bar chart indicating the quantified proteins (min 5/6 biological replicates) and their allocation according to UniProt in the secretome of *ex vivo* brain slices cultures comparing hiSPECS DDA (light green) and DIA (dark green). For details of glycoprotein* see Figure 11. **b)** Illustration of the log10 LFQ values of the quantified proteins in the brain slice secretome. Proteins are ranked and grouped into quartiles relative to their LFQ value (1st quartile contains proteins with highest LFQ values). According to their annotations in UniProt with membrane, secreted or cytoplasm the percentile of proteins is indicated as well as the coverage in the brain secretome resource in total or by individual cell types. **c)** Proteins detected in the brain slice

secretome which revealed cell type specificity in the secretome resource are listed according to their belonging quartile. Figures retrieved from (Tüshaus et al., 2020).

For a final proof of principle of the utility of the hiSPECS method in combination with the brain secretome resource to study *ex vivo* brain tissue, we induced an inflammatory response by a 6 h treatment with lipopolysaccharide (LPS). Upon LPS treatment the secretome revealed dramatic changes up to 250-fold. On the one hand, proteins were detected known to increase upon LPS stimulation in the secretome of macrophages (shown in red), e.g. TIMP1, CSF1 and IL12B (Meissner et al., 2013). On the other hand, the increased secretion of proteins such as APLP1, BCAN and several others, were detected which were not known to respond to LPS treatment (Figure 27a). Overall, 107 proteins were significantly up or down regulated ($p<0.05$) including 50% secreted and 26% shed proteins (TM+GPI) (Figure 27b). Interestingly, among the significantly regulate proteins were several CTSP of the brain secretome resource, such as C1QA and C1QB (astrocytes), GRN and HEXB (microglia), APLP1 and CHL1 (neurons) and ADIPOQ and CD44 (oligodendrocytes). Hence, immune cells are not the only cells responding to LPS, but instead these findings indicate that all brain cell types respond with protein level changes to the inflammation stimulus indicating a systematic response of the whole network. Taken together, hiSPECS and the cell type-resolved secretome resource are powerful tools to study inflammation in *ex vivo* brain tissue and pinpoint effected cell types.

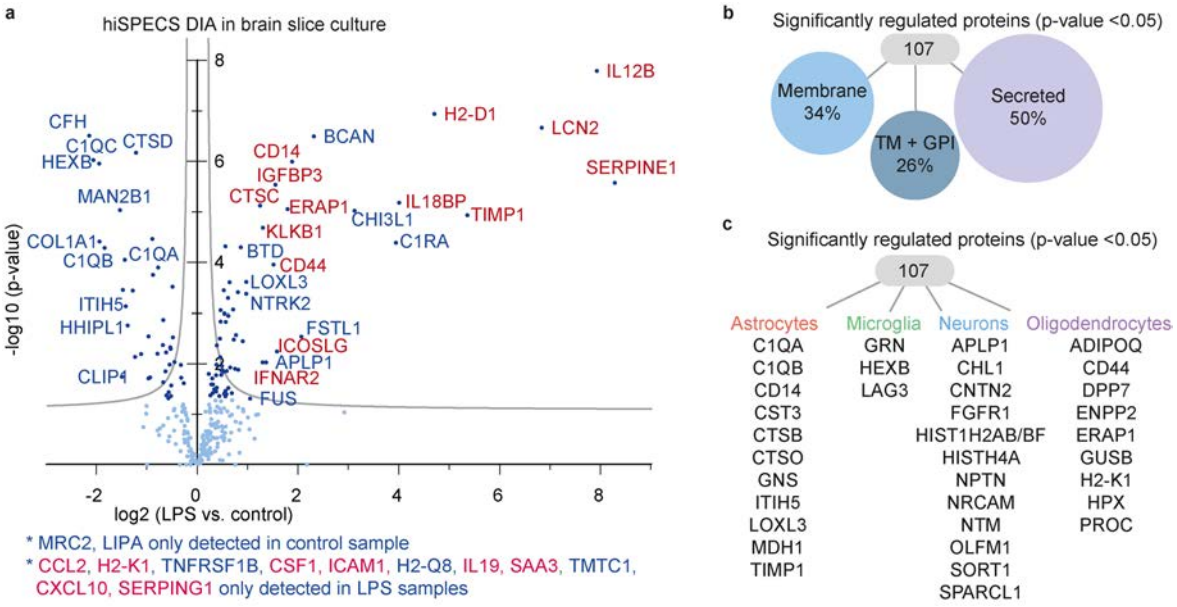

Figure 27 The inflammatory response of brain slices cultures. a) Volcano plot depicting the protein abundance changes in the secretome of brain slices within a 24 h collection window after a 6 h LPS stimulation analyzed by hiSPECS DIA. The fold change (log2) is plotted against the p-value (negative log10) with dark blue dots indicating

significant regulation meaning a p-value below 0.05. Hyperbolic selection curves colored in grey illustrate a permutation-based false discovery rate (FDR) estimation of 5% (N=6). Red letters indicate proteins found by.(Meissner et al., 2013) to increase in the secretome of immune cells upon LPS stimulation in cultured macrophages. **b-c)** Proteins significantly up or down regulated (p<0.05) in a) grouped according to their UniProt keywords in b) or proteins revealing cell type specific secretion in the brain secretome resource in c). Figures retrieved from (Tüshaus et al., 2020).

In summary, the newly established hiSPECS DIA method allows not only in depth secretome analysis of *in vitro* cultured primary cells and *ex vivo* brain slices in a miniaturized manner, but also established a brain secretome resource of the major brain cell types which utility was illustrated by tracing back the cellular origin of secreted proteins e.g. of biomarkers in CSF and the inflammation response of brain tissue.

4.7 Establishing iRHOM1 as the major regulator of ADAM17 in the brain

ADAM17 has a well-established role in inflammatory diseases and as the major sheddase of TNFα and most EGFR ligands, which were elaborated in great details in the periphery (Zunke et al., 2017). However, little is known about the cellular functions and signaling pathways of ADAM17 in the brain. Several structure-function analysis elucidated the trafficking mechanisms of ADAM17 by the iRHOM proteins to the cell surface and iRHOM1 has been suggested to be the major regulator of ADAM17 activity in brain cells except immune cells (Li et al., 2015; Lichtenthaler et al., 2015). In spite of the unique relationship between iRHOM1 and ADAM17 in the brain, until today systematic studies are missing to shed light onto their biological functions. Hence, the third and final major aim of my thesis was elucidating the function of the iRHOM1/ADAM17 complex in the brain.

In a first step, we aimed to determine the expression profile of iRHOM1 and iRHOM2 in the adult mouse brain. Due to the lack of antibodies suitable for this purpose, an indirect expression analysis based on the LacZ reporter gene was performed. LacZ encodes β-galactosidase and was knocked into the individual iRHOM genes during genome targeting of the *iRhom1*$^{4\text{-}11/4\text{-}11}$ (Li et al., 2015) and *iRhom2*$^{-/-}$ (McIlwain et al., 2012) mice. In this way, β-galactosidase expression is controlled by the same regulatory elements as iRHOM1 or iRHOM2 in wildtype mice. The presence/activity of β-galactosidase can be visualized by incubation with its chromogenic substrate X-Gal, which results in blue precipitates (Figure 28). Sagittal brain slices of adult (>8 weeks), homozygous *iRhom1*$^{4\text{-}11/4\text{-}11}$ and *iRHOM2*$^{-/-}$ animals were used for expression analysis (N=3) and co-staining of wildtype mice was used as a control for non-specific β-galactosidase-independent staining. iRHOM1 was found to be highly expressed in the brain compared to iRHOM2

and revealed a brain region-specific expression profile. The most dominant iRHOM1 expression was observed in cerebral cortex, olfactory bulb, cerebellum and hippocampus, mainly in the dentate gyrus. In contrast, iRHOM2 expression in the brain seemed to be in general low and the blue-positive cells were detected in the inner part of the olfactory bulb, the brain meninges, and part of the hypothalamus, potentially the median eminence or nucleus. Together, taking advantage of the LacZ reporter, iRHOM1 and iRHOM2 expression were studied in the brain, which revealed distinct, region-specific expression profiles of the iRHOM proteins and underlined the predominate role of iRHOM1 in the brain.

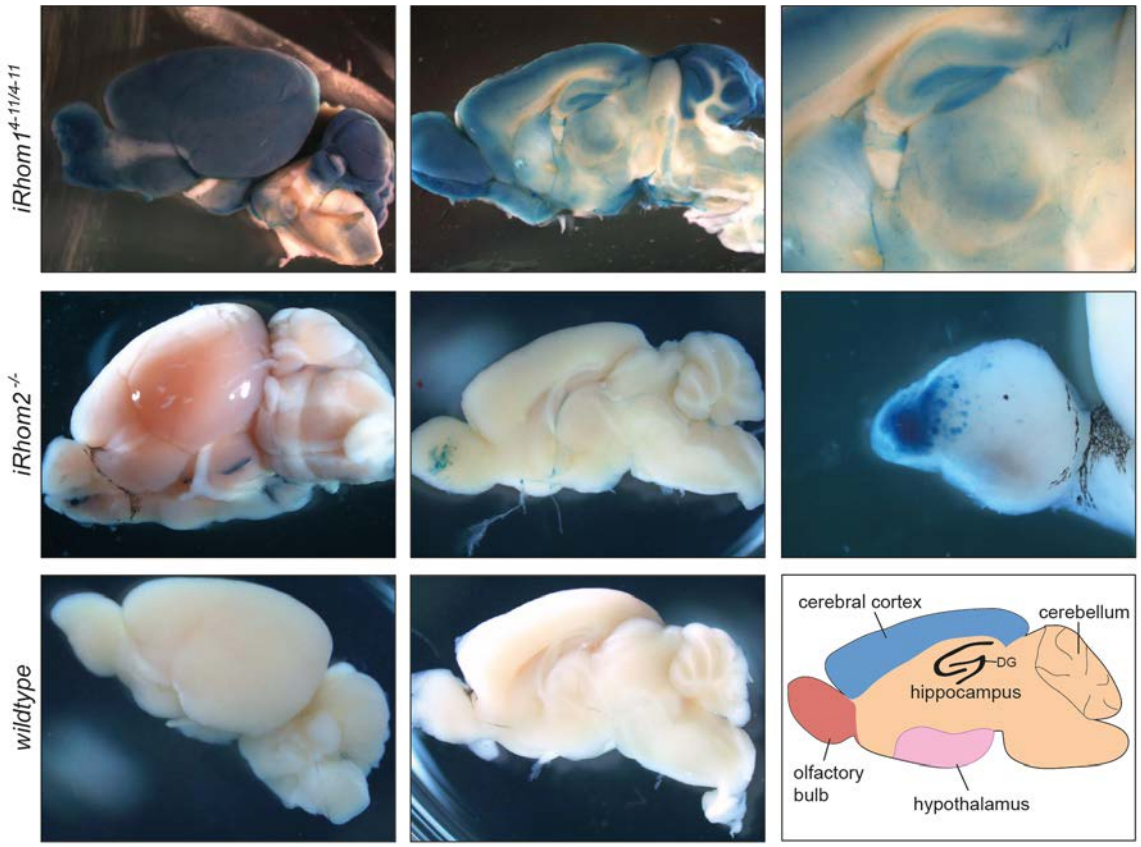

Figure 28 iRHOM1 and iRHOM2 expression profile in the brain. X-gal staining of sagittal brain slices of adult homozygous *iRhom1*$^{4\text{-}11/4\text{-}11}$, *iRHOM2*$^{-/-}$ and *wildtype* mouse brains. Blue staining reflects expression of the reporter gene LacZ which encodes β-galactosidase and indirectly reports about iRHOM expression. The brain regions most affected are shown in the lower right corner. The two pictures on the right are magnifications of regions with high blue staining. Dentate gyrus (DG)

In order to facilitate the analysis of iRHOM1 in the brain, we aimed to produce a novel highly-specific iRHOM1 antibody. Therefore, a peptide which corresponds to the first 19 amino acids of the N-terminus of iRHOM1 was injected into rats by our collaborator Regina Feederle and colleagues (Figure 29a). Interestingly, these 19 amino acids are completely preserved between human and mouse iRHOM1. One antibody clone (20A8)

revealed a specific iRHOM1 signal at the expected molecular weight size of 100kDa in brain homogenates, primary neurons and mouse embryonic fibroblasts (MEFs) (Figure 29b+c). A detailed characterization of the antibody was published together with the Blobel laboratory (Weskamp et al., 2020).

Next, we asked the question if *iRhom1*$^{4\text{-}11/4\text{-}11}$ mice are a suitable model to study the lack of ADAM17 activity in the brain. Considering that both *ADAM17*$^{-/-}$ and *iRhom1*$^{2\text{-}18/2\text{-}18}$ mice suffer from premature death, *iRhom1*$^{4\text{-}11/4\text{-}11}$ mice may give the unique opportunity to study iRHOM1/ADAM17 biological functions in adult mice. ADAM17 exists in two different conformations in the cell which cause the typical two-band pattern in Western blot analysis (Figure 29). The upper molecular weight band (around 130 kDa) corresponds to the inactive/immature ADAM17 which still contains its prodomain. In contrast, the lower band (around 90 kDa) corresponds to the active/mature ADAM17 which lost the prodomain and is catalytically active. Interestingly, Western blot analysis of brain homogenates of *iRhom1*$^{4\text{-}11/4\text{-}11}$ mice revealed the loss of mature ADAM17 (Figure 29b). Moreover, cultured primary cortical neurons isolated from *iRhom1*$^{4\text{-}11/4\text{-}11}$ mice also lack the mature band of ADAM17 (Figure 29b). Hence, we hypothesize that *iRhom1*$^{4\text{-}11/4\text{-}11}$ neurons and the majority of other *iRhom1*$^{4\text{-}11/4\text{-}11}$ brain cells lack ADAM17 activity and *iRhom1*$^{4\text{-}11/4\text{-}11}$ mice are a suitable model to study ADAM17 brain function in adulthood. Importantly, although we cannot exclude that truncated iRHOM1 protein might remain in *iRhom1*$^{4\text{-}11/4\text{-}11}$ mice and this potentially might explain the mild phenotypes seen in *iRhom1*$^{4\text{-}11/4\text{-}11}$ mice as compared to the *iRhom1*$^{2\text{-}18/2\text{-}18}$ mice, this truncated form does not seem to be sufficient to mature ADAM17 but rather suggests additional functions of the iRHOM1 protein, potentially independent of ADAM17.

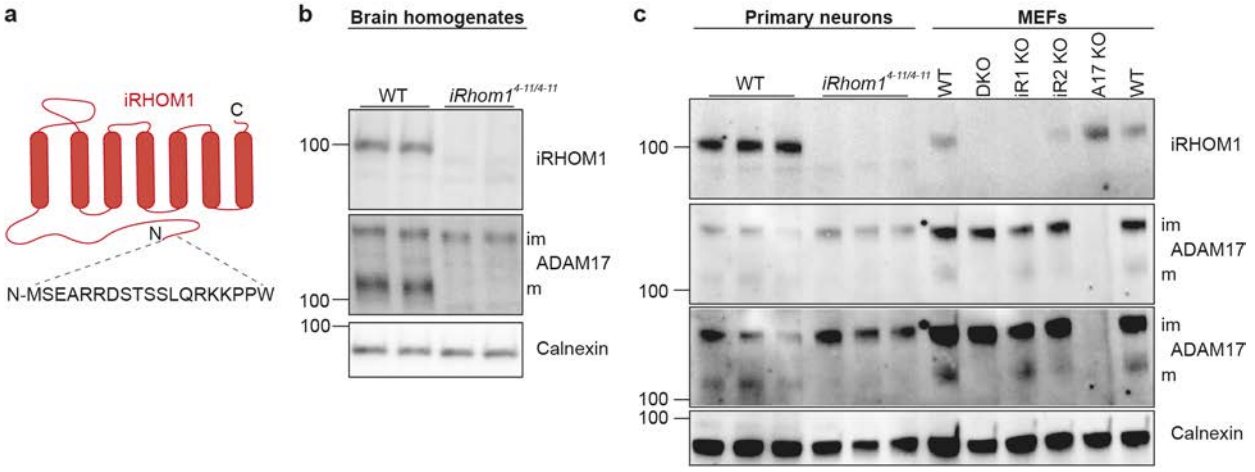

Figure 29 Antibody validation against the N-terminus of iRHOM1. a) The N-terminal 19 amino acids of iRHOM1 were used to produce a new iRHOM1 antibody in rats by the collaborating laboratory of Regina Feederle. Western blot analysis of brain homogenates (N=5) **b)**, primary neurons and mouse embryonic fibroblast (MEF) cells **c)** of iRHOM1, ADAM17 and calnexin (loading control) (N=6). The immature (im) and mature (m) band of ADAM17 is highlighted (short and long exposure shown). MEF cells of the following genotypes were used as control for the running behavior of the iRHOM1 and ADAM17 bands: *wildtype* (WT), *iRhom1*$^{4\text{-}11/4\text{-}11}$ and *iRHOM2*$^{-/-}$ (DKO), *iRhom1*$^{4\text{-}11/4\text{-}11}$ (iR1 KO), *iRHOM2*$^{-/-}$ (iR2 KO), *ADAM17*$^{-/-}$ (A17 KO).

4.8 Elucidating the substrate repertoire of iRHOM1/ADAM17 in the brain

Proteases such as ADAM17 are involved in diverse signaling pathways in the cell by shedding a broad spectrum of substrates. In general, ADAM17 is known to preferably cleave single-pass transmembrane or GPI-anchored proteins (Zunke et al., 2017), the specific substrate profile may however vary between different cell types and depend on the specialized expression profile and physiological tasks of the cell. While single brain substrates of ADAM17, such as neogenin (van Erp et al., 2015), HB-EGF (Palazuelos et al., 2014) and SMEA5B (Browne et al., 2012) have been studied in more detail, a broader picture of the overall brain substrate repertoire is lacking. To this end, we not only applied the optimized hiSPECS DIA method to determine ADAM17 substrates in primary neurons and astrocytes *in vitro* but also used CSF analysis to elucidate the *in vivo* substrate repertoire of ADAM17 in the brain.

In a first step, we aimed to determine the constitutive substrates of ADAM17 in primary cultured neurons. Therefore, neurons were isolated from E16.5 embryos of littermates either homozygous for *iRhom1*$^{4\text{-}11/4\text{-}11}$ or wildtype (N=6). The supernatant was collected after a 48h ManNAz labeling step and analyzed using the hiSPECS DIA protocol as described in detail before (Figure 7). Since *iRhom1*$^{4\text{-}11/4\text{-}11}$ neurons lack the mature/ active ADAM17 (Figure 29c), all single-pass transmembrane and GPI-anchored proteins significantly reduced in the supernatant of *iRhom1*$^{4\text{-}11/4\text{-}11}$ neurons compared to control

neurons were classified as potential ADAM17 substrate candidates (Figure 30, Table 10). Of note, several known ADAM17 substrates such as ALCAM (Rosso et al., 2007), SEMA5B (Browne et al., 2012), SORL1 (Tsukamoto et al., 2014) and CD44 (Kamarajan et al., 2013) were reduced in the supernatant of *iRhom1*$^{4\text{-}11/4\text{-}11}$ neurons which strengthened the hypothesis that these neurons lack ADAM17 activity. On top of this, several new substrate candidates were identified, such as MEGF10 and MEGF11, which are known to trigger neuronal mosaic formation (Kay et al., 2012), or CADM4, CNTNAP2, CNTN1, PTPRM and PTPRU, which are all cell adhesion proteins according to UniProt. Notably, several known BACE1 substrates including SEZ6 and SEZ6L (Pigoni et al., 2020; Pigoni et al., 2016)as well as ADAM10 substrates such as NRCAM, EPHA4 and PTPRK (Kuhn et al., 2016) showed slightly increased protein abundance in the supernatant of *iRhom1*$^{4\text{-}11/4\text{-}11}$ neurons. This finding may hint towards additional functions of iRHOM1 or a mechanism in *iRhom1*$^{4\text{-}11/4\text{-}11}$ neurons which may compensate the loss of ADAM17 activity by upregulating ADAM10 and BACE1 activity.

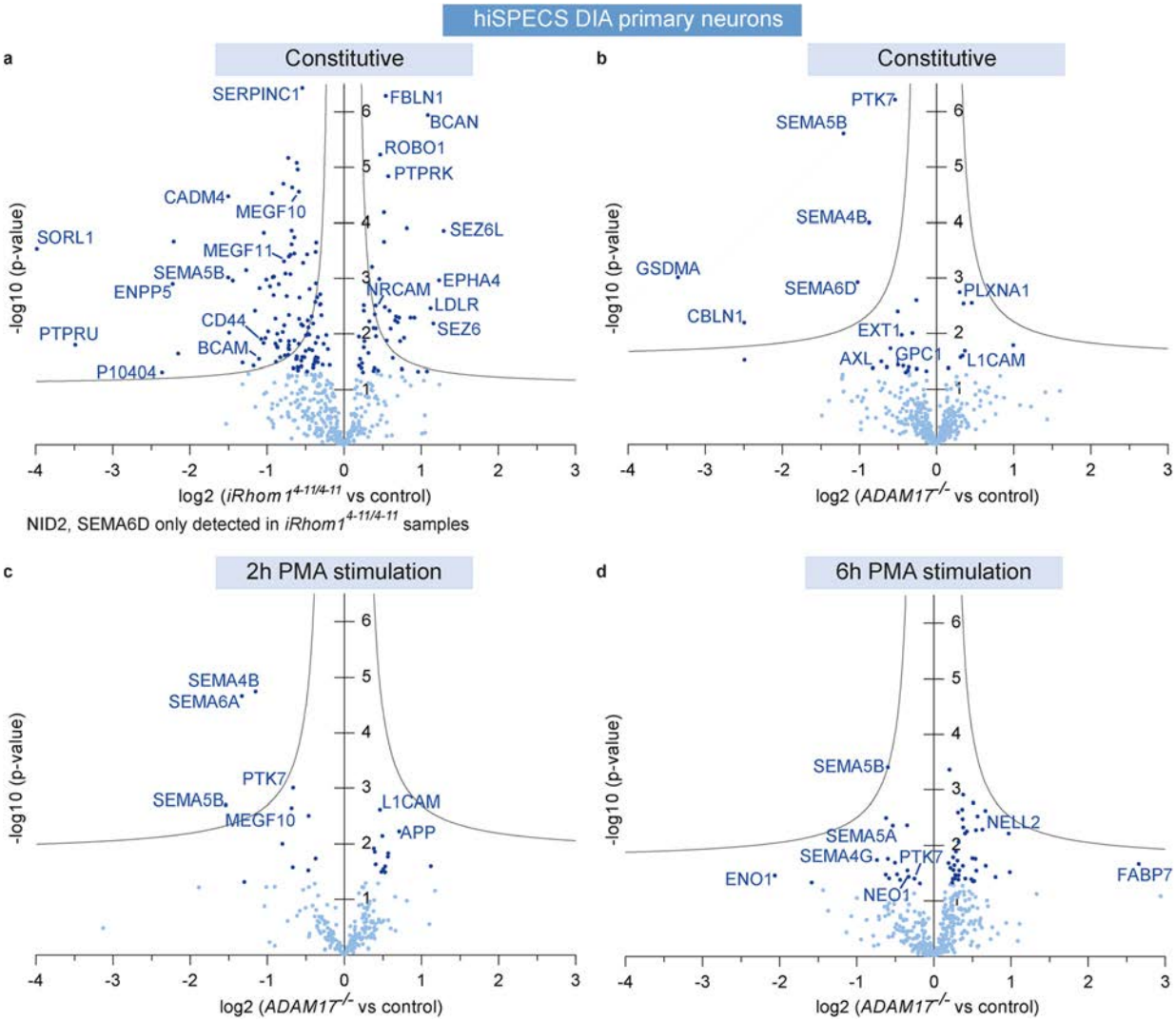

Figure 30 ADAM17 substrate repertoire in primary neurons. Volcano plot depicting the protein abundance changes in the secretome of primary *iRhom1*$^{4\text{-}11/4\text{-}11}$ or *ADAM17*$^{-/-}$ vs. control neurons within a 48 h collection window **a)** and **b)**, a 2h in **c)** or 6h in **d**) PMA stimulation/ collection window. The fold change (log2) is plotted against the p-value (negative log10) with dark blue dots indicating significant regulation meaning a p-value below 0.05. Hyperbolic selection curves colored in grey illustrate a permutation-based false discovery rate (FDR) estimate of 5%.

Next, neurons were isolated from a conditional ADAM17 knockout mouse model (ADAM17flox/flox). At the 1st day in vitro (DIV), neurons were infected with either a lentivirus expressing CRE recombinase in order to specifically excision ADAM17 or a GFP control lentivirus which allows the estimation of transduction efficiency. ManNAz labeling was performed for 48h (5-7 DIV) followed by media collection to identify constitutive ADAM17 substrates (Figure 30b). Moreover, ADAM17 is known to be rapidly activated by the experimental stimulus PMA (Lorenzen et al., 2016). In order to establish the stimulated substrate repertoire of ADAM17, neurons were treated for 2h (Figure 30c)

or 6h (Figure 30d) with PMA after the 48h ManNAz labeling step and a washing step was performed to exclude previously accumulated secretome proteins. Media of all conditions were analyzed using the hiSPECS DIA method and significantly reduced single-pass transmembrane or GPI-anchored proteins were considered as potential ADAM17 substrate candidates (summarized in Table 10). Known ADAM17 substrates AXL (Orme et al., 2016) and GPC1 (Kawahara et al., 2017) were identified under constitutive conditions as well as SEMA5B (Browne et al., 2012) and PTK7 (Na et al., 2012) which were additionally identified under stimulated conditions. MEGF10 and SEMA4B, novel ADAM17 substrate candidates identified in the *iRhom1*$^{4\text{-}11/4\text{-}11}$ neurons, could be confirmed in the ADAM17 floxed neurons. Moreover, several other semaphorin family members known to play a role in neuron morphology (Alto et al., 2017) (SEMA4G, SEMA5A, SEMA6A, SEMA6D) were identified as ADAM17 substrate candidates. Of note, the increase of BACE1 and ADAM10 substrates was exclusively detected in supernatants of *iRhom1*$^{4\text{-}11/4\text{-}11}$ neurons, suggesting a modulatory role of iRHOM1 rather than ADAM17 in this potential compensatory cell response. Together, the hiSPECS DIA method was successfully used to identify novel as well as known ADAM17 substrate candidates in primary neurons.

Table 10 ADAM17 substrate candidates in primary neurons. Significantly reduced hits which are single-pass transmembrane proteins or GPI-anchored in the different hiSPECS DIA analysis of primary astrocytes. Candidates which were validated as ADAM17 substrates in previous publications are listed.

Gene name	UniProt Ac	*iRhom1*$^{4\text{-}11/4\text{-}11}$ (N=6)	*ADAM17*$^{-/-}$ conditional (N=8)	*ADAM17*$^{-/-}$ 2h PMA (N=5)	*ADAM17*$^{-/-}$ 6h PMA (N=5)	Known ADAM17 substrate
Adam12	Q61824	+				
Adam9	Q61072	+				
Alcam	Q61490	+				(Rosso et al., 2007)
Atrn	Q9WU60	+				
Axl	Q00993		+			(Orme et al., 2016)
Bcam	Q9R069	+				
Cadm4	Q8R464	+				
Cd44	P15379	+				(Kamarajan et al., 2013)
Cntn1	P12960	+				
Cntnap2	Q9CPW0	+				
Cntnap4	Q99P47				+	
Cntnap5a	Q0V8T9	+				
Enpp5	Q9EQG7	+				
Ext1	P97464		+			
Glce	Q9EPS3	+				
Glg1	Q61543	+				
Golm1	Q91XA2	+				
Gpc1	Q9QZF2		+			(Kawahara et al., 2017)
Lrrc4	Q99PH1	+				
Lsamp	Q8BLK3			+		
Lypd4	Q8BVP6	+				
Megf10	Q6DIB5	+		+		
Megf11	Q80T91	+				
Neo1	P97798				+	(van Erp et al., 2015)
Nfasc	Q810U3				+	
Ntm	Q99PJ0			+		
Omg	Q63912	+	+			
P10404	P10404	+				
Pld3	O35405	+				

Ptk7	Q8BKG3		+	+	+	(Na et al., 2012)
Ptprm	P28828	+				
Ptpru	B1AUH1	+				
Reck	Q9Z0J1	+				
Rgma	Q6PCX7		+			
Sema4b	Q62179	+	+	+		
Sema4g	Q9WUH7				+	
Sema5a	Q62217		+		+	
Sema5b	Q60519	+	+	+	+	(Browne et al., 2012)
Sema6a	O35464			+		
Sema6d	Q76KF0-3		+			
Slitrk5	Q810B7				+	
Sorl1	O88307	+				(Tsukamoto et al., 2014)

To understand the substrate repertoire of ADAM17 in another primary cell type, the same experiments described in detail before with neurons were repeated using primary astrocytes. In contrast to neurons, astrocytes were cultured for 3 weeks prior to the ManNAz labeling step. Overall, fewer ADAM17 substrates candidates were identified in astrocytes compared to neurons (Figure 30, Figure 31). This phenomenon might be explained by the, in general observed, less pronounced contribution of ectodomain shedding to the astrocytic secretome compared to neuronal secretome (Figure 17). Moreover, other proteases such as ADAM10 may have a more dominant role in astrocytes compared to ADAM17. Of note, the known ADAM17 substrates VCAM1 (Garton et al., 2003), EPHB4 (Weskamp et al., 2010), NEO1 (van Erp et al., 2015), CDH5 (Weskamp et al., 2010) and SEMA4D (Zhu et al., 2007) were detected validating the experimental approach (Figure 30, Table 11Table 11). Newly identified ADAM17 substrate candidates in primary astrocytes including e.g. the cell-cell adhesion protein CDH13, which together with CDH5, EPHB4, STAB1 and EFMB2, are involved in blood vessel development (GO term Biological process (BP), see Figure 33)

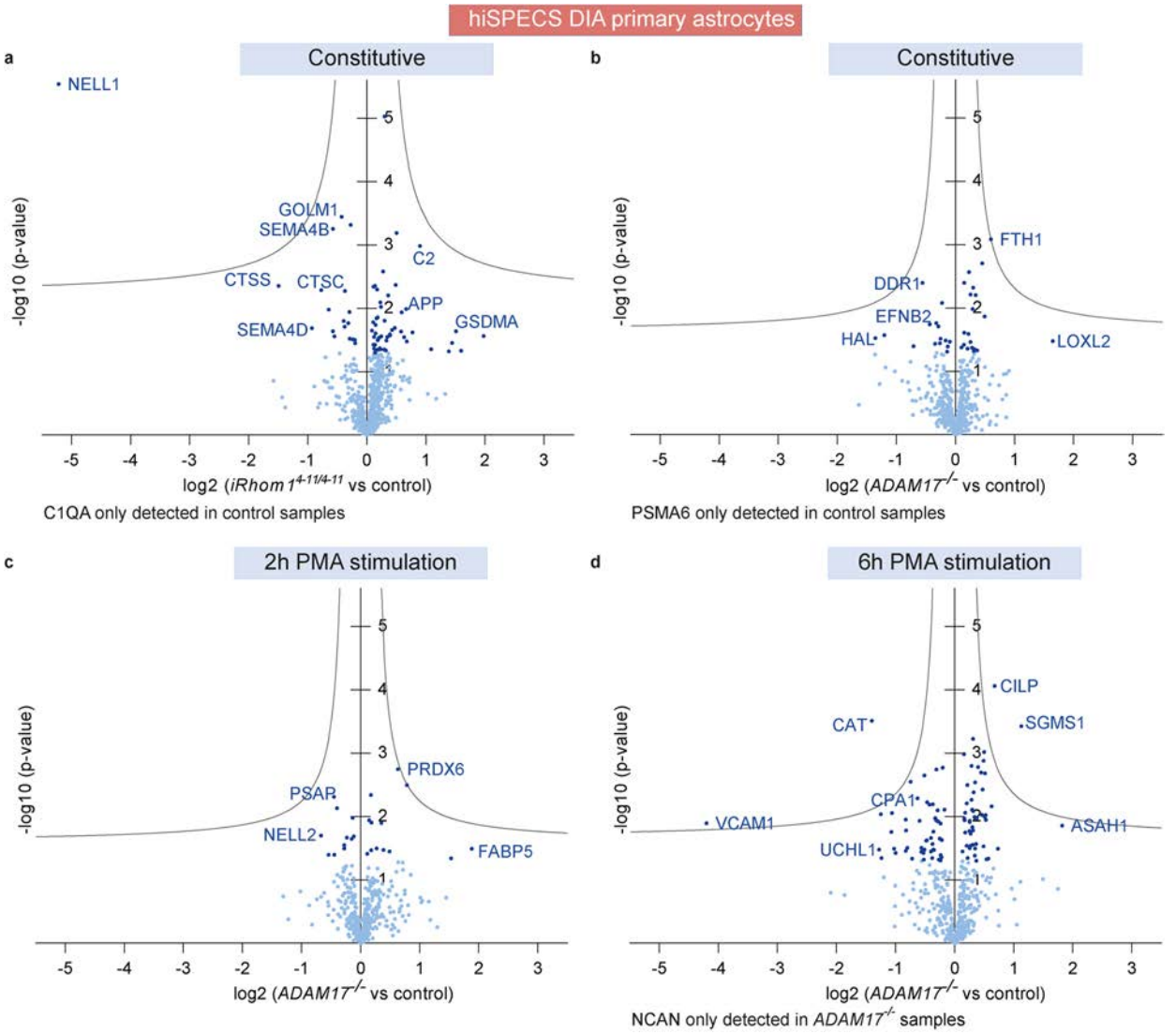

Figure 31 ADAM17 substrate repertoire in primary astrocytes. Volcano plot depicting the protein abundance changes in the secretome of primary *iRhom1*$^{4\text{-}11/4\text{-}11}$ or *ADAM17*$^{-/-}$ vs. control astrocytes within a 48 h collection window **a)** and **b)**, a 2h in **c)** or 6h in **d**) PMA stimulation/ collection window. The fold change (log2) is plotted against the p-value (negative log10) with dark blue dots indicating significant regulation meaning a p-value below 0.05. Hyperbolic selection curves colored in grey illustrate a permutation-based false discovery rate (FDR) estimate of 5%.

Table 11: ADAM17 substrate candidates in primary astrocytes. Significantly reduced hits which are single-pass transmembrane proteins or GPI-anchored in the different hiSPECS DIA analysis of primary astrocytes. Candidates which were validated as ADAM17 substrates in previous publications are highlighted.

Gene name	UniProt Ac	*iRhom1*$^{4\text{-}11/4\text{-}11}$ (N=6)	*ADAM17*$^{-/-}$ conditional (N=6)	*ADAM17*$^{-/-}$ 2h PMA (N=5)	*ADAM17*$^{-/-}$ 6h PMA (N=4)	Known ADAM17 substrate
Cdh13	Q9WTR5				+	
Cdh5	P55284		+			(Weskamp et al., 2010)
Ddr1	Q03146		+			
Efnb2	P52800		+			
Ephb4	P54761		+			(Weskamp et al., 2010)
Ext1	P97464				+	
Ext2	P70428			+		
Galnt10	Q6P9S7				+	
Glg1	Q61543				+	
Golm1	Q91XA2	+				
H2-D1	P01899	+				
Ifnar2	O35664	+				
Lfng	O09010		+			

Man2a1	P27046				+	
Mxra8	Q9DBV4				+	
Neo1	P97798				+	(van Erp et al., 2015)
Ret	P35546		+	+		
Sema4b	Q62179	+				
Sema4d	O09126	+			+	(Zhu et al., 2007)
Sema6a	O35464	+				
Stab1	Q8R4Y4		+		+	
Vcam1	P29533				+	(Garton et al., 2003)

In order to elaborate not only the *in vitro* but also the *in vivo* substrate repertoire of ADAM17, CSF samples of 3-month-old *iRhom1*$^{4\text{-}11/4\text{-}11}$ mice and wildtype littermates were analyzed using mass spectrometry-based proteome analysis (N=4). As shown before Western blot analysis revealed that brain homogenates of *iRhom1*$^{4\text{-}11/4\text{-}11}$ mice lack mature ADAM17 (Figure 30b) indicating that in most brain cells ADAM17 is inactive. However, little remaining ADAM17 activity cannot be excluded and may contribute to the CSF secretome composition e.g. due to cells expressing iRHOM2. In total, eleven single-pass transmembrane or GPI-anchored proteins revealed significant reduction down to 50% (Figure 32a+b) in the CSF of *iRhom1*$^{4\text{-}11/4\text{-}11}$ mice compared to wildtype mice. In order to validate the quality of the CSF analysis, the localization of all quantified proteins (at least 3 of 4 biological replicates in one group) was determined according to UniProt annotations/keywords. Most of the quantified proteins were either annotated as secreted or membrane protein confirming the quality of the CSF samples (Figure 32c). Moreover, the identified peptides of ADAM17 substrate candidates were exclusively mapped to their protein domains using QARIP (Ivankov et al., 2013). The fact that all peptides were allocated to the extracellular domain and not to the cytotail or transmembrane domains strengthens the hypothesis that shed ectodomains rather than full-length proteins were quantified in the CSF samples (Figure 32d). Noteworthy, LAG3 an α-synuclein receptor linked to Parkinson's disease (Li et al., 2007), VCAM1 (Garton et al., 2003) and the AD-risk gene TREM2 (Feuerbach et al., 2017; Schlepckow et al., 2017) were published before to be proteolytically processed by ADMA17 and were also identified as ADAM17 substrate candidates (Figure 32b). In addition, MEGF10, which was also identified in neurons as ADAM17 substrate candidate (Table 10) and other novel substrate candidates were elucidated, such as the endocytosis receptor MRC2, the ephrin receptor EPHB6, the low-density lipoprotein receptor LDLR, the synapse protein NPTXR and the neuronal cell adhesion protein NCAM2 (UniProt Consortium, 2018). Of note, when using the hiSPECS secretome resource (Figure 12) to trace back the cellular origin of the

substrate candidates a very diverse picture including all cell types was drawn (e.g. TREM2/LAG3 microglia specific, NCAM2 oligodendrocyte specific, NPTXR/B4GALNT1 neuron specific; Figure 32b), which underlines the hypothesis that *iRhom1*$^{4\text{-}11/4\text{-}11}$ mice lack ADAM17 in most brain cells.

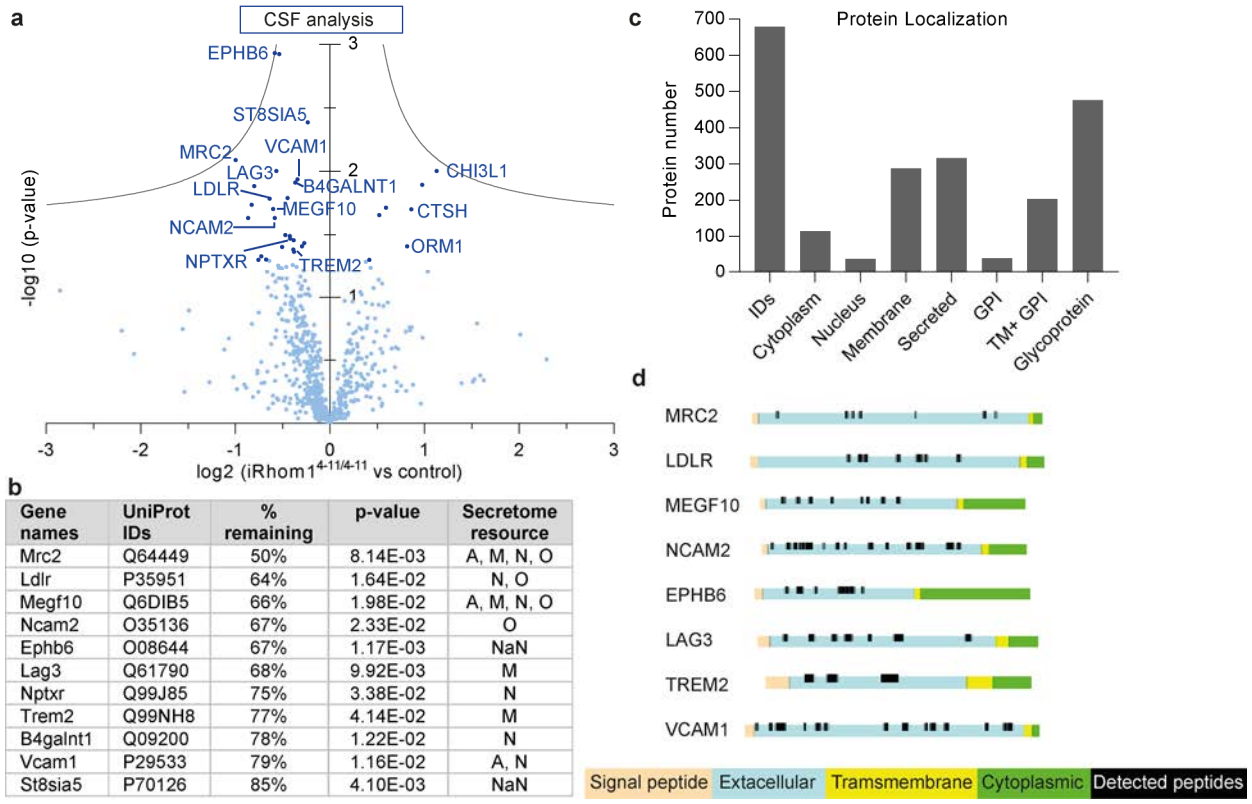

b

Gene names	UniProt IDs	% remaining	p-value	Secretome resource
Mrc2	Q64449	50%	8.14E-03	A, M, N, O
Ldlr	P35951	64%	1.64E-02	N, O
Megf10	Q6DIB5	66%	1.98E-02	A, M, N, O
Ncam2	O35136	67%	2.33E-02	O
Ephb6	O08644	67%	1.17E-03	NaN
Lag3	Q61790	68%	9.92E-03	M
Nptxr	Q99J85	75%	3.38E-02	N
Trem2	Q99NH8	77%	4.14E-02	M
B4galnt1	Q09200	78%	1.22E-02	N
Vcam1	P29533	79%	1.16E-02	A, N
St8sia5	P70126	85%	4.10E-03	NaN

Figure 32 CSF analysis of *iRhom1*$^{4\text{-}11/4\text{-}11}$ mice. a) Volcano plot depicting the protein abundance changes between the CSF of 3 months old *iRhom1*$^{4\text{-}11/4\text{-}11}$ vs. wildtype mice. The fold change (log2) is plotted against the p-value (negative log10) with dark blue dots indicating significant regulation meaning a p-value below 0.05. Hyperbolic selection curves colored in grey illustrate a permutation-based false discovery rate (FDR) estimate of 5% (N=4). **b)** List of potential ADAM17 substrate candidates based on significant downregulation of single-pass transmembrane or GPI-anchored proteins in a). Indicated are gene name, UniProt ID, percentage reaming in *iRhom1*$^{4\text{-}11/4\text{-}11}$ CSF, p-value (t-test), and the cell types are indicated in which they were detected in the hiSPECS secretome resource. A: astrocytes, M: microglia, N: neurons, O: oligodendrocytes **c)** Bar chart indicating the quantified proteins (min. 3/4 biological replicates) and their allocation according to UniProt in the in the CSF samples. **d)** Peptide (black) of ADAM17 substrate candidates of b) identified in the CSF analysis and their localization within the different protein domains: signal peptides (beige), extracellular (blue), transmembrane (yellow) and cytoplasmic (green). All peptides could be allocated to the extracellular domain which suggests a release by ectodomain shedding rather than full-length protein release into the CSF.

In the next step, alkaline phosphatase (AP) assays were performed on selected substrate candidates of the *in vitro* and *in vivo* secretome screens to gain independent evidence that the candidates identified are ADAM17 substrates. Substrates fused to an N-terminal AP-tag were overexpressed in *ADAM17*$^{-/-}$ or wildtype MEFs. AP activity was measured in the supernatant and lysates to normalize for expression differences. The signal of cells treated for 45 min with PMA was normalized to non-treated controls. Interestingly, all six candidates tested revealed an increase upon PMA-stimulation in wildtype but not

ADAM17 deficient MEFs (Figure 33a). Together, the AP-assay confirmed that MRC2, EPHB5, SORL1, MEGF10, TREM2 and SEMA5B as ADAM17 substrates in a PMA-stimulated manner.

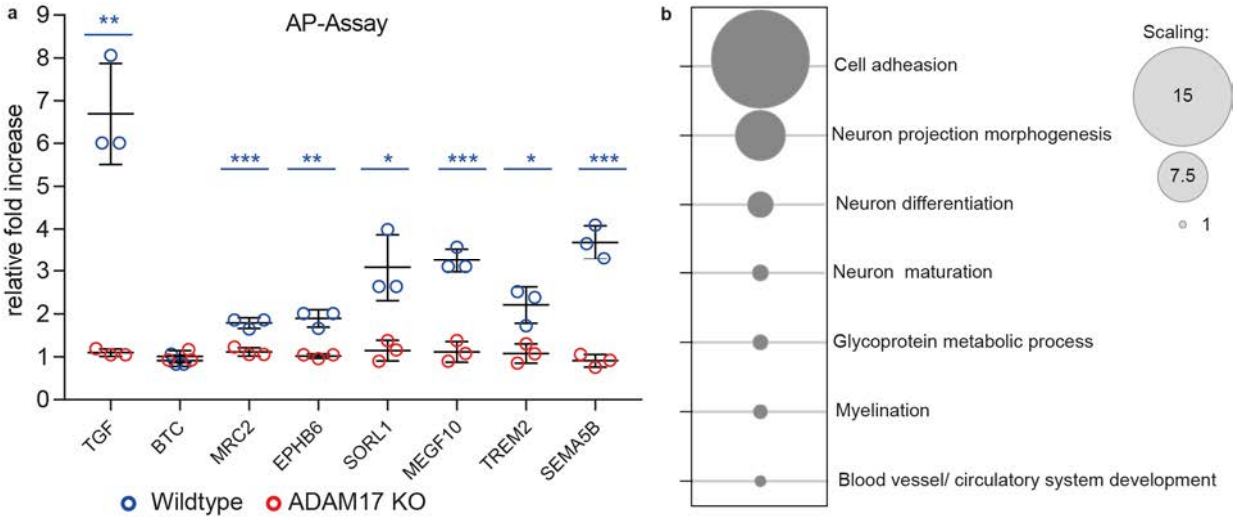

Figure 33 Validation of ADAM17 substrate candidates. a) ADAM17 KO (red) or wildtype (blue) MEFs overexpressing AP-tagged substrate candidates with or without 45 min PMA treatment (N=3). AP activity in the supernatant was normalized to the lysate expression level and relative to samples without PMA treatment. None of the ADAM17 KO samples showed significant difference. TGFα (p=1.13E-03), MRC2 (p=3.75E-04), EPHB6 (p=1.49E-03), SORL1 (p=9.65E-03), MEGF10 (p=1.42E-04), TREM2 (p=7.99E-03) and SEMA5B (p=2.9E-04) reveal significantly increased levels upon PMA treatment (unpaired t-test). **b)** GO analysis by functional annotation clustering of the proteins identified as potential ADAM17 substrate candidates in the secretome analysis of primary neurons and astrocytes and CSF analysis (Figure 31, Figure 32, **Figure 32**) compared to the whole mouse proteome (background) for the term biological process (FAT) using DAVID 6.8 (Huang da et al., 2009a, b). Enrichment scores are mirrored in the dot size

In order to estimate the physiological significance of the shedding events by ADAM17 in the brain, a pathway analysis of all identified ADAM17 substrate candidates *in vitro* and *in vivo* was performed. Using the GO term biological process and the murine proteome as background revealed the most enriched term to be cell adhesion, followed by neuron projection morphogenesis, neuron differentiation and maturation, glycoprotein metabolic process, myelination and blood vessel/circulatory system development (Figure 33b).

In summary, the newly established hiSPECS DIA method was applied to elucidate ADAM17 substrate in primary neurons and astrocytes. Together with the CSF analysis of *iRhom1*$^{4\text{-}11/4\text{-}11}$ mice, this thesis sheds light for the first time onto the overall substrate repertoire of ADAM17 in the brain and lays the foundation to study the physiological significance of these shedding events in a targeted and substrate dependent manner.

4.9 Evaluating ADAM17-dependent neuronal morphology changes

The majority of ADAM17 substrate candidates have been linked to cell adhesion and several of those to neuronal morphogenesis including proteins such as NEO1, RGMA and the semaphorin family members. Moreover ADAM17 has previously been shown to regulate neurite outgrowth by cleaving NCAM1 (Kalus et al., 2006). In order to evaluate the effect of ADAM17 on neuron morphology changes, Sholl analysis was performed. Sholl analysis is based on sparse labeling of neurons in order to trace all neurites belonging to a single neuron. Next, the soma of the neuron is defined as the center and concentric circles apart by 10-µm each are computed and the intersections with a total of 10 circles (100 µm) automatically determined using ImageJ software. In this thesis, primary hippocampal neurons lacking ADAM17 were compared to control neurons by Sholl analysis. First, the neurons were isolated from ADAM17flox/flox embryos (E16.5) and transfected with CRE-GFP to knockout ADAM17 or only GFP as control construct using calcium phosphate transfection at DIV1. In this manner only single cells are transfected to a high degree which enables morphological analysis of single neurons without crossing with the adjacent GFP-positive neurons. Cells were fixed DIV7 and the Sholl morphology analysis was conducted of a total of three biological replicates (exemplary images shown in Figure 34a). To illustrate neuritic complexity, a Sholl profile was constructed by plotting the average number of intersections of neurites against the distance of the circles from the center of the soma (Figure 34b+c). Using this elaborate and detailed analysis no significant difference between neurons expressing or lacking ADAM17 could be established under the experimental conditions. Further analysis may be required to pinpoint minor changes which can be not evaluated using the applied basic Sholl analysis.

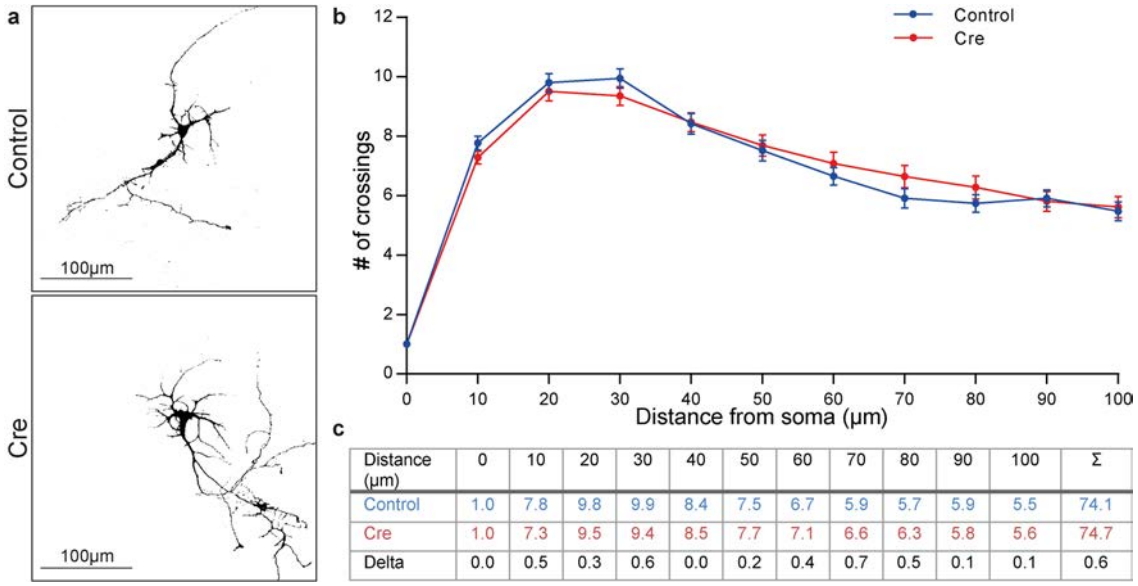

c

Distance (µm)	0	10	20	30	40	50	60	70	80	90	100	Σ
Control	1.0	7.8	9.8	9.9	8.4	7.5	6.7	5.9	5.7	5.9	5.5	74.1
Cre	1.0	7.3	9.5	9.4	8.5	7.7	7.1	6.6	6.3	5.8	5.6	74.7
Delta	0.0	0.5	0.3	0.6	0.0	0.2	0.4	0.7	0.5	0.1	0.1	0.6

Figure 34 Sholl analysis of control neurons and neurons lacking ADAM17. a) Representative thresholder pictures of hippocampal neurons transfected with Cre recombinase causing the knockdown of ADAM17 or a control plasmid at 6DIV. The soma of the neuron was set as center for the Sholl analysis. **b-c)** Sholl analysis profiles of control (N=162) and Cre neurons (N=168) originating from three different biological replicates. The average number of crossings is plotted against the distance from the soma (µm) which were measured every 10µm up to a distance of 100µm. The error bars indicate the SEM.

4.10 Discovering the brain vessel proteome of *iRhom1*$^{4\text{-}11/4\text{-}11}$ mice

Finally, we aimed to evaluate the role of iRHOM1/ADAM17 in the brain vasculature. In a publicly available resource of single cell RNA-sequencing data of brain cells associated with vasculature by the Betsholtz laboratory (Vanlandewijck et al., 2018) (He et al., 2018), iRHOM1 and ADAM17 revealed high expression in pericytes, smooth muscle cells, vascular fibroblasts-like cells, endothelial cells and astrocytes. In contrast, iRHOM2 seemed to be exclusively expressed in endothelial cells. Taking advantage of the β-galactosidase (β-GAL) reporter expressed under control of the iRHOM1 promoter in *iRhom1*$^{4\text{-}11/4\text{-}11}$ mice revealed high expression around blood vessels in immunofluorescence (IF) staining of brain sections. Interestingly, the reporter signal co-localized with the astrocyte marker GFAP (Figure 35a). Together those expression data led us to the hypothesis that ADAM17 maturation in brain vessels is mainly dependent on iRHOM1 except endothelial cells and that *iRhom1*$^{4\text{-}11/4\text{-}11}$ vessels may be affected in an ADAM17-activity dependent manner. To this end, brain vessels were isolated from *iRhom1*$^{4\text{-}11/4\text{-}11}$ and control littermates according to an established protocol (Zellner et al., 2018). Whole proteome analysis by mass spectrometry, revealed pronounced protein abundance changes in the vessels derived from *iRhom1*$^{4\text{-}11/4\text{-}11}$ mice (Figure 35b). iRHOM1 peptides were exclusively found in the vessel proteome of control mice

confirming the setup of the experiment. Interestingly, the ADAM17 protein abundance was reduced by 30% which might point towards a stabilizing function of iRHOM1. Several proteins including the myosin family members MYH1, MYH2 and MYH8 were strongly reduced in *iRhom1*$^{4\text{-}11/4\text{-}11}$ vessels (Figure 35c). GO term enrichment analysis of the significantly regulated proteins revealed terms such as muscle contraction and cytoskeletal organization, whereas KEGG pathway analysis pointed out tight junction as the major enriched term (Figure 35d). Together, the expression analysis and the dramatic vessel proteome changes suggest major functions of iRHOM1/ADAM17 in brain vessels. This groundwork may lay the foundation for exciting follow-up experiments to unravel the mechanism controlled by iRHOM1/ADAM17 in the brain vasculature and physiological significant functions such as the maintenance of the blood brain barrier.

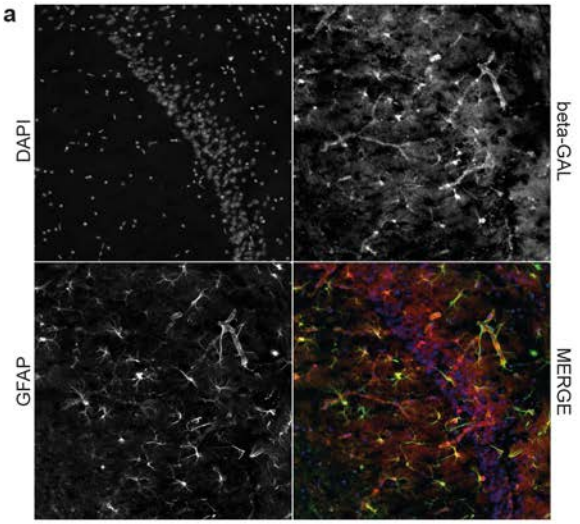

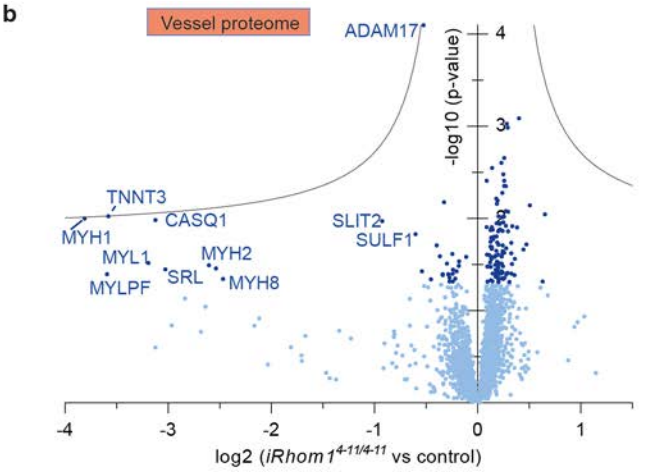

Timm22 only detected in *iRhom1*$^{4\text{-}11/4\text{-}11}$ samples
APOBEC2, CA3, CXXC1, D17H6S53E, GCSG, iRHOM1, KLHL41, MAP2K2, NSUN2, PICK1, PUM2, , RPS6KA3, SYNPO2, TAF6, USP24
only detected in control samples

c

Gene name	UniProt AC	% remaining	p-value
Myh1	Q5SX40	7%	9.97E-03
Mylpf	P97457	8%	4.01E-02
Tnnt3	Q9QZ47	8%	9.46E-03
Myl1	P05977	11%	3.02E-02
Casq1	O09165	11%	1.03E-02
Srl	Q7TQ48	12%	3.57E-02
Myh2	G3UW82	16%	3.19E-02
Acta1	P68134	17%	3.46E-02
Myh8	P13542	18%	4.53E-02
Slit2	Q9R1B9	53%	1.06E-02
Sulf1	Q8K007	66%	1.47E-02
Sema3f	O88632	69%	3.73E-02
Adam17	Q9Z0F8	70%	7.99E-05
Fam129a	Q3UW53	73%	4.53E-02

d

GOterm	Enrichment score	Key Term
BP_FAT	6.97	Muscle system process
BP_FAT	2.13	Muscle contraction
BP_FAT	1.34	Regulation of muscle contraction
BP_FAT	1.13	Cytoskeleton organization
CC_FAT	6.49	Mycofibril, contractile fiber
CC_FAT	0.68	Ribonucleoprotein complex
CC_FAT	0.67	Endoplasmic reticulum
MF_FAT	1.36	Ion binding
MF_FAT	1.03	Cytoskeletal protein binding
MF_FAT	0.43	Motor activity
KEGG		Tight junction (Myh1, Myh2, Myh8)

Figure 35 Brain vessel proteome of *iRhom1*$^{4\text{-}11/4\text{-}11}$ mice. a) Staining of *iRhom1*$^{4\text{-}11/4\text{-}11}$ brain sections for nuclei (using DAPI), GFAP (astrocyte marker), β-galactosidase (iRHOM1 expression reporter) reveals high iRHOM1 levels in astrocytes. **b)** Volcano plot depicting the protein abundance changes in the brain vessel proteome of *iRhom1*$^{4\text{-}11/4\text{-}11}$ vs. control mice (3 months old, N=6). The fold change (log2) is plotted against the p-value (negative log10) with dark blue dots indicating significant regulation (p-value <0.05). Hyperbolic selection curves colored in grey illustrate a permutation-based FDR estimate of 5%. **c)** List of proteins significantly downregulated in *iRhom1*$^{4\text{-}11/4\text{-}11}$ vessels. **d)** GO/KEGG analysis by functional annotation clustering of the significantly altered proteins compared to all proteins quantified for the indicated terms by DAVID 6.8 (Huang da et al., 2009a, b).

5 DISCUSSION

This thesis can be summarized into three major topics, that will be discussed in separate sections, i) optimization of the hiSPECS method ii) establishment of the hiSPECS secretome resource and iii) evaluation of the brain function of ADAM17.

5.1 Chances and limitations of secretome analysis

So far, proteomic secretome analyses of primary cells could only be achieved by either using laborious sample preparation, or by excluding protein supplements from the culture media (Schira-Heinen et al., 2019). However, exclusion of media supplements, such as FBS or B27, has been shown to trigger a stress response inducing dramatic changes in the expression profile and alters the secretome composition in a rapid manner (Eichelbaum et al., 2012). In order to circumvent the starvation mediated changes, two methods have been introduced in the past which rely on click chemistry-mediated enrichment of cell derived proteins. Yet, both methods require more than 10 Million cells as input material and a high degree of fractionation either on protein or on peptide level (Eichelbaum et al., 2012; Kuhn et al., 2012). Moreover, the method introduced by Eichelbaum et al. was based on the incorporation of the artificial amino acid azidohomoalanine, a cost intensive and potentially toxic approach (Eichelbaum et al., 2012). Therefore, the scope of this thesis was to optimize the SPECS method, which was previously published by our laboratory, to enable single-shot secretome analysis in a highly efficient manner.

Establishment of the new hiSPECS protocol allowed miniaturization while increasing proteome coverage. Skipping the fractionation steps greatly improved the reproducibility of the secretome analysis and reduced measurement time on the mass spectrometer by 5-fold while allowing highly parallelized sample preparation of up to 24 samples. Moreover, the simplicity of the protocol and the cost-efficient measurement time makes hiSPECS also a useful tool for researchers not specialized on mass spectrometry to study the secretome which can simply measure their samples of interest in their mass spectrometry facility of choice. Most importantly, the cell number required for each biological replicate was dramatically reduced from 40 to 1 Million cells. This makes hiSPECS secretome analysis also a suitable method to study secretion of less abundant cell types in the brain such as microglia of which around 1 Million cells can be isolated

from an adult mouse brain. Moreover, it enables to study secretion differences in a brain-region resolved manner e.g. neurons isolated from the hippocampus to cerebral cortex. Moreover, it can be used to elucidate the substrate repertoire of membrane bound proteases such as BACE1 and ADAM17 under physiological-like cell culture conditions. Additionally, hiSPECS is able to elaborate the secretome of brain slices and detect secretome changes upon stimulation with e.g. LPS. Altogether, the benchmarking of the newly established hiSPECS to the previous published SPECS method highlighted the superiority of hiSPECS in regard of proteome coverage while miniaturizing resources. We are optimistic that in the future hiSPECS can be applied to study the secretome of low abundant cell types, elaborate the substrate repertoire of additional proteases in a cell type-specific manner and help to study systematic mechanism which control secretion.

Even though hiSPECS greatly improved secretome analysis, optimization is a continuous process and it is important to highlight the limitations of the technique in order to achieve further progress and potential further miniaturization in the future. hiSPECS is blind to secretome proteins which fail to incorporate the ManNAz sugar as azido modified sialic acid into their glycotrees. Although most secretome proteins were shown to be glycosylated (Kuhn et al., 2016) it might be of advantage to label not only sialic acid-carrying glycoproteins with ManNAz, but additionally use click-able sugar derivatives such as GlcNAz, or GalNAz which target O-linked glycoproteins. Moreover, using an additional lectin e.g. wheat germ agglutinin (WGA) together with ConA may allow better enrichment of the target proteins (Zielinska et al., 2010). Furthermore, additional studies are required which focus on glycosylation of brain cell types which may unravel systematic differences in their structure and function and may potentially uncover an influence on the labeling efficiency with e.g. ManNAz between the cell types. A recent study focusing on sialyation *in vivo* published a list of proteins which carry a sialic acid, including CADM4, NEO1, TF, MUG1 and CTSB (Li et al., 2019). These proteins were found to be robustly secreted from neurons, astrocytes, microglia and oligodendrocytes in our secretome resource. This finding provides evidence that sialyation of glycoproteins is present in all cell types, however, we cannot rule out minor systematic differences in the glycosylation pattern of brain cells. A dedicated glycomics analysis of cultured brain cell types would have to be employed to investigate general differences in glycosylation.

Noteworthy, our results show that DIA outperforms DDA in regard of proteome coverage in secretome and CSF analysis, an observation especially pronounced in the low abundant protein range. The usage of custom made libraries, as the ones prepared in our study, containing fragmentation and retention time information of DDA analyses of similar sample types were shown to achieve the best results (Ludwig et al., 2018). In contrast, large libraries aiming for complete proteome coverage of the organism/tissue of interest were shown to reduce reproducibility and peptide count. Likely true signals are lost due to multiple testing corrections leading to an enlarged number of false negatives (Muntel et al., 2015). Generally, improvements of this custom library in regard e.g. of completeness or reproducibility allows reanalysis of the DIA data and may gain deeper proteome coverage to a later time point. One potential path, which might be able to boost the peptides detected per protein, would be the integration of computationally predicted fragmentation spectra information (Gessulat et al., 2019) of identified proteins. This would be especially interesting for proteins identified with only one unique peptide and could result in a more reliable protein quantification. Moreover, combined quantification on MS1 and MS2 level has been recently shown to improve DIA quantification (Huang et al., 2020). Recently, new algorithms such as DIA umpire or DirectDIA were developed which overcome the requirement of spectral libraries. These algorithms extract pseudo MS/MS spectra through peak alignment of precursor *m/z* signals from MS1 scans with peptide fragment *m/z* signals in the corresponding DIA fragmentation window. Precursor and fragment ions with a perfect retention time overlap are used to generate pseudo MS/MS spectra for conventional database searches (Muntel et al., 2019). The ongoing optimizing of those algorithms may potentially yield in enhanced protein quantification based on library-free DIA. Thereby it may overcome the to date biggest drawback of DIA analyses which is the need of preparing customized libraries in order to gain deep proteome coverage whose preparation is time and cost intensive.

Even though we could significantly improve the sensitivity of secretome analysis with hiSPECS, the low protein amounts are still a limiting factor for mass spectrometric analysis. In this regard, advances in data analysis and mass spectrometer instruments, such as hybrid ion mobility mass spectrometers (Meier et al., 2018), will further improve the sensitivity of our hiSPECS method. Recently developed mass spectrometers such as the Bruker TimsTOF pro or the Exploris 480 mass spectrometers show substantially

improved sensitivity and potentially will facilitate even better results (Zhang et al., 2020). Together, technical improvements of the mass spectrometer and the DIA analysis as well as more efficient enrichment of the secreted target proteins has the potential to further miniaturize the cell number required to study the secretome.

5.2 Systematic analysis of the hiSPECS secretome resource

In the scope of this thesis, we determined the secretome of neurons, microglia, astrocytes and oligodendrocytes, which are the four most dominant brain cell types, using the newly established hiSPECS DIA method. Previous studies have described the secretome of brain cells, however most studies were either restricted to cell lines (Eichelbaum et al., 2014; Nijaguna et al., 2015; Tsumagari et al., 2017; Woo et al., 2015) or conducted under starvation conditions meaning without media supplements (Brown et al., 2013; Meissner et al., 2013; Skorupa et al., 2013; Stiess et al., 2015; Zhou et al., 2012). This study, elaborated for the first time a brain secretome resource by analyzing and comparing the secretion of the four major brain cell types using primary murine cell cultures in a standardized manner.

Systematic analysis of the mouse brain secretome resource provided new insights into cell-type resolved secretion differences. To evaluate the similarity of protein quantification between biological replicates of the same cell type but also between different cell types, a correlation analysis based on Pearson correlation coefficients of the log2 transformed LFQ intensities was employed. This analysis showed a high correlation between biological replicates of the same cell type validating the robustness of the hiSPECS method and the general experimental setup. Furthermore, the relatively higher correlation between oligodendrocyte and astrocyte secretome indicate a closer relationship, which may be explained by their common origin from the same linage during development (Hirano et al., 1988) - a phenomenon also observed in whole lysate analysis by (Sharma et al., 2015). In contrast, the neuronal secretome correlated least to the other glia cell types. While soluble secreted proteins in general revealed a higher abundance in the secretome compared to shed ectodomains, the shedding event itself was remarkably more pronounced in neurons compared to glia cells. The unique secretion pattern of each cell type which included proteins specifically secreted from one cell type (>5-fold enriched or exclusively secreted from one cell type) were used to trace the cell type of origin of the identified CSF proteins and to pinpoint the cellular response of brain slices upon LPS

treatment. Moreover, around 42% of the quantified proteins in the resource were secreted in a cell type specific manner (5-fold in a pairwise comparison or quantified in only one secretome) indicating a unique secretome finger print.

5.3 Mechanisms controlling cell type specific protein secretion

To understand to which extent protein abundance levels within the cells were mirrored in their secretomes, the secretome data were compared to a previous study (Sharma et al., 2015), which determined the cellular proteome of the same brain cell types. Surprisingly, specific secretion of a protein went hand in hand with specific expression of the protein only in about 10-50% of the cases depending on the cell type. This indicates, that additional mechanisms must be in place controlling cell type specific secretion. One mechanism further analyzed in this study, which can at least explain specific secretion of ectodomains, was the cell type selective expression of the responsible proteases. To this end, the substrate repertoire of BACE1 was determined in primary neurons, the cell type BACE1 is predominantly expressed in (Voytyuk et al., 2018). Two examples strengthening our hypothesis of cell type-specific secretion due to specific expression of the protease were CACHD1 and APLP1, which were ubiquitously present in all cell lysates of the analyzed brain cell types but were specifically secreted from neurons. This mechanism, however, explains cell specific secretion of shed ectodomains only of a small fraction of proteins. Additional regulator proteins such as iRHOMs for ADAM17 and TSPANs for ADAM10, which are responsible for the activation/maturation of the ADAM proteases, have been suggested to influence the substrate accessibility and cleavage rate (Koo et al., 2020; Maretzky et al., 2013; Matthews et al., 2017). Moreover, the responsible proteases of most transmembrane proteins remains elusive and future studies are needed to shed light on their unique substrate repertoire. Additionally it would be interesting to know to which extent proteins are cleaved by different proteases – a phenomenon observed for APP (Lichtenthaler et al., 2018). However, hiSPECS is not suitable to study the cleavage of one substrate by several proteases because it only quantifies the total protein ectodomain in the supernatant and does not distinguish e.g. by different cleavage sites. To this end, a method named TAILS (terminal amine isotopic labeling of substrates) would be suitable to use and might be a fruitful add-on to the hiSPECS analysis to determine protease cleavage sites (Kleifeld et al., 2010; Kleifeld et al., 2011; Schlage et al., 2015).

In general, mechanisms controlling the passage of certain proteins trough the secretory pathway may explain cell type-specific secretion. For example, CAB45 was shown to be required for trafficking of specific proteins through the TGN (Blank et al., 2017). Moreover, anchor proteins have been described such as the retention in endoplasmic reticulum 1 (RER1) protein, which retain binding partners such as subunits of the γ-secretase and potentially APP in the ER (Park et al., 2012). Other proteins such as the newly validated BACE1 substrate ADAM22 have been shown to contain sequence motifs in their cytotail, which mediate 14-3-3 protein binding and are required for ADAM22 to pass the TGN and reach the cell surface (Gödde et al., 2006). Cell-type specific expression of these trafficking proteins may explain cell type specific secretion patterns observed in our resource. However, little is known and further studies are needed to explore mechanisms controlling these interesting phenomenon potentially triggering secretion differences. The novel hiSPECS methods now facilitates to study the underlying mechanisms of protein shedding in detail due to the increased sensitivity and higher throughput. Potentially, the investigation of knockout, knockdown or inhibition of membrane-bound protease and their modulators with hiSPECS will improve the general understanding of shedding in the near future.

5.4 ADAM22 and CD200 are two new BACE1 substrates

After setting up the hiSPECS method we have applied it to investigate the substrate repertoire of BACE1 in primary murine neurons. BACE1 is a major drug target in AD research because its inhibition lowers the formation of Aβ peptides. However, inhibitors tested in clinical trials were terminated because of severe side effects (Hampel et al., 2020; Imbimbo et al., 2019). Therefore, it is essential to understand the overall substrate repertoire of BACE1 in order to evaluate these inhibitors and potential prevent side effects in the future. Previously, BACE1 has been shown to cleave a broad spectrum of substrates. Proteomic studies have identified more than 40 substrate candidates involved in diverse cellular functions including SEZ6, SEZ6L, CHL1 and APP (Dislich et al., 2015; Kuhn et al., 2012; Stutzer et al., 2013; Zhou et al., 2012). In this study, neurons have been treated with the BACE inhibitor C3, which is known to inhibit BACE1 and BACE2. The latter however, is not expressed in neurons and thereby changes determined in the neuronal secretome using the hiSPECS DIA method were accounted to the loss of BACE1 cleavage. Of note, we identified several known BACE1 substrates found in

previous proteomic studies of neurons or CSF which validated our experimental approach including APLP1, CACHD1, CHL1, CNTN2, FGFR1, GLG1, LRRN1, PLXDC2, SEEMA4B, SEZ6 and SEZ6L. On top, we identified 20 new BACE1 substrate candidates in primary neurons, for example CD200 and ADAM22 revealed strong reduction in the secretome upon C3 inhibition and were further validated as BACE1 substrate using independent methods such as Western blot analysis and ELISA. Noteworthy, the soluble ectodomain of ADAM22 runs on SDS-PAGE at a molecular weight of about 60 kDa which might have been the reason why it was not robustly detected using the old SPECS protocol because this particular area needed to be excluded from the MS analyses due to high albumin contamination. All in all, ADAM22 and CD200 can now be added to the long list of validated neuronal BACE1 substrates.

ADAM22, a proteolytically inactive ADAM family member, was shown to bind LGI1 and the postsynaptic density protein 95 (PSD95). Thereby, it controls AMPA receptor surface levels and plays a role in synapse maturation and epilepsy (Fukata et al., 2006; Gödde et al., 2006; Hsia et al., 2019; Sagane et al., 2005). On the other hand, CD200 was determined to have an anti-inflammatory effect on microglia by binding to its receptor CD200R1 which is exclusively expressed in immune cells (Chen et al., 2008; Yi et al., 2016). Further studies will be required to determine, if only the full-length proteins on the cell surface are biologically active or if on top the shed ectodomains of CD200 and ADAM22 carry potentially different biological activity. This phenomenon has been observed for other substrates e.g. TNFα, where the soluble ectodomain triggers pro-inflammatory signaling and the full length acts rather anti-inflammatory (Black et al., 1997; Grell, 1995). Meaning the biological task in the cell may be different for the full-length CD200/ADAM22 compared to the released soluble ectodomains. Hypothetically, the cell adhesion function of ADAM22 is likely to be terminated by the shedding event. In contrast, its binding to LGI1 in the synaptic cleft might remain. On the other hand, soluble CD200 was shown to maintain the binding ability to its sole receptor CD200R1 (Frank et al., 2018; Walker et al., 2013). However, future studies will have to elaborate if the soluble ectodomain or only the full-length CD200 can activate CD200R1 and trigger its phosphorylation. Alternatively, the soluble ectodomain might act as a decoy cue which prevents full-length CD200 binding and downstream signaling. Of note, the intracellular domain of CD200 released upon γ-secretase cleavage was shown to regulate

transcription in neurons (Chen et al., 2018). Importantly, γ-secretase substrates with an ectodomain of approximately more than 100 amino acids require an initial cleavage step by another protease to make it accessible for γ-secretase (Güner et al., 2020), meaning that BACE1 cleavage of CD200 might be the initial trigger for downstream transcriptional regulation. Altogether, further studies are required to pinpoint the function of CD200/ADAM22 cleavage by BACE1 and the influence on microglia activation or synapse maturation. These studies may potentially help to explain and prevent side effects observed in clinical trials evaluating BACE1 inhibitors as Alzheimer's disease therapy strategy (Hsiao et al., 2019).

5.5 Tracing the cellular origin of secreted proteins from brain slices and in CSF

In humans, CSF is the body-fluid of choice for biomarker research aiming to reflect the health or disease state of the brain e.g. during the progression of neurodegenerative diseases such as AD (Bader et al., 2020; Bai et al., 2020; Ewers et al., 2019; Johnson et al., 2020; Llibre-Guerra et al., 2019; Sathe et al., 2019; Schindler et al., 2019; Whelan et al., 2019). Nowadays, the ratio of Aβ species and phosphorylated tau are measured in patient CSF samples to diagnose AD (Budelier et al., 2019). However, early diagnosis of AD remains difficult and the urgent need for better biomarkers are the reason for several large-scale proteomic studies to determine the whole proteome changes in patient CSF using mass spectrometry (Bader et al., 2020; Bai et al., 2020; Johnson et al., 2020; Sathe et al., 2019; Whelan et al., 2019). Decades of research focusing on the processing of APP by different proteases contributed to the knowledge of the origin of the different Aβ species (Budelier et al., 2019). In contrast, the origin of newly suggested biomarkers such as CD44 (Johnson et al., 2020) often remains elusive. This problem is not limited to AD, but also other biomarker studies of other brain diseases lack this fundamental information. Moreover, studies of transgenic mice revealing alterations in the CSF composition may be hampered my missing the cellular origin. Therefore, determining the cellular origin of CSF proteins of interest has the potential to pinpoint the affected cell types and to accelerate detailed follow-up studies which may unravel the cause of the particular protein abundance change.

To this end, we analyzed the CSF of wildtype mice and used the secretome resource to trace back the origin of CSF proteins. Overall, the cellular origin of around 65% of the

quantified CSF glycoproteins were assessed including the newly proposed AD biomarker CD44 (Johnson et al., 2020). While revealing high protein abundance in the lysates of astrocytes, microglia and to a lower extent in oligodendrocytes (Sharma et al., 2015), we found CD44 to be selectively secreted from oligodendrocytes. We are convinced that future studies, not only on CD44 but also other CSF proteins of elusive origin, may greatly benefit from our secretome resource which will help to target the most appropriate cell type for future analysis or potentially pharmacological targeting.

To the best of our knowledge, this secretome study provides the most complete resource to determine the cellular origin of CSF proteins. Nevertheless, it is only a first mile stone and further studies are required to draw a more complete picture of brain cell secretion. As discussed before, hiSPECS is blind to proteins without glycosylation. Moreover, the CSF is also influenced by the periphery e.g. by blood proteins passing the blood brain barrier. Furthermore, the secretome resource itself lacks the information of low abundant cell types such as those of the choroid plexus, which is the source of CSF (Lun et al., 2015), including e.g. pericytes. The resource is also missing brain region-specific differences, for example, neurons from the cerebellum likely secrete different proteins than hippocampal neurons. Moreover, the secretome may very well be influenced by the maturation and activation state of the cells and alter during ageing or upon stimulation e.g. with inflammatory stimuli. In addition, co-culture of astrocytes and neurons was shown before to alter their secretome composition (Stiess et al., 2015). To this end, secretome analysis of co-cultured cell might be highly informative in the future. However, to elucidate which secreted protein is released from which cell type in the co-culture an additional e.g. SILAC labeling step would be required. Finally, we have analyzed cultivated cells which are only an estimate of the *in vivo* situation and previous publications clearly showed that expression profiles of primary cells changed upon cultivation (Sharma et al., 2015). Ideally the cellular origin of CSF proteins would be traced back in the living animal in which the cellular network maintain intact using protein labeling in a specific cell type, however, until today this is not possible due to technical hurdles.

One way to maintain cells in their complex multicellular network is the usage of *ex vivo* brain slices. In this study, we showed that hiSPECS DIA was suitable to determine the secretome of organotypic cortico-hippocampal brain slices. Moreover, we elaborated to

which extent the different brain cell types contribute to the secretome. Thereby, we determined a predominant role of proteins released by oligodendrocytes considering the 25% most abundant secretome proteins. To understand how the secretome would change under inflammatory conditions, the brain slices were treated with LPS. Interestingly, proteins shown to be specifically secreted in the secretome resource from a particular cell type revealed a dramatic upregulation upon LPS treatment including proteins of neuronal, astrocytic, microglia and oligodendrocytic origin. This indicates that not only the brain immune cells, microglia, revealed a strong inflammation response but also neurons and oligodendrocytes. However, further studies are required to distinguish between primary and secondary effects meaning if for example, the upregulation of neuronal proteins was a direct effect of LPS or a secondary effect caused by inflammatory microglia and the release of cytokines or other signaling proteins. It is also not known if the LPS treatment shifts the secretion/expression profile of a certain cell type in a way that cells upregulate the secretion of certain proteins which would be not datable in the secretome under non-inflammatory conditions for example in our secretome resource.

5.6 iRHOM1 - the major regulator of ADAM17 in the brain

Next, we investigated the role of ADAM17 in neurons and astrocytes. While many studies are focused on immune cells such as macrophages, the role of ADAM17 is hardly studied in brain cells. In this context, iRHOM1 has previously been suggested as the major regulator of ADAM17 in the brain due to the lack of mature ADAM17 in brain lysates of *iRhom1*$^{4\text{-}11/4\text{-}11}$ mice (Li et al., 2015). Therefore, we first investigated the expression of iRHOM1 and iRHOM2 in the brains using X-gal staining (Figure 28). The results of this analysis confirmed and validated the predominant role of iRHOM1 in the brain (Figure 29). The staining revealed high expression of iRHOM1 compared to very limited expression of iRHOM2 in the brain. Interestingly, the expression of iRHOM1 varied in different brain regions and the highest expression was found in cerebellum, olfactory bulb, cerebral cortex and the dentate gyrus of the hippocampus. In the scope of this thesis *iRhom1*$^{4\text{-}11/4\text{-}11}$ samples are used to model the loss of ADAM17 activity in cells not expressing iRHOM2. We hypothesize that this is the case in the majority of brain cells and brain vasculature including neurons, astrocytes, pericytes and smooth muscle cells. However, we cannot exclude a minor iRHOM2 expression in those cell types that is below

the X-gal detection limit. Moreover, most data rely on RNA or reporter gene expression and further studies are needed to verify these findings on the protein level.

As described in detail in the introduction (Figure 4), different iRHOM1 knockout mice have been published revealing different phenotypes. The mice used throughout this thesis developed by (Li et al., 2015) (called *iRhom1*$^{4\text{-}11/4\text{-}11}$) reveal no obvious phenotype, while the mice generated by (Christova et al., 2013) (called *iRHOM1*$^{2\text{-}18/2\text{-}18}$) suffer from premature death and hemorrhages. It is important to highlight that an independent analysis, which recreated these mouse strains using CRISPR Cas9 targeting strategy was uploaded on bioRxiv, a preprint sever, and verified the discrepancy in the phenotypes (Hosur et al., 2020). Further studies are required to understand the molecular mechanism underlying these different phenotypes. One possibility that may cause the discrepancy is that in *iRhom1*$^{4\text{-}11/4\text{-}11}$ mice, a truncated form of iRHOM1 may still remain and it is sufficient for several biological functions in the cells. Alternatively, the remaining RNA in *iRhom1*$^{4\text{-}11/4\text{-}11}$ mice may trigger a compensatory effect on related proteins as described for other mouse models by (El-Brolosy et al., 2019). Together, the discrepancy of the phenotypes may point towards additional functions of iRHOM1 in the cell independent of maturation of ADAM17 and could, for example, include pathways such as ERAD, which was shown to depend on of drosophila iRHOM (Dulloo et al., 2019). We cannot exclude that these mechanisms may influence our study and potentially affect the expression profile of e.g. iRHOM1 in the cells (Figure 28). Therefore, RNA-sequencing analysis comparing the different mouse strains might be informative. In summary, we are far from understanding the mechanism explaining the differences between the iRHOM1 knockout mouse strains published. Therefore, we would like to emphasize that within this thesis *iRhom1*$^{4\text{-}11/4\text{-}11}$ mice were not used to study the loss of the iRHOM1 protein itself but rather used to model loss of ADAM17 activity in cells, where iRHOM2 cannot compensate the loss of iRHOM1 e.g. in neurons. This model is especially interesting because the direct knockout of ADAM17 in mice causes premature death around birth.

5.7 The substrate repertoire of ADAM17 in the brain

So far, more than 80 proteins have been described as ADAM17 substrates, linking it to diverse biological functions ranking from triggering a rapid inflammatory response to basic developmental processes (Zunke et al., 2017). However, little is known about ADAM17 in the brain and to which extent substrates identified in the periphery are also shed by

ADAM17 in the CNS. This study provides the first large-scale proteomic analysis aiming to identify the substrate repertoire of ADAM17 in the brain using secretome analysis of primary neurons, astrocytes and CSF analysis. Several known ADAM17 substrates were detected in the screening, including AXL, ALCAM, GPC1, SEMA5B, SORL1 and VCAM1, verifying the experimental setup. Additionally, more than 50 novel substrate candidates were identified including five semaphorin family members (SEMA4B, SEMA4G, SEMA5A, SEMA6A, SEMA6D). Together with the two known ADAM17 substrates SEMA5B (Browne et al., 2012) and SEMA4D (Zhu et al., 2007), these findings indicate a strong regulatory role of ADAM17 in semaphorin signaling, a protein family known to shape neuronal morphology and axonal outgrowth (Alto et al., 2017).

Using the cell-type resolved secretome resource we traced the cellular origin of significantly reduced proteins in the CSF of *iRhom1*$^{4\text{-}11/4\text{-}11}$ mice. Interestingly, proteins specifically secreted from all four cell types were detected, including e.g. NCAM2 from oligodendrocytes, LAG3 and TREM2 from microglia, NPTXR and B4GALNT1 from neurons and VCAM1 from neurons and astrocytes. On isolated primary cell culture level we only analyzed ADAM17 activity-dependent secretome in neurons and astrocytes (& Figure 31). Hence, we lack the information of isolated oligodendrocytes and future studies will be needed to verify the CSF findings which might be of special interest considering that ADAM17 has been shown before to regulate myelination (Fredrickx et al., 2020; Hsia et al., 2019; Palazuelos et al., 2014; Palazuelos et al., 2015).

On top of the constitutive shedding, we also analyzed ADAM17 dependent shedding upon stimulating neurons or astrocytes with PMA (Figure 30 & Figure 31). Even though PMA is a well-established ADAM17 activator broadly used in the field, these results shall be viewed with caution, because PMA is not a natural stimulus present in humans *in vivo*. Therefore, identification of an ADAM17 specific activator occurring in the brain would likely improve future substrate analysis and verify the *in vivo* relevance of our PMA experiments.

The three new ADAM17 substrate candidates EPHB6, MEGF10 and MRC2 were validated in an independent AP-shedding assay (Figure 33). Previously, EPHB6 was determined to bind to ephrin-B1 and ephrin-B2 and was linked to axon growth cone guidance (Freywald et al., 2003; Matsuoka et al., 2005). MEGF10 was shown to be involved in mosaic spacing (Kay et al., 2012), a receptor for C1Q, crucial in phagocytosis,

and to be required for the clearance of apoptotic cells by astrocytes (Iram et al., 2016). MRC2 (also known as ENDO180), a glycoprotein receptor, was shown to regulate the extracellular matrix and to be involved in endocytosis (Engelholm et al., 2009; Kjøller et al., 2004). Further studies are required to evaluate how iRHOM1/ADAM17 are regulating the diverse functions of three substrates.

AP-shedding assays are commonly used in the field to validate ADAM17 substrates (Maretzky et al., 2013; McIlwain et al., 2012; Tang et al., 2020). In our study, we also applied these assays to verify EPHB6, MEGF10 and MRC2 as ADAM17 substrates in a heterologous system using overexpression and PMA stimulation. However, additional experiments determining the direct cleavage of these substrates by ADAM17 in primary cells under endogenous conditions will help to further clarify the significance of these findings.

Furthermore, in addition to CSF proteomics, we applied hiSPECS on primary neurons and astrocytes of two different genetically engineered mice to identify new ADAM17 substrates. On the one hand, ADAM17 flox mice in combination with viral CRE infection and on the other hand, cells of *iRhom1*$^{4\text{-}11/4\text{-}11}$ mice, which we hypothesize to lack the ADAM17 activity in cells not expressing iRHOM2 as discussed above. Surprisingly, the overlap of ADAM17 substrate candidates between the two systems was not as pronounced as we had expected in the first place.

In neurons, substrates such as SEMA5B were found in all analysis. However, many of the other candidates were not as reputably identified. One reason for the discrepancy might be that in the ADAM17flox/viral Cre model, the loss of ADAM17 was around 85% in the neuronal culture. However, homomorphic ADAM17 mutant mice with only around 5% of the total ADAM17 level are viable (Chalaris et al., 2010), indicating that even little ADAM17 expression might be sufficient to maintain the essential substrate cleavage and signaling. This may explain the generally observed stronger abundance reduction of ADAM17 substrate candidates in the secretome of *iRhom1*$^{4\text{-}11/4\text{-}11}$ neurons. In this experiment, neuronal cultures of littermates either homozygous for the control allele or *iRhom1*$^{4\text{-}11/4\text{-}11}$ were compared which likely reflected the more complete loss of ADAM17 activity as compared to ADAM17 floxed neurons. An additional unexpected observation in the secretome of *iRhom1*$^{4\text{-}11/4\text{-}11}$ neurons, was the increased shedding of BACE1 and ADAM10 substrates, such as SEZ6 and NRCAM identified in previous studies (Kuhn et

al., 2016; Kuhn et al., 2012). These may indicate a compensation of loss of ADAM17 activity by upregulating BACE1 and ADAM10 activity. Further studies will be needed to elaborate if this potential compensation is happening on the RNA or protein level. Of note, this phenomenon was only overserved in the secretome of *iRhom1*$^{4\text{-}11/4\text{-}11}$ neurons and not ADAM17 floxed neurons, which may either indicate that a complete loss of ADAM17 function is required to induce this compensation or that iRHOM1 carries out additional tasks in the cell beyond ADAM17 maturation. Potentially, iRHOM1 may have additional clients/binding partners in the cell through which it may be involved in diverse cellular functions. Noteworthy, iRHOM2 is unstable in the absence of ADAM17 (Weskamp et al., 2020), which may be an indication for iRHOM2 having the sole client ADAM17 in the cell. In contrast, iRHOM1 remains stable in MEF cells lacking ADAM17 and reveals even a slight upregulation on protein level (Weskamp et al., 2020). This finding, may be a compensatory effect and may strengthen the hypothesis of iRHOM1 carrying out additional functions in the cell besides the maturation of ADAM17.

5.8 Exploring cellular functions of ADAM17 in the brain

Pathway analysis of the ADAM17 substrate candidates indicated cell adhesion and neuronal morphogenesis as enriched GO terms. To investigate the potential role of ADAM17 in neuron morphology, we performed Sholl analysis to understand to which extent the lack of ADAM17 influences dendritic branching. However, using standard Sholl analysis no major differences were detected between neurons expressing or lacking ADAM17. Of note, minor changes may not be detectable with the applied method and more detailed analysis which e.g. distinguish between the order of dendrites (O'Neill et al., 2015) might be required to elaborate the role of ADAM17 in dendritic branching. Moreover, the majority of neurons maintain untransfected using calcium phosphate transfection. These untransfected cells remain with ADAM17 activity and continue releasing ectodomains of ADAM17 substrates, which may act non-cell autonomously and compensate the loss of ADAM17 in single neurons analyzed in the Sholl analysis. Alternatively, analysis of axon extension/outgrowth, a feature not analyzed with Sholl analysis, may be an interesting path for future studies to understand neuronal ADAM17 function because e.g. SEMA5B was determined as axon guidance cue (Browne et al., 2012).

Our findings using IF staining and the single cell RNA-sequencing data obtained by the Betsholtz laboratory (He et al., 2018; Vanlandewijck et al., 2018) established high expression of iRHOM1 and ADAM17 in cells forming brain vessels. To better understand the role of ADAM17 activity in brain vasculature, whole proteome changes were determined between isolated brain vessels of *iRhom1*$^{4\text{-}11/4\text{-}11}$ and control mice. Dramatic downregulation of MYH1, MYH2 and MYH8 in *iRhom1*$^{4\text{-}11/4\text{-}11}$ vessels potentially indicate changes in the cytoskeleton (Squire et al., 2017). Pathway analysis of the significantly downregulated proteins pointed towards muscle and tight junction related alterations. Although we have not specifically followed up on these results, and additional experiments will be required, to find out if these proteomic data set may suggest deficits in *iRhom1*$^{4\text{-}11/4\text{-}11}$ smooth muscle cells and potentially the maintenance of the blood brain barrier. We hypothesize that *iRhom1*$^{4\text{-}11/4\text{-}11}$ mice lack ADAM17 activity in most vasculature cells despite endothelial cells in which iRHOM2 was shown to be expressed (He et al., 2018; Vanlandewijck et al., 2018). Therefore, studies in conditional knockout mice which would lack ADAM17 in a specific vasculature cell type may help to pinpoint its cellular function in e.g. pericytes, astrocytes or smooth muscle cells. Moreover, analysis of the whole vessel proteome did not reveal the substrate repertoire of ADAM17 in these cells. Therefore, secretome analysis of vessel cultures may be highly interesting. However, while hiSPECS might be powerful enough to decipher the vessel proteome, technical hurdles of culturing vessels, a method not yet established in the field, would need to be overcome first. Nevertheless, it is important to highlight that ADAM17 knockout as well as *iRHOM1*$^{2\text{-}181/2\text{-}18}$ mice suffer from hemorrhage (Canault et al., 2010; Christova et al., 2013). Future studies will have to proof if these phenotypes are related to the molecular changes observed in *iRhom1*$^{4\text{-}11/4\text{-}11}$ vessels. However, elucidating the cellular mechanism causing the changes upon loss of ADAM17 function may potentially help to explain the appearance of hemorrhage in ADAM17 KO mice for the first time.

6 CONCLUSION and OUTLOOK

In conclusion, in this thesis the hiSPECS method was established by eminently optimizing the previously published SPECS protocol (Kuhn et al., 2012). hiSPECS allows efficient secretome analysis of minor amounts of primary cells in the presence of serum supplements in a highly robust and reproducible manner. This novel method will likely have a great impact on the understudied field of secretome research by facilitating secretome studies of diverse primary cells which may help to gain fundamental insights into unexplored mechanisms controlling secretion in the future. These studies have the potential to unravel new systematic trafficking mechanism controlling cell type specific secretion which may advance basic research as well as the understanding of neurodegenerative diseases.

Next, we applied the hiSPECS method to decipher the secretome of primary neurons, oligodendrocytes, astrocytes and microglia under physiological-like conditions. Systematic analysis using bioinformatics and cross comparison to a previous study which determined the whole lysate proteome of the same major brain cell times (Sharma et al., 2015) allowed us to shed light on the specific secretion profiles of each brain cell type. For the first time we set out to establish a mouse brain secretome resource to elaborate the cellular origin of CSF biomarker proteins. We are convinced that this rich resource will be of great interest to the neuroscience community and future studies will help to expand the resource by studying e.g. less abundant cell types. This way we may be able to pinpoint the cellular origin of biomarkers even more precisely and target follow-up studies more efficiently.

Finally, we identified the substrate repertoire of ADAM17 in the brain using primary neurons, astrocytes and CSF analysis. Moreover, we linked ADAM17 activity to alterations of the brain vessel proteome. Additional studies are on the one hand required to shed light on the molecular mechanism causing these alterations and on the other hand to study ADAM17 activity in other brain cell types such as oligodendrocytes. Elucidating the brain functions of ADAM17 in greater detail will likely open new path for understanding the role of ADAM17 in neurodegenerative disease, its evaluation as potential drug target in brain diseases and the general understanding of the maintenance of the BBB. While we are confident that *iRhom1*$^{4\text{-}11/4\text{-}11}$ mice are a suitable model to study loss of ADAM17 activity in the majority of brain cell types, we are convinced that the field

of iRHOM/ADAM17 research would extremely benefit by future studies elucidating molecular mechanism causing the different phenotypes of iRHOM1 knockout mice. Those studies may potentially highlight mechanisms of cellular compensation or identify additional functions of iRHOM1 in the cells besides ADAM17 maturation. Moreover, they might provide essential insights into general targeting strategies of knockout mouse models and the compensatory effects trigger by the different approaches.

7 REFERENCES

Adrain, C., Zettl, M., Christova, Y., Taylor, N., and Freeman, M. (2012). Tumor necrosis factor signaling requires iRhom2 to promote trafficking and activation of TACE. Science (New York, NY) *335*, 225-228.

Aebersold, R., and Mann, M. (2016). Mass-spectrometric exploration of proteome structure and function. Nature *537*, 347-355.

Aggarwal, S., Talukdar, N.C., and Yadav, A.K. (2019). Advances in Higher Order Multiplexing Techniques in Proteomics. Journal of proteome research *18*, 2360-2369.

Alto, L.T., and Terman, J.R. (2017). Semaphorins and their Signaling Mechanisms. Methods in molecular biology (Clifton, NJ) *1493*, 1-25.

Alzheimer, A. (1907). Uber eine eigenartige Erkrankung der Hirnrinde. Zentralbl Nervenh Psych *18*, 177-179.

Alzheimer, A., Stelzmann, R.A., Schnitzlein, H.N., and Murtagh, F.R. (1995). An English translation of Alzheimer's 1907 paper, "Uber eine eigenartige Erkankung der Hirnrinde". Clinical anatomy (New York, NY) *8*, 429-431.

Bader, J.M., Geyer, P.E., Müller, J.B., Strauss, M.T., Koch, M., Leypoldt, F., Koertvelyessy, P., Bittner, D., Schipke, C.G., Incesoy, E.I., Peters, O., Deigendesch, N., Simons, M., Jensen, M.K., Zetterberg, H., and Mann, M. (2020). Proteome profiling in cerebrospinal fluid reveals novel biomarkers of Alzheimer's disease. Molecular systems biology *16*, e9356.

Bai, B., Wang, X., Li, Y., Chen, P.C., Yu, K., Dey, K.K., Yarbro, J.M., Han, X., Lutz, B.M., Rao, S., Jiao, Y., Sifford, J.M., Han, J., Wang, M., Tan, H., Shaw, T.I., Cho, J.H., Zhou, S., Wang, H., Niu, M., Mancieri, A., Messler, K.A., Sun, X., Wu, Z., Pagala, V., High, A.A., Bi, W., Zhang, H., Chi, H., Haroutunian, V., Zhang, B., Beach, T.G., Yu, G., and Peng, J. (2020). Deep Multilayer Brain Proteomics Identifies Molecular Networks in Alzheimer's Disease Progression. Neuron *105*, 975-991.e977.

Bandsma, R.H., van Goor, H., Yourshaw, M., Horlings, R.K., Jonkman, M.F., Schölvinck, E.H., Karrenbeld, A., Scheenstra, R., Kömhoff, M., Rump, P., Koopman-Keemink, Y., Nelson, S.F., Escher, J.C., Cutz, E., and Martín, M.G. (2015). Loss of ADAM17 is associated with severe multiorgan dysfunction. Human pathology *46*, 923-928.

Black, R.A., Rauch, C.T., Kozlosky, C.J., Peschon, J.J., Slack, J.L., Wolfson, M.F., Castner, B.J., Stocking, K.L., Reddy, P., Srinivasan, S., Nelson, N., Boiani, N., Schooley, K.A., Gerhart, M., Davis, R., Fitzner, J.N., Johnson, R.S., Paxton, R.J., March, C.J., and Cerretti, D.P. (1997). A metalloproteinase disintegrin that releases tumour-necrosis factor-alpha from cells. Nature *385*, 729-733.

Blank, B., and von Blume, J. (2017). Cab45-Unraveling key features of a novel secretory cargo sorter at the trans-Golgi network. European journal of cell biology *96*, 383-390.

Blaydon, D.C., Biancheri, P., Di, W.L., Plagnol, V., Cabral, R.M., Brooke, M.A., van Heel, D.A., Ruschendorf, F., Toynbee, M., Walne, A., O'Toole, E.A., Martin, J.E., Lindley, K., Vulliamy, T., Abrams, D.J., MacDonald, T.T., Harper, J.I., and Kelsell, D.P. (2011). Inflammatory skin and bowel disease linked to ADAM17 deletion. The New England journal of medicine *365*, 1502-1508.

Blaydon, D.C., Etheridge, S.L., Risk, J.M., Hennies, H.C., Gay, L.J., Carroll, R., Plagnol, V., McRonald, F.E., Stevens, H.P., Spurr, N.K., Bishop, D.T., Ellis, A., Jankowski, J., Field, J.K., Leigh, I.M., South, A.P., and Kelsell, D.P. (2012). RHBDF2

mutations are associated with tylosis, a familial esophageal cancer syndrome. American journal of human genetics *90*, 340-346.

Blobel, C.P. (2002). Functional and biochemical characterization of ADAMs and their predicted role in protein ectodomain shedding. Inflammation research : official journal of the European Histamine Research Society [et al] *51*, 83-84.

Blobel, C.P. (2005). ADAMs: key components in EGFR signalling and development. Nature reviews Molecular cell biology *6*, 32-43.

Brown, K.J., Seol, H., Pillai, D.K., Sankoorikal, B.J., Formolo, C.A., Mac, J., Edwards, N.J., Rose, M.C., and Hathout, Y. (2013). The human secretome atlas initiative: implications in health and disease conditions. Biochim Biophys Acta *1834*, 2454-2461.

Brown, M.S., Ye, J., Rawson, R.B., and Goldstein, J.L. (2000). Regulated intramembrane proteolysis: a control mechanism conserved from bacteria to humans. Cell *100*, 391-398.

Browne, K., Wang, W., Liu, R.Q., Piva, M., and O'Connor, T.P. (2012). Transmembrane semaphorin5B is proteolytically processed into a repulsive neural guidance cue. J Neurochem *123*, 135-146.

Bruderer, R., Bernhardt, O.M., Gandhi, T., Miladinović, S.M., Cheng, L.-Y., Messner, S., Ehrenberger, T., Zanotelli, V., Butscheid, Y., Escher, C., Vitek, O., Rinner, O., and Reiter, L. (2015). Extending the limits of quantitative proteome profiling with data-independent acquisition and application to acetaminophen-treated three-dimensional liver microtissues. Molecular & cellular proteomics : MCP *14*, 1400-1410.

Bruderer, R., Bernhardt, O.M., Gandhi, T., and Reiter, L. (2016). High-precision iRT prediction in the targeted analysis of data-independent acquisition and its impact on identification and quantitation. Proteomics *16*, 2246-2256.

Bruderer, R., Bernhardt, O.M., Gandhi, T., Xuan, Y., Sondermann, J., Schmidt, M., Gomez-Varela, D., and Reiter, L. (2017). Optimization of Experimental Parameters in Data-Independent Mass Spectrometry Significantly Increases Depth and Reproducibility of Results. Molecular & cellular proteomics : MCP *16*, 2296-2309.

Brummer, T., Pigoni, M., Rossello, A., Wang, H., Noy, P.J., Tomlinson, M.G., Blobel, C.P., and Lichtenthaler, S.F. (2018). The metalloprotease ADAM10 (a disintegrin and metalloprotease 10) undergoes rapid, postlysis autocatalytic degradation. FASEB journal : official publication of the Federation of American Societies for Experimental Biology *32*, 3560-3573.

Budelier, M.M., and Bateman, R.J. (2019). Biomarkers of Alzheimer Disease. The journal of applied laboratory medicine.

Canault, M., Certel, K., Schatzberg, D., Wagner, D.D., and Hynes, R.O. (2010). The Lack of ADAM17 Activity during Embryonic Development Causes Hemorrhage and Impairs Vessel Formation. PloS one *5*, e13433.

Capone, C., Dabertrand, F., Baron-Menguy, C., Chalaris, A., Ghezali, L., Domenga-Denier, V., Schmidt, S., Huneau, C., Rose-John, S., Nelson, M.T., and Joutel, A. (2016). Mechanistic insights into a TIMP3-sensitive pathway constitutively engaged in the regulation of cerebral hemodynamics. eLife *5*, e17536.

Carlyle, B.C., Kitchen, R.R., Kanyo, J.E., Voss, E.Z., Pletikos, M., Sousa, A.M.M., Lam, T.T., Gerstein, M.B., Sestan, N., and Nairn, A.C. (2017). A multiregional proteomic survey of the postnatal human brain. Nature neuroscience *20*, 1787-1795.

Cavadas, M., Oikonomidi, I., Gaspar, C.J., Burbridge, E., Badenes, M., Felix, I., Bolado, A., Hu, T., Bileck, A., Gerner, C., Domingos, P.M., von Kriegsheim, A., and Adrain, C. (2017). Phosphorylation of iRhom2 Controls Stimulated Proteolytic Shedding by the Metalloprotease ADAM17/TACE. Cell reports *21*, 745-757.

Chalaris, A., Adam, N., Sina, C., Rosenstiel, P., Lehmann-Koch, J., Schirmacher, P., Hartmann, D., Cichy, J., Gavrilova, O., Schreiber, S., Jostock, T., Matthews, V., Häsler, R., Becker, C., Neurath, M.F., Reiß, K., Saftig, P., Scheller, J., and Rose-John, S. (2010). Critical role of the disintegrin metalloprotease ADAM17 for intestinal inflammation and regeneration in mice. Journal of Experimental Medicine *207*, 1617-1624.

Chatr-Aryamontri, A., Breitkreutz, B.J., Oughtred, R., Boucher, L., Heinicke, S., Chen, D., Stark, C., Breitkreutz, A., Kolas, N., O'Donnell, L., Reguly, T., Nixon, J., Ramage, L., Winter, A., Sellam, A., Chang, C., Hirschman, J., Theesfeld, C., Rust, J., Livstone, M.S., Dolinski, K., and Tyers, M. (2015). The BioGRID interaction database: 2015 update. Nucleic acids research *43*, D470-478.

Chen, Z., Chen, D.-X., Kai, Y., Khatri, I., Lamptey, B., and Gorczynski, R.M. (2008). Identification of an Expressed Truncated Form of CD200, CD200tr, which is a Physiologic Antagonist of CD200-Induced Suppression. Transplantation *86*.

Chen, Z., Kapus, A., Khatri, I., Kos, O., Zhu, F., and Gorczynski, R.M. (2018). Cell membrane-bound CD200 signals both via an extracellular domain and following nuclear translocation of a cytoplasmic fragment. Leukemia research *69*, 72-80.

Cho, R.W., Park, J.M., Wolff, S.B.E., Xu, D., Hopf, C., Kim, J.-a., Reddy, R.C., Petralia, R.S., Perin, M.S., Linden, D.J., and Worley, P.F. (2008). mGluR1/5-Dependent Long-Term Depression Requires the Regulated Ectodomain Cleavage of Neuronal Pentraxin NPR by TACE. Neuron *57*, 858-871.

Christova, Y., Adrain, C., Bambrough, P., Ibrahim, A., and Freeman, M. (2013). Mammalian iRhoms have distinct physiological functions including an essential role in TACE regulation. EMBO reports *14*, 884-890.

Cox, J., Neuhauser, N., Michalski, A., Scheltema, R.A., Olsen, J.V., and Mann, M. (2011). Andromeda: a peptide search engine integrated into the MaxQuant environment. Journal of proteome research *10*, 1794-1805.

Daria, A., Colombo, A., Llovera, G., Hampel, H., Willem, M., Liesz, A., Haass, C., and Tahirovic, S. (2017). Young microglia restore amyloid plaque clearance of aged microglia. The EMBO journal *36*, 583-603.

De Strooper, B., Annaert, W., Cupers, P., Saftig, P., Craessaerts, K., Mumm, J.S., Schroeter, E.H., Schrijvers, V., Wolfe, M.S., Ray, W.J., Goate, A., and Kopan, R. (1999). A presenilin-1-dependent γ-secretase-like protease mediates release of Notch intracellular domain. Nature *398*, 518-522.

Deng, M., Loughran, P.A., Zhang, L., Scott, M.J., and Billiar, T.R. (2015). Shedding of the tumor necrosis factor (TNF) receptor from the surface of hepatocytes during sepsis limits inflammation through cGMP signaling. Science signaling *8*, ra11.

Deshmukh, A.S., Cox, J., Jensen, L.J., Meissner, F., and Mann, M. (2015). Secretome Analysis of Lipid-Induced Insulin Resistance in Skeletal Muscle Cells by a Combined Experimental and Bioinformatics Workflow. Journal of proteome research *14*, 4885-4895.

Diaz-Papkovich, A., Anderson-Trocme, L., Ben-Eghan, C., and Gravel, S. (2019). UMAP reveals cryptic population structure and phenotype heterogeneity in large genomic cohorts. PLoS genetics *15*, e1008432.

Dislich, B., Wohlrab, F., Bachhuber, T., Muller, S.A., Kuhn, P.H., Hogl, S., Meyer-Luehmann, M., and Lichtenthaler, S.F. (2015). Label-free Quantitative Proteomics of Mouse Cerebrospinal Fluid Detects beta-Site APP Cleaving Enzyme (BACE1) Protease Substrates In Vivo. Molecular & cellular proteomics : MCP *14*, 2550-2563.

Dulloo, I., Muliyil, S., and Freeman, M. (2019). The molecular, cellular and pathophysiological roles of iRhom pseudoproteases. Open biology *9*, 190003.

Egan, M.F., Kost, J., Tariot, P.N., Aisen, P.S., Cummings, J.L., Vellas, B., Sur, C., Mukai, Y., Voss, T., Furtek, C., Mahoney, E., Harper Mozley, L., Vandenberghe, R., Mo, Y., and Michelson, D. (2018). Randomized Trial of Verubecestat for Mild-to-Moderate Alzheimer's Disease. The New England journal of medicine *378*, 1691-1703.

Eichelbaum, K., and Krijgsveld, J. (2014). Rapid temporal dynamics of transcription, protein synthesis, and secretion during macrophage activation. Molecular & cellular proteomics : MCP *13*, 792-810.

Eichelbaum, K., Winter, M., Berriel Diaz, M., Herzig, S., and Krijgsveld, J. (2012). Selective enrichment of newly synthesized proteins for quantitative secretome analysis. Nature biotechnology *30*, 984-990.

El-Brolosy, M.A., Kontarakis, Z., Rossi, A., Kuenne, C., Günther, S., Fukuda, N., Kikhi, K., Boezio, G.L.M., Takacs, C.M., Lai, S.L., Fukuda, R., Gerri, C., Giraldez, A.J., and Stainier, D.Y.R. (2019). Genetic compensation triggered by mutant mRNA degradation. Nature *568*, 193-197.

Engelholm, L.H., Ingvarsen, S., Jürgensen, H.J., Hillig, T., Madsen, D.H., Nielsen, B.S., and Behrendt, N. (2009). The collagen receptor uPARAP/Endo180. Frontiers in bioscience (Landmark edition) *14*, 2103-2114.

Ewers, M., Franzmeier, N., Suarez-Calvet, M., Morenas-Rodriguez, E., Caballero, M.A.A., Kleinberger, G., Piccio, L., Cruchaga, C., Deming, Y., Dichgans, M., Trojanowski, J.Q., Shaw, L.M., Weiner, M.W., and Haass, C. (2019). Increased soluble TREM2 in cerebrospinal fluid is associated with reduced cognitive and clinical decline in Alzheimer's disease. Science translational medicine *11*.

Fang, P., Wang, X.J., Xue, Y., Liu, M.Q., Zeng, W.F., Zhang, Y., Zhang, L., Gao, X., Yan, G.Q., Yao, J., Shen, H.L., and Yang, P.Y. (2016). In-depth mapping of the mouse brain N-glycoproteome reveals widespread N-glycosylation of diverse brain proteins. Oncotarget *7*, 38796-38809.

Fenn, J.B., Mann, M., Meng, C.K., Wong, S.F., and Whitehouse, C.M. (1990). Electrospray ionization–principles and practice. Mass spectrometry reviews *9*, 37-70.

Feuerbach, D., Schindler, P., Barske, C., Joller, S., Beng-Louka, E., Worringer, K.A., Kommineni, S., Kaykas, A., Ho, D.J., Ye, C., Welzenbach, K., Elain, G., Klein, L., Brzak, I., Mir, A.K., Farady, C.J., Aichholz, R., Popp, S., George, N., and Neumann, U. (2017). ADAM17 is the main sheddase for the generation of human triggering receptor expressed in myeloid cells (hTREM2) ectodomain and cleaves TREM2 after Histidine 157. Neuroscience letters *660*, 109-114.

Frank, M.G., Fonken, L.K., Annis, J.L., Watkins, L.R., and Maier, S.F. (2018). Stress disinhibits microglia via down-regulation of CD200R: A mechanism of neuroinflammatory priming. Brain, behavior, and immunity *69*, 62-73.

Fredrickx, E., Colombo, E., Canevazzi, P., La Marca, R., Pellegatta, M., Dina, G., Podini, P., Nave, K.A., Quattrini, A., and Taveggia, C. (2020). Ablation of neuronal ADAM17 impairs oligodendrocyte differentiation and myelination. Glia *68*, 1148-1164.

Freywald, A., Sharfe, N., Rashotte, C., Grunberger, T., and Roifman, C.M. (2003). The EphB6 receptor inhibits JNK activation in T lymphocytes and modulates T cell receptor-mediated responses. The Journal of biological chemistry *278*, 10150-10156.

Fukata, Y., Adesnik, H., Iwanaga, T., Bredt, D.S., Nicoll, R.A., and Fukata, M. (2006). Epilepsy-related ligand/receptor complex LGI1 and ADAM22 regulate synaptic transmission. Science (New York, NY) *313*, 1792-1795.

Garton, K.J., Gough, P.J., Philalay, J., Wille, P.T., Blobel, C.P., Whitehead, R.H., Dempsey, P.J., and Raines, E.W. (2003). Stimulated shedding of vascular cell adhesion molecule 1 (VCAM-1) is mediated by tumor necrosis factor-alpha-converting enzyme (ADAM 17). The Journal of biological chemistry *278*, 37459-37464.

Gessulat, S., Schmidt, T., Zolg, D.P., Samaras, P., Schnatbaum, K., Zerweck, J., Knaute, T., Rechenberger, J., Delanghe, B., Huhmer, A., Reimer, U., Ehrlich, H.-C., Aiche, S., Kuster, B., and Wilhelm, M. (2019). Prosit: proteome-wide prediction of peptide tandem mass spectra by deep learning. Nature methods *16*, 509-518.

Gillet, L.C., Navarro, P., Tate, S., Rost, H., Selevsek, N., Reiter, L., Bonner, R., and Aebersold, R. (2012). Targeted data extraction of the MS/MS spectra generated by data-independent acquisition: a new concept for consistent and accurate proteome analysis. Molecular & cellular proteomics : MCP *11*, O111.016717.

Gödde, N.J., D'Abaco, G.M., Paradiso, L., and Novak, U. (2006). Efficient ADAM22 surface expression is mediated by phosphorylation-dependent interaction with 14-3-3 protein family members. Journal of cell science *119*, 3296-3305.

Grell, M. (1995). Tumor necrosis factor (TNF) receptors in cellular signaling of soluble and membrane-expressed TNF. Journal of inflammation *47*, 8-17.

Grieve, A.G., Xu, H., Kunzel, U., Bambrough, P., Sieber, B., and Freeman, M. (2017). Phosphorylation of iRhom2 at the plasma membrane controls mammalian TACE-dependent inflammatory and growth factor signalling. eLife *6*.

Groot, A.J., Habets, R., Yahyanejad, S., Hodin, C.M., Reiss, K., Saftig, P., Theys, J., and Vooijs, M. (2014). Regulated proteolysis of NOTCH2 and NOTCH3 receptors by ADAM10 and presenilins. Molecular and cellular biology *34*, 2822-2832.

Guan, F., Tan, Z., Li, X., Pang, X., Zhu, Y., Li, D., and Yang, G. (2015). A lectin-based isolation/enrichment strategy for improved coverage of N-glycan analysis. Carbohydrate Research *416*, 7-13.

Güner, G., and Lichtenthaler, S.F. (2020). The substrate repertoire of γ-secretase/presenilin. Seminars in cell & developmental biology.

Hampel, H., Vassar, R., De Strooper, B., Hardy, J., Willem, M., Singh, N., Zhou, J., Yan, R., Vanmechelen, E., De Vos, A., Nistico, R., Corbo, M., Imbimbo, B.P., Streffer, J., Voytyuk, I., Timmers, M., Tahami Monfared, A.A., Irizarry, M., Albala, B., Koyama, A., Watanabe, N., Kimura, T., Yarenis, L., Lista, S., Kramer, L., and

Vergallo, A. (2020). The beta-Secretase BACE1 in Alzheimer's Disease. Biological psychiatry.

Hartl, D., May, P., Gu, W., Mayhaus, M., Pichler, S., Spaniol, C., Glaab, E., Bobbili, D.R., Antony, P., Koegelsberger, S., Kurz, A., Grimmer, T., Morgan, K., Vardarajan, B.N., Reitz, C., Hardy, J., Bras, J., Guerreiro, R., Balling, R., Schneider, J.G., and Riemenschneider, M. (2020). A rare loss-of-function variant of ADAM17 is associated with late-onset familial Alzheimer disease. Molecular psychiatry *25*, 629-639.

Hauck, S.M., Dietter, J., Kramer, R.L., Hofmaier, F., Zipplies, J.K., Amann, B., Feuchtinger, A., Deeg, C.A., and Ueffing, M. (2010). Deciphering membrane-associated molecular processes in target tissue of autoimmune uveitis by label-free quantitative mass spectrometry. Molecular & cellular proteomics : MCP *9*, 2292-2305.

Haxaire, C., Hakobyan, N., Pannellini, T., Carballo, C., McIlwain, D., Mak, T.W., Rodeo, S., Acharya, S., Li, D., Szymonifka, J., Song, X., Monette, S., Srivastava, A., Salmon, J.E., and Blobel, C.P. (2018). Blood-induced bone loss in murine hemophilic arthropathy is prevented by blocking the iRhom2/ADAM17/TNF-alpha pathway. Blood *132*, 1064-1074.

He, L., Vanlandewijck, M., Mäe, M.A., Andrae, J., Ando, K., Del Gaudio, F., Nahar, K., Lebouvier, T., Laviña, B., Gouveia, L., Sun, Y., Raschperger, E., Segerstolpe, Å., Liu, J., Gustafsson, S., Räsänen, M., Zarb, Y., Mochizuki, N., Keller, A., Lendahl, U., and Betsholtz, C. (2018). Single-cell RNA sequencing of mouse brain and lung vascular and vessel-associated cell types. Scientific data *5*, 180160.

Hemming, M.L., Elias, J.E., Gygi, S.P., and Selkoe, D.J. (2009). Identification of beta-secretase (BACE1) substrates using quantitative proteomics. PloS one *4*, e8477.

Herber, J., Njavro, J., Feederle, R., Schepers, U., Muller, U.C., Brase, S., Muller, S.A., and Lichtenthaler, S.F. (2018). Click Chemistry-mediated Biotinylation Reveals a Function for the Protease BACE1 in Modulating the Neuronal Surface Glycoproteome. Molecular & cellular proteomics : MCP *17*, 1487-1501.

Hirano, M., and Goldman, J.E. (1988). Gliogenesis in rat spinal cord: evidence for origin of astrocytes and oligodendrocytes from radial precursors. Journal of neuroscience research *21*, 155-167.

Hosur, V., Low, B.E., Li, D., Stafford, G.A., Kohar, V., Shultz, L.D., and Wiles, M.V. (2020). Genes adapt to outsmart gene targeting strategies in mutant mouse strains by skipping exons to reinitiate transcription and translation. bioRxiv, 2020.2004.2022.041087.

Hsia, H.E., Kumar, R., Luca, R., Takeda, M., Courchet, J., Nakashima, J., Wu, S., Goebbels, S., An, W., Eickholt, B.J., Polleux, F., Rotin, D., Wu, H., Rossner, M.J., Bagni, C., Rhee, J.S., Brose, N., and Kawabe, H. (2014). Ubiquitin E3 ligase Nedd4-1 acts as a downstream target of PI3K/PTEN-mTORC1 signaling to promote neurite growth. Proceedings of the National Academy of Sciences of the United States of America *111*, 13205-13210.

Hsia, H.E., Tushaus, J., Brummer, T., Zheng, Y., Scilabra, S.D., and Lichtenthaler, S.F. (2019). Functions of 'A disintegrin and metalloproteases (ADAMs)' in the mammalian nervous system. Cellular and molecular life sciences : CMLS *76*, 3055-3081.

Hsiao, C.C., Rombouts, F., and Gijsen, H.J.M. (2019). New evolutions in the BACE1 inhibitor field from 2014 to 2018. Bioorganic & medicinal chemistry letters *29*, 761-777.

Hu, X., Hicks, C.W., He, W., Wong, P., Macklin, W.B., Trapp, B.D., and Yan, R. (2006). Bace1 modulates myelination in the central and peripheral nervous system. Nature neuroscience *9*, 1520-1525.

Huang da, W., Sherman, B.T., and Lempicki, R.A. (2009a). Bioinformatics enrichment tools: paths toward the comprehensive functional analysis of large gene lists. Nucleic acids research *37*, 1-13.

Huang da, W., Sherman, B.T., and Lempicki, R.A. (2009b). Systematic and integrative analysis of large gene lists using DAVID bioinformatics resources. Nature protocols *4*, 44-57.

Huang, T., Bruderer, R., Muntel, J., Xuan, Y., Vitek, O., and Reiter, L. (2020). Combining Precursor and Fragment Information for Improved Detection of Differential Abundance in Data Independent Acquisition. Molecular & cellular proteomics : MCP *19*, 421-430.

Hughes, C.S., Moggridge, S., Müller, T., Sorensen, P.H., Morin, G.B., and Krijgsveld, J. (2019). Single-pot, solid-phase-enhanced sample preparation for proteomics experiments. Nature protocols *14*, 68-85.

Huse, J.T., and Doms, R.W. (2000). Closing in on the amyloid cascade: recent insights into the cell biology of Alzheimer's disease. Molecular neurobiology *22*, 81-98.

Imbimbo, B.P., and Watling, M. (2019). Investigational BACE inhibitors for the treatment of Alzheimer's disease. Expert Opin Investig Drugs *28*, 967-975.

Iram, T., Ramirez-Ortiz, Z., Byrne, M.H., Coleman, U.A., Kingery, N.D., Means, T.K., Frenkel, D., and El Khoury, J. (2016). Megf10 Is a Receptor for C1Q That Mediates Clearance of Apoptotic Cells by Astrocytes. J Neurosci *36*, 5185-5192.

Ivankov, D.N., Bogatyreva, N.S., Hönigschmid, P., Dislich, B., Hogl, S., Kuhn, P.-H., Frishman, D., and Lichtenthaler, S.F. (2013). QARIP: a web server for quantitative proteomic analysis of regulated intramembrane proteolysis. Nucleic acids research *41*, W459-W464.

Jackson, L.F., Qiu, T.H., Sunnarborg, S.W., Chang, A., Zhang, C., Patterson, C., and Lee, D.C. (2003). Defective valvulogenesis in HB-EGF and TACE-null mice is associated with aberrant BMP signaling. The EMBO journal *22*, 2704-2716.

Johnson, E.C.B., Dammer, E.B., Duong, D.M., Ping, L., Zhou, M., Yin, L., Higginbotham, L.A., Guajardo, A., White, B., Troncoso, J.C., Thambisetty, M., Montine, T.J., Lee, E.B., Trojanowski, J.Q., Beach, T.G., Reiman, E.M., Haroutunian, V., Wang, M., Schadt, E., Zhang, B., Dickson, D.W., Ertekin-Taner, N., Golde, T.E., Petyuk, V.A., De Jager, P.L., Bennett, D.A., Wingo, T.S., Rangaraju, S., Hajjar, I., Shulman, J.M., Lah, J.J., Levey, A.I., and Seyfried, N.T. (2020). Large-scale proteomic analysis of Alzheimer’s disease brain and cerebrospinal fluid reveals early changes in energy metabolism associated with microglia and astrocyte activation. Nature Medicine.

Joshi, H.J., Jorgensen, A., Schjoldager, K.T., Halim, A., Dworkin, L.A., Steentoft, C., Wandall, H.H., Clausen, H., and Vakhrushev, S.Y. (2018). GlycoDomainViewer: a bioinformatics tool for contextual exploration of glycoproteomes. Glycobiology *28*, 131-136.

Kalus, I., Bormann, U., Mzoughi, M., Schachner, M., and Kleene, R. (2006). Proteolytic cleavage of the neural cell adhesion molecule by ADAM17/TACE is involved in neurite outgrowth. Journal of Neurochemistry *98*, 78-88.

Kamarajan, P., Shin, J.M., Qian, X., Matte, B., Zhu, J.Y., and Kapila, Y.L. (2013). ADAM17-mediated CD44 cleavage promotes orasphere formation or stemness and tumorigenesis in HNSCC. Cancer medicine *2*, 793-802.

Kawahara, R., Granato, D.C., Yokoo, S., Domingues, R.R., Trindade, D.M., and Paes Leme, A.F. (2017). Mass spectrometry-based proteomics revealed Glypican-1 as a novel ADAM17 substrate. Journal of Proteomics *151*, 53-65.

Kay, J.N., Chu, M.W., and Sanes, J.R. (2012). MEGF10 and MEGF11 mediate homotypic interactions required for mosaic spacing of retinal neurons. Nature *483*, 465-469.

Kefaloyianni, E., Muthu, M.L., Kaeppler, J., Sun, X., Sabbisetti, V., Chalaris, A., Rose-John, S., Wong, E., Sagi, I., Waikar, S.S., Rennke, H., Humphreys, B.D., Bonventre, J.V., and Herrlich, A. (2016). ADAM17 substrate release in proximal tubule drives kidney fibrosis. JCI Insight *1*, e87023.

Kim, J., Gee, H.Y., and Lee, M.G. (2018). Unconventional protein secretion – new insights into the pathogenesis and therapeutic targets of human diseases. Journal of cell science *131*, jcs213686.

Kjøller, L., Engelholm, L.H., Høyer-Hansen, M., Danø, K., Bugge, T.H., and Behrendt, N. (2004). uPARAP/endo180 directs lysosomal delivery and degradation of collagen IV. Experimental cell research *293*, 106-116.

Kleifeld, O., Doucet, A., auf dem Keller, U., Prudova, A., Schilling, O., Kainthan, R.K., Starr, A.E., Foster, L.J., Kizhakkedathu, J.N., and Overall, C.M. (2010). Isotopic labeling of terminal amines in complex samples identifies protein N-termini and protease cleavage products. Nature biotechnology *28*, 281-288.

Kleifeld, O., Doucet, A., Prudova, A., auf dem Keller, U., Gioia, M., Kizhakkedathu, J.N., and Overall, C.M. (2011). Identifying and quantifying proteolytic events and the natural N terminome by terminal amine isotopic labeling of substrates. Nature protocols *6*, 1578-1611.

Koo, C.Z., Harrison, N., Noy, P.J., Szyroka, J., Matthews, A.L., Hsia, H.E., Müller, S.A., Tüshaus, J., Goulding, J., Willis, K., Apicella, C., Cragoe, B., Davis, E., Keles, M., Malinova, A., McFarlane, T.A., Morrison, P.R., Nguyen, H.T.H., Sykes, M.C., Ahmed, H., Di Maio, A., Seipold, L., Saftig, P., Cull, E., Pliotas, C., Rubinstein, E., Poulter, N.S., Briddon, S.J., Holliday, N.D., Lichtenthaler, S.F., and Tomlinson, M.G. (2020). The tetraspanin Tspan15 is an essential subunit of an ADAM10 scissor complex. The Journal of biological chemistry.

Kuhn, P.-H., Wang, H., Dislich, B., Colombo, A., Zeitschel, U., Ellwart, J.W., Kremmer, E., Rossner, S., and Lichtenthaler, S.F. (2010). ADAM10 is the physiologically relevant, constitutive alpha-secretase of the amyloid precursor protein in primary neurons. The EMBO journal *29*, 3020-3032.

Kuhn, P.H., Colombo, A.V., Schusser, B., Dreymueller, D., Wetzel, S., Schepers, U., Herber, J., Ludwig, A., Kremmer, E., Montag, D., Muller, U., Schweizer, M., Saftig, P., Brase, S., and Lichtenthaler, S.F. (2016). Systematic substrate identification indicates a central role for the metalloprotease ADAM10 in axon targeting and synapse function. eLife *5*.

Kuhn, P.H., Koroniak, K., Hogl, S., Colombo, A., Zeitschel, U., Willem, M., Volbracht, C., Schepers, U., Imhof, A., Hoffmeister, A., Haass, C., Rossner, S., Brase, S., and Lichtenthaler, S.F. (2012). Secretome protein enrichment identifies physiological

BACE1 protease substrates in neurons. The EMBO journal *31*, 3157-3168.

Kuhn, P.H., Voss, M., Haug-Kroper, M., Schroder, B., Schepers, U., Brase, S., Haass, C., Lichtenthaler, S.F., and Fluhrer, R. (2015). Secretome analysis identifies novel signal Peptide peptidase-like 3 (Sppl3) substrates and reveals a role of Sppl3 in multiple Golgi glycosylation pathways. Molecular & cellular proteomics : MCP *14*, 1584-1598.

Kunzel, U., Grieve, A.G., Meng, Y., Sieber, B., Cowley, S.A., and Freeman, M. (2018). FRMD8 promotes inflammatory and growth factor signalling by stabilising the iRhom/ADAM17 sheddase complex. eLife *7*.

La Marca, R., Cerri, F., Horiuchi, K., Bachi, A., Feltri, M.L., Wrabetz, L., Blobel, C.P., Quattrini, A., Salzer, J.L., and Taveggia, C. (2011). TACE (ADAM17) inhibits Schwann cell myelination. Nature neuroscience *14*, 857-865.

Langhammer, C.G., Previtera, M.L., Sweet, E.S., Sran, S.S., Chen, M., and Firestein, B.L. (2010). Automated Sholl analysis of digitized neuronal morphology at multiple scales: Whole cell Sholl analysis versus Sholl analysis of arbor subregions. Cytometry Part A : the journal of the International Society for Analytical Cytology *77*, 1160-1168.

Lee, T.H., Cheng, K.K., Hoo, R.L., Siu, P.M., and Yau, S.Y. (2019). The Novel Perspectives of Adipokines on Brain Health. International journal of molecular sciences *20*.

Li, F., and Ding, J. (2019). Sialylation is involved in cell fate decision during development, reprogramming and cancer progression. Protein & Cell *10*, 550-565.

Li, N., Wang, Y., Forbes, K., Vignali, K., Heale, B., Saftig, P., Hartmann, D., Black, R., Rossi, J., Blobel, C., Dempsey, P., Workman, C., and Vignali, D. (2007). Metalloproteases regulate T-cell proliferation and effector function via LAG-3. The EMBO journal *26*, 494-504.

Li, X., Maretzky, T., Perez-Aguilar, J.M., Monette, S., Weskamp, G., Le Gall, S., Beutler, B., Weinstein, H., and Blobel, C.P. (2017). Structural modeling defines transmembrane residues in ADAM17 that are crucial for Rhbdf2-ADAM17-dependent proteolysis. Journal of cell science *130*, 868-878.

Li, X., Maretzky, T., Weskamp, G., Monette, S., Qing, X., Issuree, P.D., Crawford, H.C., McIlwain, D.R., Mak, T.W., Salmon, J.E., and Blobel, C.P. (2015). iRhoms 1 and 2 are essential upstream regulators of ADAM17-dependent EGFR signaling. Proceedings of the National Academy of Sciences of the United States of America *112*, 6080-6085.

Lichtenthaler, S.F., Lemberg, M.K., and Fluhrer, R. (2018). Proteolytic ectodomain shedding of membrane proteins in mammals-hardware, concepts, and recent developments. The EMBO journal *37*.

Lichtenthaler, S.F., O'Hara, B.F., and Blobel, C.P. (2015). iRhoms in the brain - a new frontier? Cell cycle (Georgetown, Tex) *14*, 3003-3004.

Liu, L., and Duff, K. (2008). A technique for serial collection of cerebrospinal fluid from the cisterna magna in mouse. Journal of visualized experiments : JoVE.

Liu, M.Q., Zeng, W.F., Fang, P., Cao, W.Q., Liu, C., Yan, G.Q., Zhang, Y., Peng, C., Wu, J.Q., Zhang, X.J., Tu, H.J., Chi, H., Sun, R.X., Cao, Y., Dong, M.Q., Jiang, B.Y., Huang, J.M., Shen, H.L., Wong, C.C.L., He, S.M., and Yang, P.Y. (2017). pGlyco 2.0 enables precision N-glycoproteomics with comprehensive quality control and one-step mass spectrometry for intact glycopeptide identification. Nature communications *8*, 438.

Llibre-Guerra, J.J., Li, Y., Schindler, S.E., Gordon, B.A., Fagan, A.M., Morris, J.C., Benzinger, T.L.S., Hassenstab, J., Wang, G., Allegri, R., Berman, S.B., Chhatwal, J., Farlow, M.R., Holtzman, D.M., Jucker, M., Levin, J., Noble, J.M., Salloway, S., Schofield, P., Karch, C., Fox, N.C., Xiong, C., Bateman, R.J., and McDade, E. (2019). Association of Longitudinal Changes in Cerebrospinal Fluid Total Tau and Phosphorylated Tau 181 and Brain Atrophy With Disease Progression in Patients With Alzheimer Disease. JAMA network open *2*, e1917126.

Lombardo, S., Chiacchiaretta, M., Tarr, A., Kim, W., Cao, T., Sigal, G., Rosahl, T.W., Xia, W., Haydon, P.G., Kennedy, M.E., and Tesco, G. (2019). BACE1 partial deletion induces synaptic plasticity deficit in adult mice. Scientific reports *9*, 19877.

Lorenzen, I., Lokau, J., Korpys, Y., Oldefest, M., Flynn, C.M., Künzel, U., Garbers, C., Freeman, M., Grötzinger, J., and Düsterhöft, S. (2016). Control of ADAM17 activity by regulation of its cellular localisation. Scientific reports *6*, 35067-35067.

Ludwig, C., Gillet, L., Rosenberger, G., Amon, S., Collins, B.C., and Aebersold, R. (2018). Data-independent acquisition-based SWATH-MS for quantitative proteomics: a tutorial. Molecular systems biology *14*, e8126.

Lun, M.P., Monuki, E.S., and Lehtinen, M.K. (2015). Development and functions of the choroid plexus-cerebrospinal fluid system. Nat Rev Neurosci *16*, 445-457.

Makarov, A. (2000). Electrostatic axially harmonic orbital trapping: a high-performance technique of mass analysis. Analytical chemistry *72*, 1156-1162.

Maretzky, T., McIlwain, D.R., Issuree, P.D., Li, X., Malapeira, J., Amin, S., Lang, P.A., Mak, T.W., and Blobel, C.P. (2013). iRhom2 controls the substrate selectivity of stimulated ADAM17-dependent ectodomain shedding. Proceedings of the National Academy of Sciences of the United States of America *110*, 11433-11438.

Maretzky, T., Schulte, M., Ludwig, A., Rose-John, S., Blobel, C., Hartmann, D., Altevogt, P., Saftig, P., and Reiss, K. (2005). L1 is sequentially processed by two differently activated metalloproteases and presenilin/gamma-secretase and regulates neural cell adhesion, cell migration, and neurite outgrowth. Molecular and cellular biology *25*, 9040-9053.

Matsuoka, H., Obama, H., Kelly, M.L., Matsui, T., and Nakamoto, M. (2005). Biphasic functions of the kinase-defective Ephb6 receptor in cell adhesion and migration. The Journal of biological chemistry *280*, 29355-29363.

Matthews, A.L., Szyroka, J., Collier, R., Noy, P.J., and Tomlinson, M.G. (2017). Scissor sisters: regulation of ADAM10 by the TspanC8 tetraspanins. Biochemical Society transactions *45*, 719-730.

McIlwain, D.R., Lang, P.A., Maretzky, T., Hamada, K., Ohishi, K., Maney, S.K., Berger, T., Murthy, A., Duncan, G., Xu, H.C., Lang, K.S., Haussinger, D., Wakeham, A., Itie-Youten, A., Khokha, R., Ohashi, P.S., Blobel, C.P., and Mak, T.W. (2012). iRhom2 regulation of TACE controls TNF-mediated protection against Listeria and responses to LPS. Science (New York, NY) *335*, 229-232.

Meier, F., Brunner, A.-D., Koch, S., Koch, H., Lubeck, M., Krause, M., Goedecke, N., Decker, J., Kosinski, T., Park, M.A., Bache, N., Hoerning, O., Cox, J., Räther, O., and Mann, M. (2018). Online Parallel Accumulation-Serial Fragmentation (PASEF) with a Novel Trapped Ion Mobility Mass Spectrometer. Molecular & cellular proteomics : MCP *17*, 2534-2545.

Meissner, F., Scheltema, R.A., Mollenkopf, H.J., and Mann, M. (2013). Direct proteomic quantification of the secretome of activated immune cells. Science (New York, NY) *340*, 475-478.

Mine, N., Iwamoto, R., and Mekada, E. (2005). HB-EGF promotes epithelial cell migration in eyelid development. Development (Cambridge, England) *132*, 4317-4326.

Moss, M.L., Jin, S.L., Milla, M.E., Bickett, D.M., Burkhart, W., Carter, H.L., Chen, W.J., Clay, W.C., Didsbury, J.R., Hassler, D., Hoffman, C.R., Kost, T.A., Lambert, M.H., Leesnitzer, M.A., McCauley, P., McGeehan, G., Mitchell, J., Moyer, M., Pahel, G., Rocque, W., Overton, L.K., Schoenen, F., Seaton, T., Su, J.L., Becherer, J.D., and et al. (1997). Cloning of a disintegrin metalloproteinase that processes precursor tumour-necrosis factor-alpha. Nature *385*, 733-736.

Mülberg, J., Schooltink, H., Stoyan, T., Günther, M., Graeve, L., Buse, G., Mackiewicz, A., Heinrich, P.C., and Rose-John, S. (1993). The soluble interleukin-6 receptor is generated by shedding. European Journal of Immunology *23*, 473-480.

Muliyil, S., Levet, C., Düsterhöft, S., Dulloo, I., Cowley, S., and Freeman, M. (2020). ADAM17-triggered TNF signalling protects the ageing Drosophila retina from lipid droplet mediated degeneration. bioRxiv, 2020.2001.2009.900209.

Müller, S.A., Scilabra, S.D., and Lichtenthaler, S.F. (2016). Proteomic Substrate Identification for Membrane Proteases in the Brain. Frontiers in molecular neuroscience *9*, 96.

Muntel, J., Kirkpatrick, J., Bruderer, R., Huang, T., Vitek, O., Ori, A., and Reiter, L. (2019). Comparison of Protein Quantification in a Complex Background by DIA and TMT Workflows with Fixed Instrument Time. Journal of proteome research *18*, 1340-1351.

Muntel, J., Xuan, Y., Berger, S.T., Reiter, L., Bachur, R., Kentsis, A., and Steen, H. (2015). Advancing Urinary Protein Biomarker Discovery by Data-Independent Acquisition on a Quadrupole-Orbitrap Mass Spectrometer. Journal of proteome research *14*, 4752-4762.

Na, H.-W., Shin, W.-S., Ludwig, A., and Lee, S.-T. (2012). The cytosolic domain of protein-tyrosine kinase 7 (PTK7), generated from sequential cleavage by a disintegrin and metalloprotease 17 (ADAM17) and γ-secretase, enhances cell proliferation and migration in colon cancer cells. The Journal of biological chemistry *287*, 25001-25009.

Nijaguna, M.B., Patil, V., Urbach, S., Shwetha, S.D., Sravani, K., Hegde, A.S., Chandramouli, B.A., Arivazhagan, A., Marin, P., Santosh, V., and Somasundaram, K. (2015). Glioblastoma-derived Macrophage Colony-stimulating Factor (MCSF) Induces Microglial Release of Insulin-like Growth Factor-binding Protein 1 (IGFBP1) to Promote Angiogenesis. The Journal of biological chemistry *290*, 23401-23415.

O'Brien, R.J., and Wong, P.C. (2011). Amyloid precursor protein processing and Alzheimer's disease. Annu Rev Neurosci *34*, 185-204.

O'Neill, K.M., Akum, B.F., Dhawan, S.T., Kwon, M., Langhammer, C.G., and Firestein, B.L. (2015). Assessing effects on dendritic arborization using novel Sholl analyses. Front Cell Neurosci *9*, 285-285.

Oikonomidi, I., Burbridge, E., Cavadas, M., Sullivan, G., Collis, B., Naegele, H., Clancy, D., Brezinova, J., Hu, T., Bileck, A., Gerner, C., Bolado, A., von Kriegsheim, A., Martin, S.J., Steinberg, F., Strisovsky, K., and Adrain, C. (2018). iTAP, a novel iRhom interactor, controls TNF secretion by policing the stability of iRhom/TACE. eLife *7*.

Olsen, J.V., Macek, B., Lange, O., Makarov, A., Horning, S., and Mann, M. (2007). Higher-energy C-trap dissociation for peptide modification analysis. Nature methods *4*, 709-712.

Ong, S.E., Blagoev, B., Kratchmarova, I., Kristensen, D.B., Steen, H., Pandey, A., and Mann, M. (2002). Stable isotope labeling by amino acids in cell culture, SILAC, as a simple and accurate approach to expression proteomics. Molecular & cellular proteomics : MCP *1*, 376-386.

Orme, J.J., Du, Y., Vanarsa, K., Mayeux, J., Li, L., Mutwally, A., Arriens, C., Min, S., Hutcheson, J., Davis, L.S., Chong, B.F., Satterthwaite, A.B., Wu, T., and Mohan, C. (2016). Heightened cleavage of Axl receptor tyrosine kinase by ADAM metalloproteases may contribute to disease pathogenesis in SLE. Clinical immunology (Orlando, Fla) *169*, 58-68.

Ou-Yang, M.H., Kurz, J.E., Nomura, T., Popovic, J., Rajapaksha, T.W., Dong, H., Contractor, A., Chetkovich, D.M., Tourtellotte, W.G., and Vassar, R. (2018). Axonal organization defects in the hippocampus of adult conditional BACE1 knockout mice. Science translational medicine *10*.

Palazuelos, J., Crawford, H.C., Klingener, M., Sun, B., Karelis, J., Raines, E.W., and Aguirre, A. (2014). TACE/ADAM17 is essential for oligodendrocyte development and CNS myelination. J Neurosci *34*, 11884-11896.

Palazuelos, J., Klingener, M., Raines, E.W., Crawford, H.C., and Aguirre, A. (2015). Oligodendrocyte Regeneration and CNS Remyelination Require TACE/ADAM17. J Neurosci *35*, 12241-12247.

Park, H.-J., Shabashvili, D., Nekorchuk, M.D., Shyqyriu, E., Jung, J.I., Ladd, T.B., Moore, B.D., Felsenstein, K.M., Golde, T.E., and Kim, S.-H. (2012). Retention in endoplasmic reticulum 1 (RER1) modulates amyloid-β (Aβ) production by altering trafficking of γ-secretase and amyloid precursor protein (APP). The Journal of biological chemistry *287*, 40629-40640.

Perry, R.H., Cooks, R.G., and Noll, R.J. (2008). Orbitrap mass spectrometry: instrumentation, ion motion and applications. Mass spectrometry reviews *27*, 661-699.

Peschon, J.J., Slack, J.L., Reddy, P., Stocking, K.L., Sunnarborg, S.W., Lee, D.C., Russell, W.E., Castner, B.J., Johnson, R.S., Fitzner, J.N., Boyce, R.W., Nelson, N., Kozlosky, C.J., Wolfson, M.F., Rauch, C.T., Cerretti, D.P., Paxton, R.J., March, C.J., and Black, R.A. (1998). An essential role for ectodomain shedding in mammalian development. Science (New York, NY) *282*, 1281-1284.

Pigoni, M., Hsia, H.E., Hartmann, J., Rudan Njavro, J., Shmueli, M.D., Müller, S.A., Güner, G., Tüshaus, J., Kuhn, P.H., Kumar, R., Gao, P., Tran, M.L., Ramazanov, B., Blank, B., Hipgrave Ederveen, A.L., Von Blume, J., Mulle, C., Gunnersen, J.M., Wuhrer, M., Rammes, G., Busche, M.A., Koeglsperger, T., and Lichtenthaler, S.F. (2020). Seizure protein 6 controls glycosylation and trafficking of kainate receptor subunits GluK2 and GluK3. The EMBO journal, e103457.

Pigoni, M., Wanngren, J., Kuhn, P.H., Munro, K.M., Gunnersen, J.M., Takeshima, H., Feederle, R., Voytyuk, I., De Strooper, B., Levasseur, M.D., Hrupka, B.J., Muller, S.A., and Lichtenthaler, S.F. (2016). Seizure protein 6 and its homolog seizure 6-like protein are physiological substrates of BACE1 in neurons. Molecular neurodegeneration *11*, 67.

Pinero, J., Bravo, A., Queralt-Rosinach, N., Gutierrez-Sacristan, A., Deu-Pons, J., Centeno, E., Garcia-Garcia, J., Sanz, F., and Furlong, L.I. (2017). DisGeNET: a

comprehensive platform integrating information on human disease-associated genes and variants. Nucleic acids research *45*, D833-d839.

Qing, X., Chinenov, Y., Redecha, P., Madaio, M., Roelofs, J.J., Farber, G., Issuree, P.D., Donlin, L., McLlwain, D.R., Mak, T.W., Blobel, C.P., and Salmon, J.E. (2018). iRhom2 promotes lupus nephritis through TNF-alpha and EGFR signaling. The Journal of clinical investigation *128*, 1397-1412.

Rappsilber, J., Ishihama, Y., and Mann, M. (2003). Stop and go extraction tips for matrix-assisted laser desorption/ionization, nanoelectrospray, and LC/MS sample pretreatment in proteomics. Analytical chemistry *75*, 663-670.

Reddy, P., Slack, J.L., Davis, R., Cerretti, D.P., Kozlosky, C.J., Blanton, R.A., Shows, D., Peschon, J.J., and Black, R.A. (2000). Functional analysis of the domain structure of tumor necrosis factor-alpha converting enzyme. The Journal of biological chemistry *275*, 14608-14614.

Rosso, O., Piazza, T., Bongarzone, I., Rossello, A., Mezzanzanica, D., Canevari, S., Orengo, A.M., Puppo, A., Ferrini, S., and Fabbi, M. (2007). The ALCAM shedding by the metalloprotease ADAM17/TACE is involved in motility of ovarian carcinoma cells. Molecular cancer research : MCR *5*, 1246-1253.

Rudan Njavro, J., Klotz, J., Dislich, B., Wanngren, J., Shmueli, M.D., Herber, J., Kuhn, P.H., Kumar, R., Koeglsperger, T., Conrad, M., Wurst, W., Feederle, R., Vlachos, A., Michalakis, S., Jedlicka, P., Muller, S.A., and Lichtenthaler, S.F. (2020). Mouse brain proteomics establishes MDGA1 and CACHD1 as in vivo substrates of the Alzheimer protease BACE1. FASEB journal : official publication of the Federation of American Societies for Experimental Biology *34*, 2465-2482.

Saftig, P., and Lichtenthaler, S.F. (2015). The alpha secretase ADAM10: A metalloprotease with multiple functions in the brain. Progress in neurobiology *135*, 1-20.

Sagane, K., Hayakawa, K., Kai, J., Hirohashi, T., Takahashi, E., Miyamoto, N., Ino, M., Oki, T., Yamazaki, K., and Nagasu, T. (2005). Ataxia and peripheral nerve hypomyelination in ADAM22-deficient mice. BMC neuroscience *6*, 33.

Sahin, U., Weskamp, G., Kelly, K., Zhou, H.-M., Higashiyama, S., Peschon, J., Hartmann, D., Saftig, P., and Blobel, C.P. (2004). Distinct roles for ADAM10 and ADAM17 in ectodomain shedding of six EGFR ligands. J Cell Biol *164*, 769-779.

Sathe, G., Na, C.H., Renuse, S., Madugundu, A.K., Albert, M., Moghekar, A., and Pandey, A. (2019). Quantitative Proteomic Profiling of Cerebrospinal Fluid to Identify Candidate Biomarkers for Alzheimer's Disease. Proteomics Clinical applications *13*, e1800105.

Schindler, S.E., Li, Y., Todd, K.W., Herries, E.M., Henson, R.L., Gray, J.D., Wang, G., Graham, D.L., Shaw, L.M., Trojanowski, J.Q., Hassenstab, J.J., Benzinger, T.L.S., Cruchaga, C., Jucker, M., Levin, J., Chhatwal, J.P., Noble, J.M., Ringman, J.M., Graff-Radford, N.R., Holtzman, D.M., Ladenson, J.H., Morris, J.C., Bateman, R.J., Xiong, C., and Fagan, A.M. (2019). Emerging cerebrospinal fluid biomarkers in autosomal dominant Alzheimer's disease. Alzheimer's & dementia : the journal of the Alzheimer's Association *15*, 655-665.

Schira-Heinen, J., Grube, L., Waldera-Lupa, D.M., Baberg, F., Langini, M., Etemad-Parishanzadeh, O., Poschmann, G., and Stuhler, K. (2019). Pitfalls and opportunities in the characterization of unconventionally secreted proteins by secretome analysis. Biochimica et biophysica acta Proteins and proteomics *1867*, 140237.

Schlage, P., Kockmann, T., Kizhakkedathu, J.N., and auf dem Keller, U. (2015). Monitoring matrix metalloproteinase activity at the epidermal-dermal interface by SILAC-iTRAQ-TAILS. Proteomics *15*, 2491-2502.

Schlepckow, K., Kleinberger, G., Fukumori, A., Feederle, R., Lichtenthaler, S.F., Steiner, H., and Haass, C. (2017). An Alzheimer-associated TREM2 variant occurs at the ADAM cleavage site and affects shedding and phagocytic function. EMBO molecular medicine *9*, 1356-1365.

Schwarz, J., Broder, C., Helmstetter, A., Schmidt, S., Yan, I., Müller, M., Schmidt-Arras, D., Becker-Pauly, C., Koch-Nolte, F., Mittrücker, H.-W., Rabe, B., Rose-John, S., and Chalaris, A. (2013). Short-term TNFα shedding is independent of cytoplasmic phosphorylation or furin cleavage of ADAM17. Biochimica et Biophysica Acta (BBA) - Molecular Cell Research *1833*, 3355-3367.

Serdaroglu, A., Muller, S.A., Schepers, U., Brase, S., Weichert, W., Lichtenthaler, S.F., and Kuhn, P.H. (2017). An optimised version of the secretome protein enrichment with click sugars (SPECS) method leads to enhanced coverage of the secretome. Proteomics *17*.

Sharma, K., Schmitt, S., Bergner, C.G., Tyanova, S., Kannaiyan, N., Manrique-Hoyos, N., Kongi, K., Cantuti, L., Hanisch, U.K., Philips, M.A., Rossner, M.J., Mann, M., and Simons, M. (2015). Cell type- and brain region-resolved mouse brain proteome. Nature neuroscience *18*, 1819-1831.

Siggs, O.M., Grieve, A., Xu, H., Bambrough, P., Christova, Y., and Freeman, M. (2014). Genetic interaction implicates iRhom2 in the regulation of EGF receptor signalling in mice. Biology open *3*, 1151-1157.

Siney, E.J., Holden, A., Casselden, E., Bulstrode, H., Thomas, G.J., and Willaime-Morawek, S. (2017). Metalloproteinases ADAM10 and ADAM17 Mediate Migration and Differentiation in Glioblastoma Sphere-Forming Cells. Molecular neurobiology *54*, 3893-3905.

Skorupa, A., Urbach, S., Vigy, O., King, M.A., Chaumont-Dubel, S., Prehn, J.H., and Marin, P. (2013). Angiogenin induces modifications in the astrocyte secretome: relevance to amyotrophic lateral sclerosis. J Proteomics *91*, 274-285.

Sommer, A., Kordowski, F., Büch, J., Maretzky, T., Evers, A., Andrä, J., Düsterhöft, S., Michalek, M., Lorenzen, I., Somasundaram, P., Tholey, A., Sönnichsen, F.D., Kunzelmann, K., Heinbockel, L., Nehls, C., Gutsmann, T., Grötzinger, J., Bhakdi, S., and Reiss, K. (2016). Phosphatidylserine exposure is required for ADAM17 sheddase function. Nature communications *7*, 11523.

Squire, J.M., Paul, D.M., and Morris, E.P. (2017). Myosin and Actin Filaments in Muscle: Structures and Interactions. Sub-cellular biochemistry *82*, 319-371.

Stachel, S.J., Coburn, C.A., Steele, T.G., Jones, K.G., Loutzenhiser, E.F., Gregro, A.R., Rajapakse, H.A., Lai, M.T., Crouthamel, M.C., Xu, M., Tugusheva, K., Lineberger, J.E., Pietrak, B.L., Espeseth, A.S., Shi, X.P., Chen-Dodson, E., Holloway, M.K., Munshi, S., Simon, A.J., Kuo, L., and Vacca, J.P. (2004). Structure-based design of potent and selective cell-permeable inhibitors of human beta-secretase (BACE-1). Journal of medicinal chemistry *47*, 6447-6450.

Stiess, M., Wegehingel, S., Nguyen, C., Nickel, W., Bradke, F., and Cambridge, S.B. (2015). A Dual SILAC Proteomic Labeling Strategy for Quantifying Constitutive and Cell-Cell Induced Protein Secretion. Journal of proteome research *14*, 3229-3238.

Stutzer, I., Selevsek, N., Esterhazy, D., Schmidt, A., Aebersold, R., and Stoffel, M. (2013). Systematic proteomic analysis identifies beta-site amyloid precursor protein

cleaving enzyme 2 and 1 (BACE2 and BACE1) substrates in pancreatic beta-cells. The Journal of biological chemistry *288*, 10536-10547.

Swaney, D.L., Wenger, C.D., and Coon, J.J. (2010). Value of using multiple proteases for large-scale mass spectrometry-based proteomics. Journal of proteome research *9*, 1323-1329.

Tang, B., Li, X., Maretzky, T., Perez-Aguilar, J.M., McIlwain, D., Xie, Y., Zheng, Y., Mak, T.W., Weinstein, H., and Blobel, C.P. (2020). Substrate-selective protein ectodomain shedding by ADAM17 and iRhom2 depends on their juxtamembrane and transmembrane domains. FASEB journal : official publication of the Federation of American Societies for Experimental Biology *34*, 4956-4969.

Tsukamoto, S., Takeuchi, M., Kawaguchi, T., Togasaki, E., Yamazaki, A., Sugita, Y., Muto, T., Sakai, S., Takeda, Y., Ohwada, C., Sakaida, E., Shimizu, N., Nishii, K., Jiang, M., Yokote, K., Bujo, H., and Nakaseko, C. (2014). Tetraspanin CD9 modulates ADAM17-mediated shedding of LR11 in leukocytes. Exp Mol Med *46*, e89-e89.

Tsumagari, K., Shirakabe, K., Ogura, M., Sato, F., Ishihama, Y., and Sehara-Fujisawa, A. (2017). Secretome analysis to elucidate metalloprotease-dependent ectodomain shedding of glycoproteins during neuronal differentiation. Genes Cells *22*, 237-244.

Tüshaus, J., Müller, S.A., Kataka, E.S., Zaucha, J., Monasor, L.S., Su, M., Güner, G., Jocher, G., Tahirovic, S., Frishman, D., Simons, M., and Lichtenthaler, S.F. (2020). Quantitative proteomics establishes the cell type-resolved mouse brain secretome. The EMBO journal e105693.

UniProt Consortium, T. (2018). UniProt: the universal protein knowledgebase. Nucleic acids research *46*, 2699.

van Erp, S., van den Heuvel, D.M.A., Fujita, Y., Robinson, R.A., Hellemons, A., Adolfs, Y., Van Battum, E.Y., Blokhuis, A.M., Kuijpers, M., Demmers, J.A.A., Hedman, H., Hoogenraad, C.C., Siebold, C., Yamashita, T., and Pasterkamp, R.J. (2015). Lrig2 Negatively Regulates Ectodomain Shedding of Axon Guidance Receptors by ADAM Proteases. Developmental cell *35*, 537-552.

Vanlandewijck, M., He, L., Mäe, M.A., Andrae, J., Ando, K., Del Gaudio, F., Nahar, K., Lebouvier, T., Laviña, B., Gouveia, L., Sun, Y., Raschperger, E., Räsänen, M., Zarb, Y., Mochizuki, N., Keller, A., Lendahl, U., and Betsholtz, C. (2018). A molecular atlas of cell types and zonation in the brain vasculature. Nature *554*, 475-480.

Vassar, R., Bennett, B.D., Babu-Khan, S., Kahn, S., Mendiaz, E.A., Denis, P., Teplow, D.B., Ross, S., Amarante, P., Loeloff, R., Luo, Y., Fisher, S., Fuller, J., Edenson, S., Lile, J., Jarosinski, M.A., Biere, A.L., Curran, E., Burgess, T., Louis, J.C., Collins, F., Treanor, J., Rogers, G., and Citron, M. (1999). Beta-secretase cleavage of Alzheimer's amyloid precursor protein by the transmembrane aspartic protease BACE. Science (New York, NY) *286*, 735-741.

Vishal, S., Sourabh, A., and Harkirat, S. (2011). Alois Alzheimer (1864-1915) and the Alzheimer syndrome. Journal of medical biography *19*, 32-33.

Voss, M., Schröder, B., and Fluhrer, R. (2013). Mechanism, specificity, and physiology of signal peptide peptidase (SPP) and SPP-like proteases. Biochimica et Biophysica Acta (BBA) - Biomembranes *1828*, 2828-2839.

Voytyuk, I., Mueller, S.A., Herber, J., Snellinx, A., Moechars, D., van Loo, G., Lichtenthaler, S.F., and De Strooper, B. (2018). BACE2 distribution in major brain

cell types and identification of novel substrates. Life Sci Alliance *1*, e201800026-e201800026.

Walker, D.G., and Lue, L.-F. (2013). Understanding the neurobiology of CD200 and the CD200 receptor: a therapeutic target for controlling inflammation in human brains? Future Neurol *8*, 10.2217/fnl.2213.2214.

Weskamp, G., Mendelson, K., Swendeman, S., Le Gall, S., Ma, Y., Lyman, S., Hinoki, A., Eguchi, S., Guaiquil, V., Horiuchi, K., and Blobel, C.P. (2010). Pathological neovascularization is reduced by inactivation of ADAM17 in endothelial cells but not in pericytes. Circulation research *106*, 932-940.

Weskamp, G., Tushaus, J., Li, D., Feederle, R., Maretzky, T., Swendemann, S., Falck-Pedersen, E., McIlwain, D.R., Mak, T.W., Salmon, J.E., Lichtenthaler, S.F., and Blobel, C.P. (2020). ADAM17 stabilizes its interacting partner inactive Rhomboid 2 (iRhom2) but not inactive Rhomboid 1 (iRhom1). The Journal of biological chemistry *295*, 4350-4358.

Whelan, C.D., Mattsson, N., Nagle, M.W., Vijayaraghavan, S., Hyde, C., Janelidze, S., Stomrud, E., Lee, J., Fitz, L., Samad, T.A., Ramaswamy, G., Margolin, R.A., Malarstig, A., and Hansson, O. (2019). Multiplex proteomics identifies novel CSF and plasma biomarkers of early Alzheimer's disease. Acta Neuropathologica Communications *7*, 169.

Wong, E., Cohen, T., Romi, E., Levin, M., Peleg, Y., Arad, U., Yaron, A., Milla, M.E., and Sagi, I. (2016). Harnessing the natural inhibitory domain to control TNFα Converting Enzyme (TACE) activity in vivo. Scientific reports *6*, 35598.

Wong, E., Maretzky, T., Peleg, Y., Blobel, C.P., and Sagi, I. (2015). The Functional Maturation of A Disintegrin and Metalloproteinase (ADAM) 9, 10, and 17 Requires Processing at a Newly Identified Proprotein Convertase (PC) Cleavage Site. The Journal of biological chemistry *290*, 12135-12146.

Woo, J., Han, D., Park, J., Kim, S.J., and Kim, Y. (2015). In-depth characterization of the secretome of mouse CNS cell lines by LC-MS/MS without prefractionation. Proteomics *15*, 3617-3622.

Yan, R., Bienkowski, M.J., Shuck, M.E., Miao, H., Tory, M.C., Pauley, A.M., Brashier, J.R., Stratman, N.C., Mathews, W.R., Buhl, A.E., Carter, D.B., Tomasselli, A.G., Parodi, L.A., Heinrikson, R.L., and Gurney, M.E. (1999). Membrane-anchored aspartyl protease with Alzheimer's disease beta-secretase activity. Nature *402*, 533-537.

Yatim, A., Benne, C., Sobhian, B., Laurent-Chabalier, S., Deas, O., Judde, J.G., Lelievre, J.D., Levy, Y., and Benkirane, M. (2012). NOTCH1 nuclear interactome reveals key regulators of its transcriptional activity and oncogenic function. Molecular cell *48*, 445-458.

Yi, M.H., Zhang, E., Kim, J.J., Baek, H., Shin, N., Kim, S., Kim, S.R., Kim, H.R., Lee, S.J., Park, J.B., Kim, Y., Kwon, O.Y., Lee, Y.H., Oh, S.H., and Kim, D.W. (2016). CD200R/Foxp3-mediated signalling regulates microglial activation. Scientific reports *6*, 34901.

Yin, R.H., Yu, J.T., and Tan, L. (2015). The Role of SORL1 in Alzheimer's Disease. Molecular neurobiology *51*, 909-918.

Yoon, S., and Baik, J.H. (2013). Dopamine D2 receptor-mediated epidermal growth factor receptor transactivation through a disintegrin and metalloprotease regulates dopaminergic neuron development via extracellular signal-related kinase activation. The Journal of biological chemistry *288*, 28435-28446.

Zellner, A., Scharrer, E., Arzberger, T., Oka, C., Domenga-Denier, V., Joutel, A., Lichtenthaler, S.F., Müller, S.A., Dichgans, M., and Haffner, C. (2018). CADASIL brain vessels show a HTRA1 loss-of-function profile. Acta neuropathologica *136*, 111-125.

Zhang, C., Han, X., Xu, X., Zhou, Z., Chen, X., Tang, Y., Cheng, J., Moazzam, N.F., Liu, F., Xu, J., Peng, W., Du, F., Zhang, B., Song, Z., Zeng, J., and Gong, A. (2018). FoxM1 drives ADAM17/EGFR activation loop to promote mesenchymal transition in glioblastoma. Cell death & disease *9*, 469.

Zhang, F., Ge, W., Ruan, G., Cai, X., and Guo, T. (2020). Data-Independent Acquisition Mass Spectrometry-Based Proteomics and Software Tools: A Glimpse in 2020. Proteomics, e1900276.

Zhou, L., Barao, S., Laga, M., Bockstael, K., Borgers, M., Gijsen, H., Annaert, W., Moechars, D., Mercken, M., Gevaert, K., and De Strooper, B. (2012). The neural cell adhesion molecules L1 and CHL1 are cleaved by BACE1 protease in vivo. The Journal of biological chemistry *287*, 25927-25940.

Zhu, L., Bergmeier, W., Wu, J., Jiang, H., Stalker, T.J., Cieslak, M., Fan, R., Boumsell, L., Kumanogoh, A., Kikutani, H., Tamagnone, L., Wagner, D.D., Milla, M.E., and Brass, L.F. (2007). Regulated surface expression and shedding support a dual role for semaphorin 4D in platelet responses to vascular injury. Proceedings of the National Academy of Sciences of the United States of America *104*, 1621-1626.

Zielinska, D.F., Gnad, F., Wisniewski, J.R., and Mann, M. (2010). Precision mapping of an in vivo N-glycoproteome reveals rigid topological and sequence constraints. Cell *141*, 897-907.

Zunke, F., and Rose-John, S. (2017). The shedding protease ADAM17: Physiology and pathophysiology. Biochimica et biophysica acta Molecular cell research *1864*, 2059-2070.

8 APPENDIX

8.1 Point-to-point protocol: hiSPECS secretome analysis

Cell culture

- Seed cells (e.g. 1 M neurons per well in a 6-well plate) for metabolic labeling
- Prepare culture medium with 50 µM of ManNAz sugar
- Wash cells once with 1xPBS
- Add 1 mL medium + ManNAz to each well of a 6-well plate
- Grow your cells in ManNAz (50 µM) containing medium for 48 h
- Harvest supernatant, spin trough 0.45 µM centrifuge tube filters, add PI (1:500)

ConA enrichment

Note: Avoid EDTA, use cut-off tip to avoid shearing of the beads; do not spin beads higher than 4000 rpm, use 1.5 mL low binding tubes

- For 1 mL medium use 60 µL ConA beads
- Wash ConA beads 2x with 1 mL Binding buffer to get rid of ethanol.
    - Centrifuge on table top centrifuge 2000 g 1 min, take off supernatant
- Add 1 mL medium to the ConA beads and rotate 2 h at 4°C
- Spin down and take off supernatant (= unbound proteins)
- 3x washing steps with Binding buffer
    - rotate 1 min over-head, spin down before taking off supernatant
- Add 500 µL Elution buffer to ConA beads and rotate for 30 min; spin down
- Place supernatant into Pierce Spin Column
- Repeat elution step with another 500 µL Elution buffer
- Place filtered eluate into a fresh 1.5 mL low binding tube
    - Run Eluate over a Membrane

Click to Magnetic DBCO beads

Note: Do not centrifuge magnetic DBCO beads, add 0.1% SDC to each solution to prevent clumping/sticking of the beads except otherwise noted

- 2x washing of magnetic DBCO beads (50 µL per 1 mL supernatant) with 1 mL mass spec grade H_20 in 1.5 mL low binding tube
- Add filtered Eluate to the magnetic beads and shake o/n (16 h, 1200 rpm) at 4°C

Washing of magnetic beads

Note: if a ring appears remove supernatant by pipetting from the bottom of the tube without touching the surface/beads. Resuspend beads properly during washing.

- Wash beads 3x 1 mL with SDS buffer; shake briefly at 1200 rpm RT
- Wash beads 3x 1 mL with 8 M UREA buffer with 0.1% SDC; rotate briefly;
- Wash beads 3x 1 mL with 20% acetonitrile with 0.1% SDC; rotate briefly;
- Add 2x 500 µL ms-dH_20 with 0.1% SDC, resuspend beads and transfer them to a new 1.5 mL low binding tube
- Denaturation:
    - Add 50 µL of 10 mM DTT in 100 mM ABC with 0.1% SDC
    - Incubate 30 min at 1200 rpm and 37°C, discard supernatant
- Alkylation:
    - Add 50 µL of 55 mM IAA in 100 mM ABC with 0.1% SDC
    - Incubate 30 min at 1200 rpm at 20°C in the dark , discard supernatant
- Wash beads 2x with 100 µL 100 mM ABC with 0.1% SDC
- Add LysC solution (0.2 µg per sample) in 100 mM ABC with 0.1% SDC
    - Incubate 3 h at 1200 rpm at 37°C
- Add Trypsin solution (0.2 µg per sample) in 100 mM ABC without 0.1% SDC
    - Incubate o/n (16 h) at 1200 rpm at 37°C
- Next morning, take off peptides and place them into a new 0.5 mL low binding tube
- Wash beads twice with 100 µL 100mM ABC without 0.1% SDC and place it to the peptides
- Acidity with 50 µL of 8% formic acid per sample
- Incubate 20 min at 4°C
- Spin down at 18.000 g for 20 min at 4°C to get rid of SDC
- Perform C18 stage tipping according to (Rappsilber et al., 2003) (4 disk, when loading the sample add 2x 150µL)
    - In the end resuspend in 18 µL 0.1% FA
- Before loading samples into the mass spec, spin down at 18.000 g for 10 min at 4 °C to remove any remaining SDC
- Add 2 µL 1:10 diluted iRTs from Biognosys
- Inject 8 µL into the mass spec for DDA and 8 µL for DIA analysis

Buffers

- Binding Buffer: 5 mM MgCl2, 5 mM MnCl2; 5 mM CaCl2, 0.5 M NaCl, in 20 mM TrisHCL pH 7.5
- Elution Buffer: 500 mM Methyl-alpha-D-mannopyranoside; 10 mM EDTA in 20 mM TrisHCl pH 7.5
- SDS buffer: 100 mM TrisHCl pH 8.5 , 1% SDS, 250 mM NaCl
- UREA Buffer: 8 M UREA in 100 mM TrisHCl pH 8.5

8.2 Point-to-point protocol: Brain vessel isolation

- Pre chill all solutions on ice before usage
- Add 6.5 mL into a 10 mL MEM Media Thomas Pestle Tissue Grinder Assemblies with Serrated Pestles (on ice)
- Cut brain with two scalpels into tiny pieces on a 10 cm dish in 1 mL MEM Media and transfer pieces into the grinder
- Start homogenization 10x, place back on ice continue with other samples continue until all pieces are gone, takes quite some time (around 10 rounds)
- Place homogenate into 50 ml falcon and wash grinder with 6 mL MEM and add it to the samples – wash grinder as well
- Add 30% Ficoll- in MEM 1:1 – 15 mL (prepare day before so it can dissolve properly during over had rotation)
- Mix by inversion 3-5 min on an overhead shaker
- Puls spin to remove liquid from lid
- Split into 2x 15 mL falcon tubes (pellet more stable)
- Centrifuge in U1 Bacteria centrifuge Beckman JS7.5 rotor
  20 min 6000 rpm decal slow 4°C
- Remove myelin layer (top) by sucking with vacuum pump
- Discard supernatant on top and place falcon upside down on tissue paper to remove as much liquid as possible
- Moisten 0.4 µm cell strainer with cold PBS
- Place 750 µL 1% BSA in PBS per brain into a tube
- Transfer vessels into one falcon with a BSA-coated p1000 tip (merge batches)
- Wash falcons and tip with 750 µL BSA – wash falcons with PBS afterwards
- Place vessels on cell strainer
- Wash 5x times with 12 mL PBS (pipette boy) and 300 ml PBS (bottle)
- Coat a 50 mL falcon with BSA (wash falcon several times with PBS)
- Put cell strainer upside down onto coated 50 mL falcon and flush out vessels with wash bottle filled with PBS, check strainer for left over pieces
- Spin down 3000 g for 5 min
- Take out pellet and place into a 1.5 mL low binding tube (Pre coated p1000 tip)
- Spin down and wash 1x times with 1 mL PBS
- Lyse vessels in 100 µL SDT buffer
  (4% SDS, 100 mM DTT, 100 mM Tris-Hcl pH 7.6)
- Incubate for 30 min at RT before homogenization with Precelly Evolution
  (10,000 rpm, 5x 30s, 30 s pause)
- Rotate for 5 min and boil 5 min at 95°C, spin down and move supernatant to fresh low binding tube.
- Wash Precellys tube with 50 µL SDT buffer, rotate for 2 min, spin down and add supernatant to previous fraction.
- Sonicate samples 5x 30 s, cool down samples in between
- Centrifuge samples for 30 min at 18,000 g
- Take of supernatant and measure concentration using 660 nm assay

8.3 LIST OF FIGURES

8.4 LIST OF TABLES

ACKNOWLEDGEMENT

This PhD thesis was conducted with the support of the Boehringer Ingelheim Fonds (BIF) by granting me a 2-year PhD fellowship, with the support of the Technical University of Munich – Institute for Advanced Study, funded by the German Excellence Initiative and the European Union Seventh Framework Program under grant agreement n° 291763 and with the support of the international Max Planck Research School (IMPRS-LS) Munich. Thank you for training, supporting me and creating a fruitful scientific network which is to the same extent helpful and enjoyable.

I would like to pay my special regards to Stefan for trusting, encouraging and respecting my work. For guiding and supporting me to grow as a young scientist. For teaching me the meaning of patience. To Stephan and Hung-En for helping me and teaching me everything required to survive in the lab. To Carl for his support, his optimism and opening the doors to his lab. To all Blobel lab members for welcoming me with open arms and showing me the magic of NYC.

I am incredibly grateful for my kind and friendly lab mates for creating an environment enjoyable to work in, for 5-years filled with support and help, for our lovely lunch times and every single coffee in the sun. To Göki for being the best lab-neighbor one could ask for, his IT support and the philosophical debates about the meaning of life and opposites. To Mar and Laura for all the positive energy and laughter. To Frau Heggeder for the most enjoyable lunch breaks full of soup.

To all my collaborators, colleges, the animal facility team, especially Claudia and Marek for their patience. To my thesis committee, thank you for the support and help on this long journey.

Last but most importantly, I would like to express my deep appreciation to my family. My parents and siblings for supporting and encouraging me to search for and find my own path in life. For their unconditional love and trust. My friends for always being my companions on the mountains and in the valleys, for loving and cheering me up. Special thanks to Ina, Jule and my Munich-pillars, Kathi, Steffi, Maria and Lisa, who all made the past 5 years the most enjoyable journey to be in.